SACLANTCEN Conference Proceedings No. 37

SACLANT ASW RESEARCH CENTRE

SELECTED PAPERS ON OCEAN-SEISMO ACOUSTICS LOW-FREQUENCY UNDERWATER ACOUSTICS

BASED ON THE SACLANTCEN CONTRIBUTIONS TO A SYMPOSIUM HELD BY SACLANTCEN ON 10-14 JUNE 1985

Organized by
Tuncay AKAL
Jonathan M. BERKSON

JUNE 1986

NORTH ATLANTIC TREATY ORGANIZATION

SACLANTCEN
LA SPEZIA, ITALY

This document is released to a NATO Government at the direction of the SACLANTCEN subject to the following conditions:

1. The recipient NATO Government agrees to use its best endeavours to ensure that the information herein disclosed, whether or not it bears a security classification, is not dealt with in any manner (a) contrary to the intent of the provisions of the Charter of the Centre, or (b) prejudicial to the rights of the owner thereof to obtain patent, copyright, or other like statutory protection therefor.

2. If the technical information was originally released to the Centre by a NATO Government subject to restrictions clearly marked on this document the recipient NATO Government agrees to use its best endeavours to abide by the terms of the restrictions so imposed by the releasing Government.

Compiled and Published by

SACLANTCEN

INITIAL DISTRIBUTION

MINISTRIES OF DEFENCE	Copies
JSPHQ Belgium	2
DND Canada	10
CHOD Denmark	8
MOD France	8
MOD Germany	15
MOD Greece	11
MOD Italy	10
MOD Netherlands	12
CHOD Norway	10
MOD Portugal	2
MOD Spain	2
MOD Turkey	5
MOD U.K.	20
SECDEF U.S.	68

NATO AUTHORITIES	Copies
Defence Planning Committee	3
NAMILCOM	2
SACLANT	10
SACLANTREPEUR	1
CINCWESTLANT/COMOCEANLANT	1
COMSTRIKFLTLANT	1
COMIBERLANT	1
CINCEASTLANT	1
COMSUBACLANT	1
COMMAIREASTLANT	1
SACEUR	2
CINCNORTH	1
CINCSOUTH	1
COMNAVSOUTH	1
COMSTRIKFORSOUTH	1
COMEDCENT	1
COMMARAIRMED	1
CINCHAN	3

SCNR FOR SACLANTCEN	Copies
SCNR Belgium	1
SCNR Canada	1
SCNR Denmark	1
SCNR Germany	1
SCNR Greece	1
SCNR Italy	1
SCNR Netherlands	1
SCNR Norway	1
SCNR Portugal	1
SCNR Turkey	1
SCNR U.K.	1
SCNR U.S.	2
SECGEN Rep. SCNR	1
NAMILCOM Rep. SCNR	1

NATIONAL LIAISON OFFICERS	
NLO Canada	1
NLO Denmark	1
NLO Germany	1
NLO Italy	1
NLO U.K.	1
NLO U.S.	1

NLR TO SACLANT	
NLR Belgium	1
NLR Canada	1
NLR Denmark	1
NLR Germany	1
NLR Greece	1
NLR Italy	1
NLR Netherlands	1
NLR Norway	1
NLR Portugal	1
NLR Turkey	1
NLR UK	1

Total initial distribution	248
SACLANTCEN Library	10
Stock	22
Total number of copies	280

SACLANTCEN CONFERENCE PROCEEDINGS NO. 37

NORTH ATLANTIC TREATY ORGANIZATION

SACLANT ASW Research Centre
Viale San Bartolomeo 400,
I-19026 San Bartolomeo (SP), Italy.

tel: national 0187 540111
international + 39 187 540111

telex: 271148 SACENT I

Selected Papers on OCEAN-SEISMO ACOUSTICS

l ...ency underwater acoustics

Based on the SACLANTCEN Contributions
to a Symposium held by SACLANTCEN
on 10-14 June 1985

Organized by
T. Akal
J. Berkson

June 1986

CONTENTS

		Page
FOREWORD		iii
Time dependence of infrasonic ambient seafloor noise on a continental shelf, by T. Akal, A. Barbagelata, G. Guidi, M. Snoek	a)	1-1 to 1-12
The use of Love waves to determine the geo-acoustic properties of marine sediments by T. Akal, H. Schmidt, P. Curzi	b)	2-1 to 2-12
Medium-induced low-frequency fluctuations in acoustic transmission loss: examples from measurements in selected geographical areas by H.B. Ali, M.G. Ferla, S. Fiori	c)	3-1 to 3-12
Directional measurements of low-frequency acoustic backscattering from the seafloor by J.M. Berkson, T. Akal, H.J. Kloosterman, J.L. Berrou	d)	4-1 to 4-7
Shear properties of ocean sediments determined from numerical modelling of Scholte wave data by F.B. Jensen, H. Schmidt	e)	5-1 to 5-10
Evaluation of low-frequency bottom back-scattering strength vs grazing angle by means of multiple beamforming by D. Marandino, T.G. Goldsberry	f)	6-1 to 6-10
Spatial variability of surficial shallow water sediment geoacoustic properties by M.D. Richardson	g)	7-1 to 7-10
Evaluation of experimental techniques for determining the plane wave reflection coefficient at the sea floor by H. Schmidt and F.B. Jensen	h)	8-1 to 8-10
Interface wave studies on the Ligurian shelf using an OBS array: experimental results and propagation models, a.o., by M. Snoek, G. Guidi, E. Michelozzi	i)	9-1 to 9-10
Low-frequency anomalies in the reflection behaviour of marine sediments by M. von Haumeder	j)	10-1 to 10-9

FOREWORD

Ralph R. Goodman
Director
SACLANT ASW Research Centre
La Spezia, Italy

Geologists and geophysicists have used both acoustic and seismic methods to study the seabed by considering the propagation of signals arising from both natural seismic events and man-made impulsive sources. Although significant advances have been made in instrumentation, such as long towed geophysical arrays, air guns and ocean bottom seismometers, the picture of the seafloor is still far from complete.

Underwater acoustics concerns itself today with the phenomena of propagation and noise at frequencies and ranges that require an understanding of acoustic interaction at both of its boundaries, the sea surface and seafloor, over depths ranging from tens to thousands of meters. Much of the earlier higher frequency (> 1 kHz) work included the characterization of the seafloor in regimes of reflection coefficients which were empirically derived from surveys. The results of these studies met with only limited success, confined as they were to those areas where survey data existed and lacking a physical understanding of the processes of reflection and scattering. The development in recent years of systematic methods of measuring the physical and acoustical characteristics of the seabed have led to a much better understanding of propagation. However these techniques are exceedingly slow and expensive and do not fulfill the needs of present day acoustics. The relatively recent recognition of the importance of the role that shear and evanescent waves in the seabed have on waterborne sound has been a major factor in the recognition of the need for acousticians and seismologists to exchange and discuss their common goals and developments.

The realization of the benefits that could be achieved from such an exchange led our Centre to sponsor the Symposium on Ocean Seismo-Acoustics, with partial support from the Office of Naval Research, London. It was held at La Spezia, Italy, June 10-14, 1985 and its purpose was to enhance cross-disciplinary dialogue and generate ideas for new research directions.

The collection of papers originating from the Symposium have been published as a volume* of the NATO Conference Series, with the papers organized into eight topics:

- Propagation: Theoretical Developments
- Propagation: Modelling and Experiments
- Propagation: Fluctuations
- Boundary Scattering
- Sediments: Seismo-Acoustic Waves and Geoacoustic Characteristics
- Seismo-Acoustic Waves: Propagation, Attenuation, and Inverse Techniques
- Seismo-Acoustic Noise
- Technology and New Approaches in Seismo-Acoustic Measurements

This present document is a compilation for normal NATO purposes of the papers presented at the Symposium by Centre staff.

---

* NATO Conference Series. IV, Marine sciences; v.16: "OCEAN SEISMO-ACOUSTICS: Low-frequency underwater acoustics", edited by Tuncay Akal and Jonathan M. Berkson, (including bibliographies and indexes). Published by Plenum Press, New York.

TIME DEPENDENCE OF INFRASONIC AMBIENT SEAFLOOR NOISE ON A CONTINENTAL SHELF

T. Akal, A. Barbagelata, G. Guidi, and M. Snoek

SACLANT ASW Research Centre
Viale San Bartolomeo 400
I-19026 La Spezia, Italy

ABSTRACT

SACLANTCEN is conducting a long term programme of ambient noise measurements that cover the frequency band from 1 to 100 Hz. A sea-bed sensor consisting of three seismometers and a hydrophone has been deployed close to the edge of the continental break in water of 100 m depth. The data are being systematically collected and telemetered via radio link to SACLANTCEN. The initial data (105 days) have been used to investigate the noise characteristics and its statistics.

INTRODUCTION

Ambient noise in the ocean has many sources. As a result, long term measurements are required to identify these sources and define the noise characteristics of an ocean area. Studies of ambient noise have shown that seismic acoustic energy in certain parts of the noise spectrum can be related to various known sources [1 to 13]. Figure 1 identifies several well known sources that transfer energy basically from biological, meteorological, geological or cultural origin into the underwater seismo-acoustic noise field.

SACLANTCEN has begun a programme to measure the time dependence of ambient noise along the Ligurian shelf edge (Fig. 2a). The frequency band of interest is 1 to 100 Hz. Initially both short (33 hr) and long (105 days) term measurements were made.

Two major factors affect ambient noise characteristics, the meteorologic conditions of the area and the distribution of the noise sources around the measurement site. In support of the interpretations of noise data, environmental and shipping data that could affect noise characteristics have been incorporated into the study.

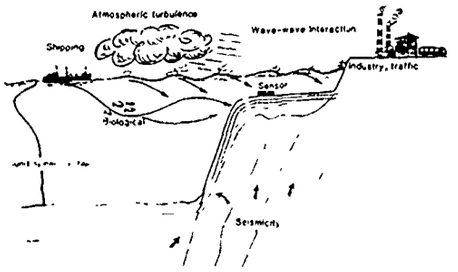

Fig. 1
Basic physical sources which transfer low-frequency energy into the underwater ambient noise field.

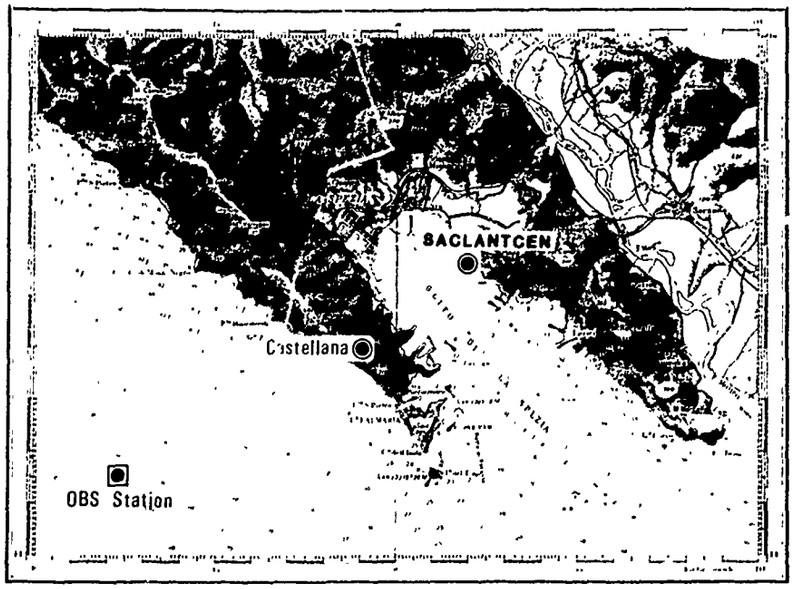

Fig. 2a The location of the measurement site.

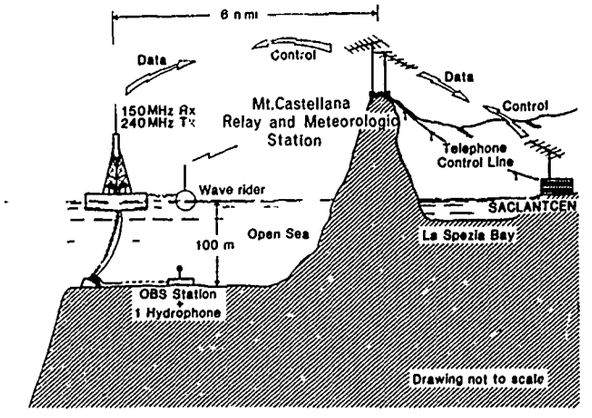

Fig. 2b
Experimental set-up.

INSTRUMENTATION

The instrumentation system used for these measurements consisted of the following components (Fig. 2b):

- the ocean bottom seismometer
- the radio transceiver (mounted on a surface buoy)
- the wave-rider buoy (attached to the surface buoy)
- the radio repeater (mounted on a mountain top)
- the receiver and control unit
- the interface to the digital computer
- the computer system.

Signals from the sensors were immediately converted into digital form. They suffered no significant degradation when transmitted through the various components to SACLANTCEN.

Ocean Bottom Seismometer (OBS)

The OBS consisted of geoacoustical and auxiliary sensors, preamplifiers and A/D electronics that are contained in a disc-shaped housing. Power is provided by a battery installed in the surface buoy and transmitted via a coaxial cable.

The geoacoustic sensors comprised three active 1 Hz geophones (Teledyne S-500) mounted orthogonally and an omnidirectional hydrophone. These sensors can be operated at any angle and need no locking for transportation and handling. They have a velocity sensitivity of 450 V-sec/m and a -5 dB passband of 1 to 100 Hz. In addition to these sensors, the system includes auxiliary sensors: two tilt meters to monitor the inclination, a compass to determine orientation, and a thermistor to measure temperature.

The four geoacoustic sensors are sampled at 600 Hz per channel. The data is converted into a floating point format and combined with low speed data from positional sensors. No gain adjustment is necessary during the experiment because the instantaneous floating point format allows the achievement of a very high dynamic range (120 dB). Calibration can be carried out by injecting stabilized AC current into the calibration coil of the geophones. The data is transmitted in biphase code to the surface buoy via a coaxial cable at 38400 bits/sec.

The Radio Buoy

The radio buoy, mounted on a 4 m diameter circular buoy moored in 100 m depth, about 8 km from the coast, contained rechargeable batteries (i.e. power for 32 hours of continuous data acquisition), a FM modulated VHF radio transmitter (220 MHz/4 W) and a standby radio receiver for power ON/OFF commands.

The Repeater

The unattended radio repeater was installed on 510 m high Mt. Castellana to overcome topographic interference between the OBS radio buoy and SACLANTCEN. The repeater received and retransmitted OBS radio buoy signals at different frequencies. A dedicated telephone line between the repeater and SACLANTCEN permitted the relay of orders to the OBS and the monitoring of the performance of the OBS instruments.

The Receiver and Control Unit

This unit, installed at SACLANTCEN, allowed the performance of the following functions: reception, demodulation and forwarding of the computer interface signals, monitoring of the performance of the geoacoustic and environmental sensors mounted on the OBS, through digital-to-analogue conversion and display of the transmitted signals, monitoring and manual control of the performance of the OBS and repeater station.

The Computer Interface

This unit, installed in the computer area, received the baseband signal from the receiver unit. Bits and words were synchronized and transferred to the digital computer in a parallel format. Commands were received from the computer which switched the full chain on and off according to a pre-set time schedule.

The Computer System

Acquisition and preprocessing were performed on a Hewlett Packard 21 MX computer with a disc unit and other peripherals. Data were immediately stored on discs for display, plot and preprocessing options and for transfer to digital tape.

MEASUREMENT AND ANALYSIS TECHNIQUES

This system was used to measure ambient sea noise for 105 days (December 1984 to March 1985). Automatic acquisitions of ambient noise of 5 minutes duration were made daily; wave-rider data and meteorological data were obtained over longer periods. Figure 3, a sample record, illustrates the variation of the ambient noise levels at different sensors for different meteorological conditions, together with the wave-rider recordings. Spectral estimates of these signals were made by applying standard techniques [14] to 25-sec time-windows over a 1 to 100 Hz frequency band, and averaging the power spectral density levels over a 1 Hz frequency bandwidth. Figure 4 shows the power spectral density of the sample signals of Fig. 3.

Noise Fluctuations in 33-hour Period

Measurements of 5, 10, 30, 60 minutes and 24 hours duration were conducted to study both the short and long-time variations of ambient noise. The power spectral density contours in a frequency/range plane provide the simplest display of the behaviour of the ambient noise field fluctuations, which are a function of both frequency and time.

Figure 5 shows an example of the changes of the ambient noise spectrum levels over a 33-hour period at different sensors. On 21 March 85, the sea surface wave field at the measurement site was flat, under a SWW wind of 3 n.mi/hr. During the day the wind increased to 15 n.mi/hr, causing waves as high as 80 cm. Twenty-seven hours after the beginning of the data acquisition, wind direction changed to North at 2 n.mi/hr. The characteristics of the ambient noise spectrum levels evident in Fig. 5 provide a natural division of the noise field into two distinct regions:

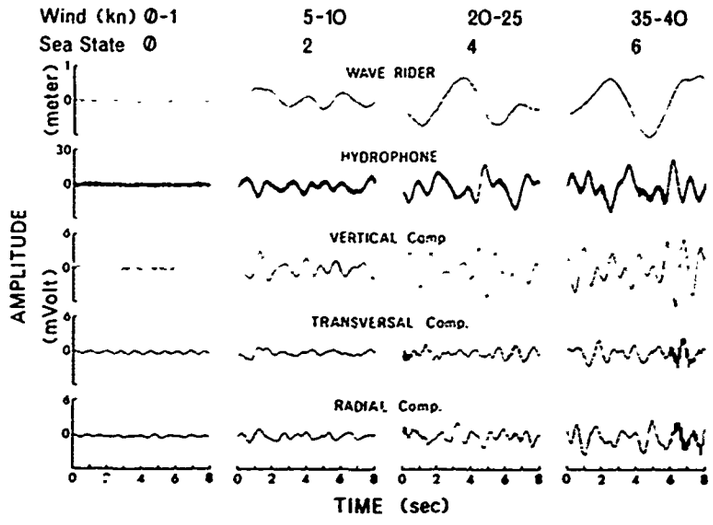

Fig. 3 Sample recordings: signals at various OBS sensors, wave-rider and meteorologic information under different meteorological conditions.

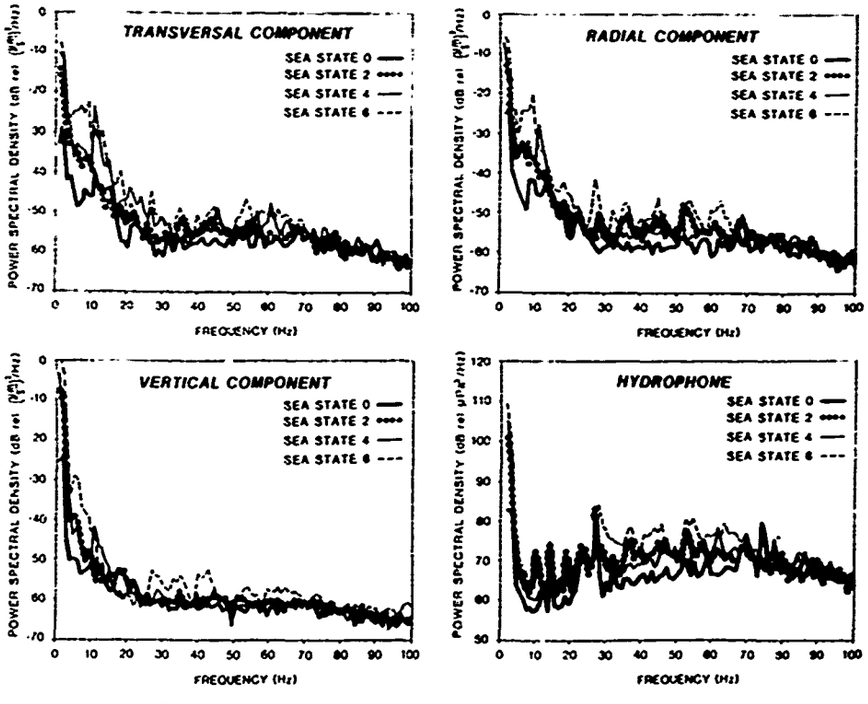

Fig. 4 Power spectral density levels of the sample signals from Fig. 3 for different sea states.

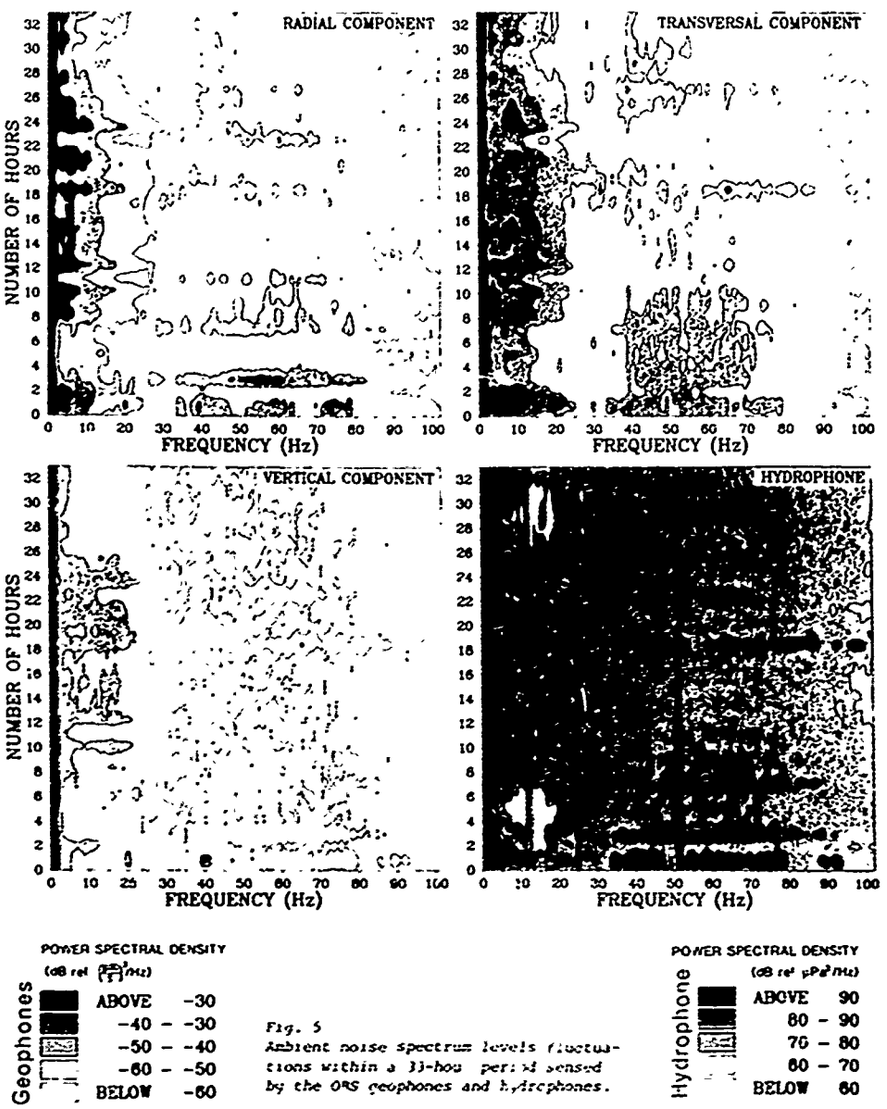

Fig. 5
Ambient noise spectrum levels fluctuations within a 33-hour period sensed by the ORS geophones and hydrophones.

- In the low frequency (1 to 30 Hz) region, horizontal sensors generally have a higher energy content than the vertical sensor and the omni-directional hydrophone has a much steeper fall-off slope than those of the seismic sensors. Increasing noise levels between the 7th and 27th hours, particularly evident in the vertical component, correspond to an increase in wind speed and sea state; conditions then reverted to those of the initial part of the measurement period.

- In the higher frequency region (30 to 100 Hz), shipping noise is demonstrated by sporadic peaks in the contours. The peaks normally correspond to the activities of medium-size trawlers and fishing boats passing through the measurement site.

Noise Fluctuations in 105-day Period

Similar procedures were applied to the data collected during the 105-day period. During this long-term period meteorological conditions and shipping were the two major sources of energy transferred into the acoustic/seismic field.

Effects of Meteorological Conditions

Figure 6 presents variations of the ambient noise spectrum levels with time and the corresponding sea states. The ambient noise fluctuations during the measurements show, as expected, that the temporal characteristics of the ambient noise spectrum levels are influenced by wind and sea conditions at low frequencies (below 30 Hz). Due to changing meteorological conditions, this frequency region reveals changes (schematically described by sea state plots) which correlate well with sea state.

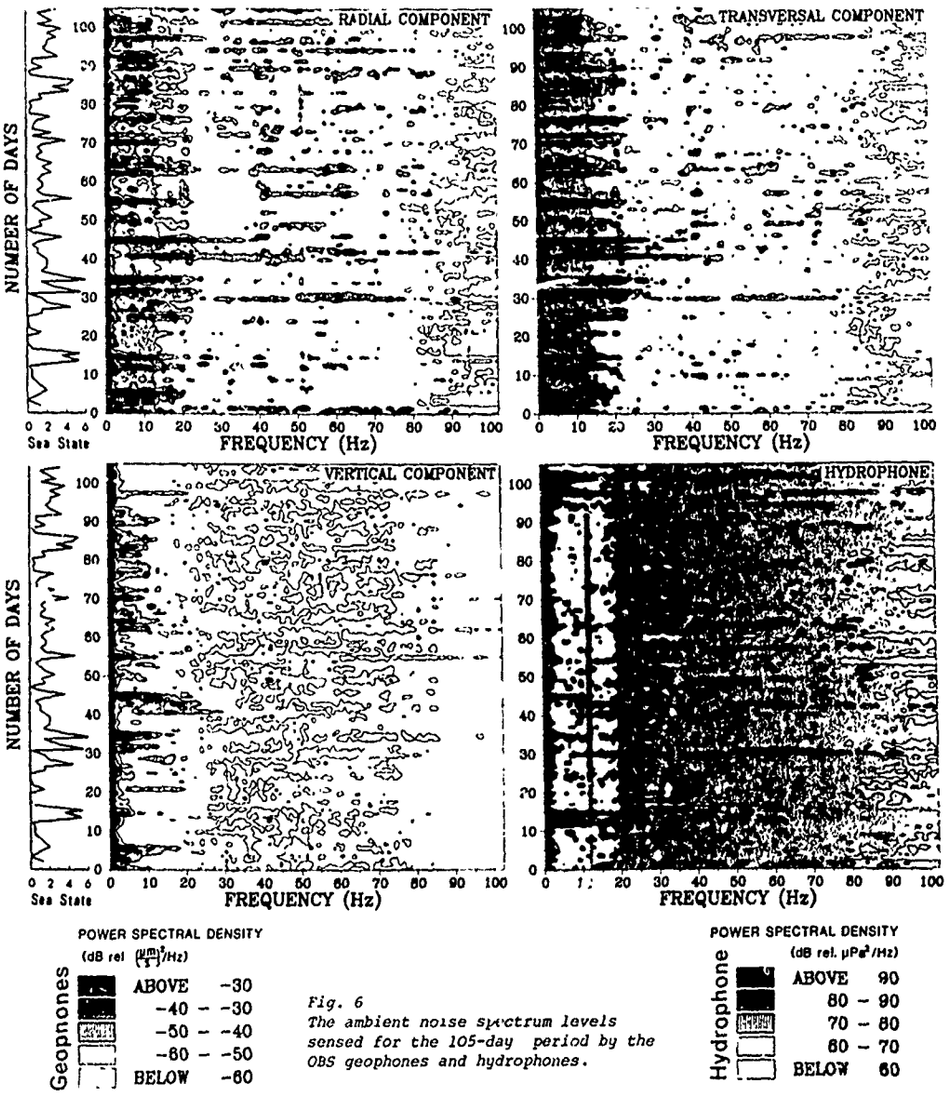

Fig. 6
The ambient noise spectrum levels sensed for the 105-day period by the OBS geophones and hydrophones.

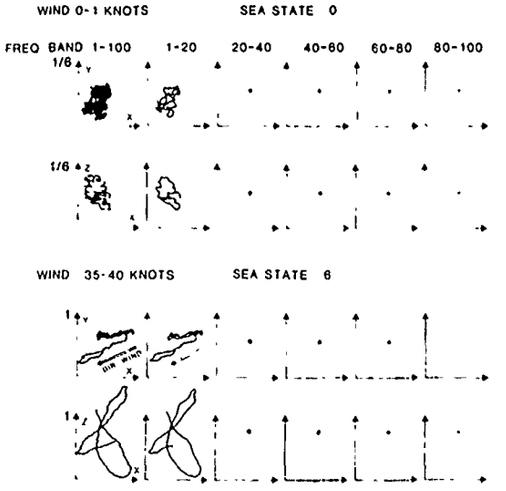

Fig. 7a
Particle motions under sea-state 0 and 6. The hodographs are displayed for different frequency bands. Note, for sea-state 6, x, y and z scales are exaggerated 6 times as compared to those for sea-state 0.

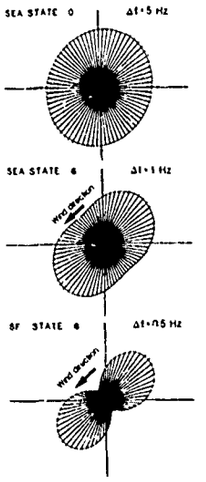

Fig. 7b
Azimuthal power pattern for two different frequency bands.

For all sensors we observed a frequency-dependent increase of spectrum levels with increasing sea state (see selection of different sea states in Fig. 4). At low frequencies, the increase is greater than at the high frequencies. Sea-state effects normally disappear above the 60 to 70 Hz band. Within the 5 to 15 Hz band peaks correspond to the sea surface waves. These peaks increase with increasing sea state while their frequency range narrows. Figure 7a displays two sets of hodographs (for the xy and xz planes) obtained at sea-states 0 and 6. The first column illustrates the particle motions within the 1 to 100 Hz frequency band while the remainder of the columns are devoted to 20 Hz bandwidths covering the 100 Hz measurement band. The energy is evidently concentrated in the 1 to 20 Hz bandwidth, for which particle motion is evident in both vertical and horizontal planes, characteristic of interface waves [15,16]. Figure 7b shows the azimuthal power patterns for sea state 0 and 6 of the same event. The patterns of sea-state were analysed with both large ($\Delta f = 5$) and narrow ($\Delta f = 0.5$) frequency bands. The directional patterns indicate the wind direction for which the sea surface waves had the same orientation.

Effects of Shipping

The high frequency region (30 to 100 Hz) is predominantly influenced by ship traffic noise. The dominant shipping of the area was coastal trawlers, fishing boats and pleasure craft (nearby shipping activity) and distant commercial shipping passing through deep water to or from Genova at distances between 20 and 130 n.mi from the station.

Figure 8 illustrates, for different sensors, the superposition of 105 power spectra, that were recorded daily for the study. To simplify this large amount of data we applied basic statistical analysis techniques [17] to obtain average power and mean power levels for each sensor.

Within the 20 to 100 Hz frequency band, various peaks are superimposed over a mean curve which displays a maximum level at about 50 to 60 Hz. These individual or grouped peaks correspond mostly to nearby shipping. Peaks grouped around 40 to 50 Hz reflect the effects of bottom trawlers (Fig. 9).

Even though the hydrophone and geophones respond to two different physical parameters (pressure and particle motion, respectively), we note that the transition regions between low and high frequencies (5 to 15 Hz) of the spectra obtained from the hydrophone and geophones display different behaviour.

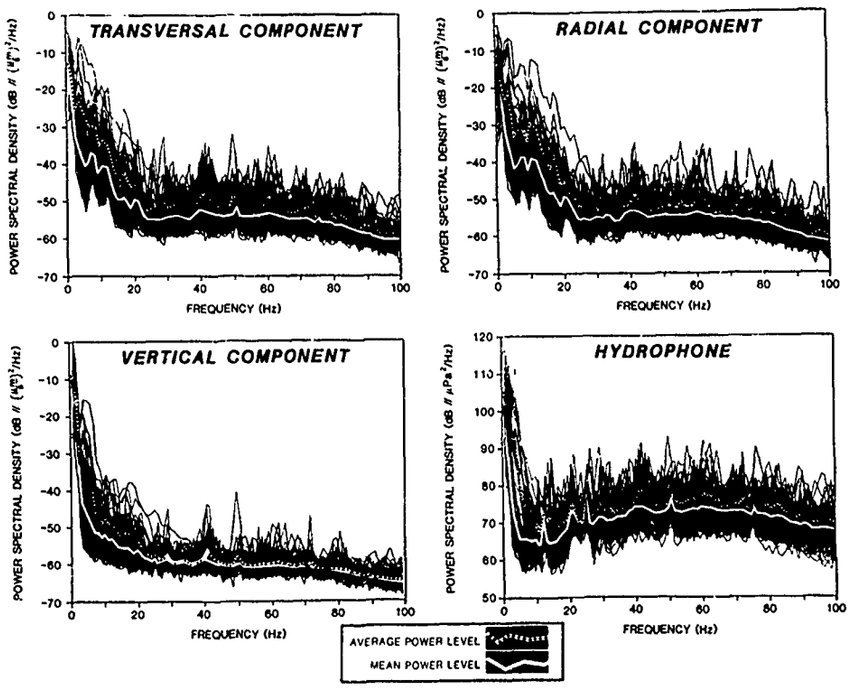

Fig. 8 Records of 105 daily measurements of ambient noise.

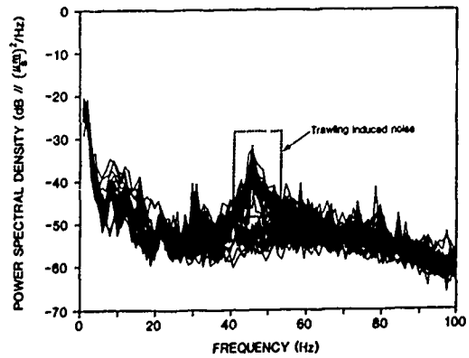

Fig. 9
Spectrum of bottom trawling induced noise.

This difference (low levels on the hydrophone spectra) is probably due to the cut-off of the waterborne propagating noise. For the water depth and the sediment type of the area, the waterborne acoustic propagation cut-off frequency corresponds to 10-15 Hz [18]. Apparently the energy is coupled into the noise field from distant shipping (deep water), and confined to the continental shelf because of the waterborne acoustic frequency cut-off process. In this case, the energy lost within the water column couples into the seismic waves which are detected by the geophones. This phenomenon appears as high energy levels within the 5 to 25 Hz frequency band on the geophone spectra. This observation and the relatively lower levels observed on the vertical geophones as compared with the horizontal ones, indicate that the noise field is mainly related to interface and Love waves.

COMPARISON WITH OTHER DATA

Experimental infrasonic ambient noise data have been reported by others. The data set for sea states 0 and 6 presented in this paper are superimposed (Fig. 10) on Kibblewhite and Ewans [13] data which summarize various other ambient noise data sets. The Mediterranean continental shelf, lacking the long swells of the open oceans, yields lower pressure amplitudes at low frequencies. The same data set compared to Wenz curves [1] within the 10 to 100 Hz band fits into the shallow water region of usual traffic noise (Fig. 11). In the 1 to 10 Hz frequency band, spectrum levels fit nicely into the seismic background and sea surface wave noise.

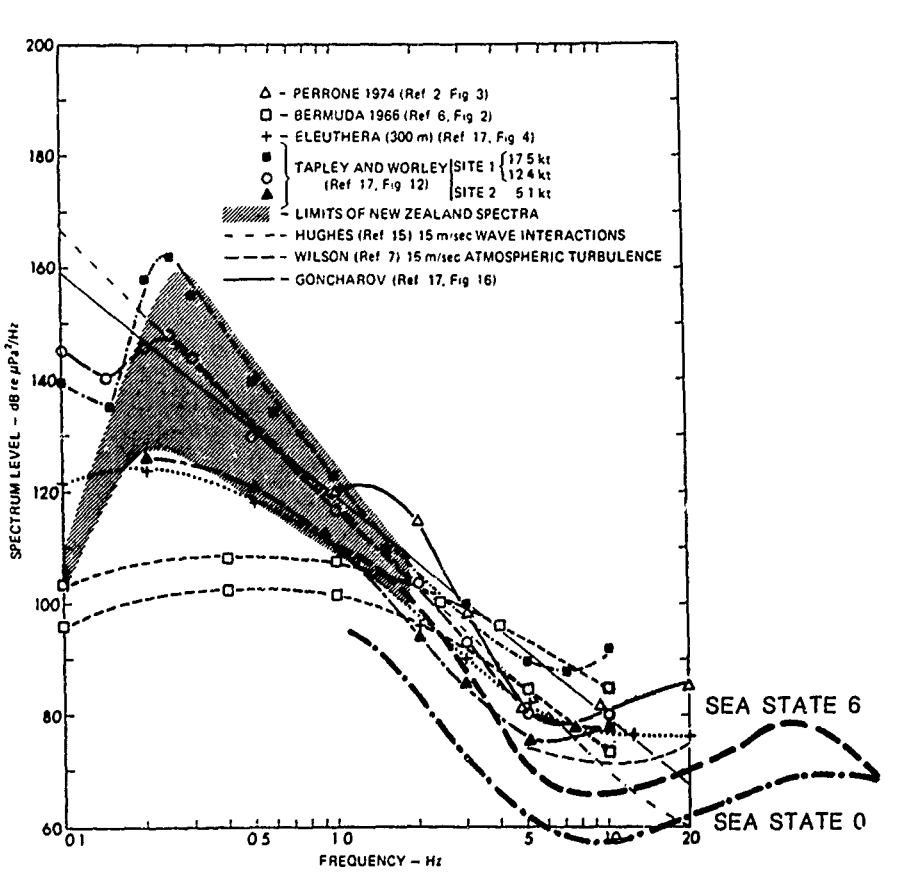

Fig. 10 Comparison of various ambient noise data sets (after [12]).

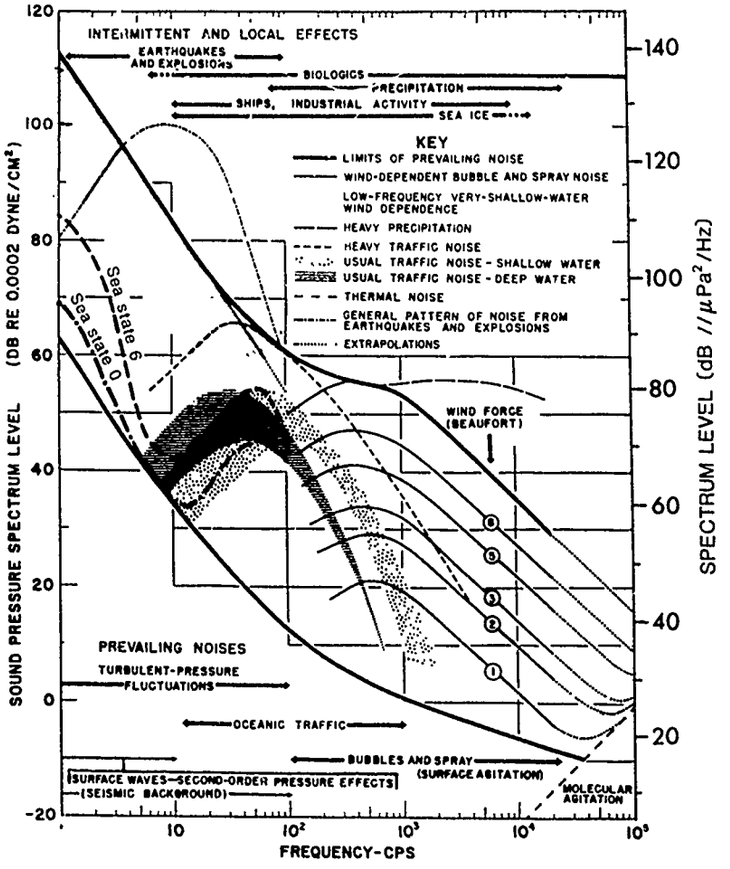

Fig. 11 Comparison of data set for sea-states 0 and 6 with Wenz curves [1].

CONCLUSION

Systematic noise data collected over the 1 to 100 Hz frequency band for a long period revealed that noise levels correlated well with wind-sea conditions and nearby shipping activity.

Meteorological noise overlaps with shipping noise in the transient region of 5 to 25 Hz band. In the same band, the hydrophone (water-borne noise) revealed very low energy levels as compared to the geophones. This effect is most probably caused by the water-borne acoustic frequency cut-off due to the decreasing water depth.

The collection of data for a longer period has produced better noise statistics for the area. The data fit well into previous ambient noise data sets. There is strong evidence that at infrasonic frequencies noise energy propagates essentially as interface waves and ducted Love waves.

REFERENCES

1. G.M. Wenz, "Acoustic Ambient Noise in the Ocean: Spectra and Sources," J. Acoust. Soc. Am. 34, 1936-1956 (1962).
2. A.J. Perrone, "Infrasonic and Low-Frequency Ambient Noise Measurements on the Grand Banks," J. Acoust. Soc. Am. 55, 754-758 (1974).
3. K. Hasselmann, " A Statistical Analysis of the Generation of Microseisms," Rev. Geophys. 1, 177-210 (1963).
4. M.A. Isakovich and B.F. Kur'yanov "Theory of Low-Frequency Noise in the Ocean," Sov. Phys.-Acoust. 16, 49-58 (1970).
5. N. Yen and A.J. Perrone, "Mechanisms and Modelling of Wind-induced Low Frequency Ambient Sea Noise," NUSC Technical Report 5833, Naval Underwater Systems Center, New London, Connecticut, 1979.
6. J.H. Wilson, "Very Low Frequency (VLF) Wind-Generated Noise Produced by Turbulent Pressure Fluctuations in the Atmosphere near the Ocean Surface," J. Acoust. Soc. Am. 66, 1499-1507 (1979).
7. M.S. Longuet-Higgins, "A Theory of the Origin of Microseisms," Philos. Trans. R. Soc. London, Ser. A 243, 1-35 (1950).
8. L.M. Brekhovskikh, "Underwater Sound Waves Generated by Surface Waves in the Ocean," Izv. Atmos. Ocean. Phys. 2, 582-587 (1966).
9. B. Hughes, "Estimates of Underwater Sound (and Infrasound) Produced by Non-linearly Interacting Ocean Waves," J. Acoust. Soc. Am. 60, 1032-1039 (1976).
10. V.V. Goncharov, "Sound Generation in the Ocean by the Interaction of Surface Waves and Turbulence," Izv. Atmos. Ocean. Phys. 6, 710-714 (1970).
11. R.A. Wagstaff, "Low Frequency Ambient Noise in the Deep Sound Channel - The Missing Component," J. Acoust. Soc. Am. 69, 1009-1013 (1981).
12. A.C. Kibblewhite and K.C. Ewans, "Wave-wave interactions, microseisms, and Infrasonic Ambient Noise in the Ocean," Technical Report Applied Research Laboratory of Texas, 1984.
13. A.C. Kibblewhite and K.C. Ewans, "A Study of Ocean and Seismic Noise at Infrasonic Frequencies (in this volume).
14. B. Schmalfeldt, "A Comparison of Seismic and Hydroacoustic Measurements at Very Low Frequencies in Different Shallow Water Areas," (in this volume).
15. D. Rauch, "On the Role of Bottom Interface Waves in Ocean Seismo-Acoustics: A Review," (in this volume).
16. M.N. Toksöz, "Microseisms and an Attempted Application to Exploration," Geophysics 29, 154-177 (1964).
17. R.A. Wagstaff, J.-L. Berrou, "Is Power Averaging the Best Estimator for Undersea Acoustic Data?" In: WAGSTAFF, R.A. and BLUY, O.Z., eds. Underwater ambient noise, proceedings of a conference held at SACLANTCEN on 11-14 May 1982, volume II, unclassified papers. SACLANTCEN CP-32. La Spezia, Italy, SACLANT ASW Research Centre, 1982: 17-1 to 17-16.
18. T. Akal, F. Jensen, "Effects of the Sea-Bed on Acoustic Propagation," In: PACE, N.G., ed., Acoustics and the Sea Bed. Proceedings of the Institute of Acoustics. Underwater Acoustics Group Conference, Bath University, 6-8 April, 1983.

THE USE OF LOVE WAVES TO DETERMINE THE GEOACOUSTIC PROPERTIES OF MARINE SEDIMENTS

T. Akal*, H. Schmidt*, P. Curzi**

*SACLANT ASW Research Centre
Viale San Bartolomeo 400
I-19026 La Spezia, Italy

**Istituto di Geologia Marina
Consiglio Nazionale delle Ricerche
Via Zamboni 65, 40127 Bologna, Italy

ABSTRACT

The importance of the geoacoustic properties of marine sediments for low-frequency shallow water propagation is well established. Reliable compressional properties can be obtained from laboratory analysis of collected samples. The shear properties, however, are highly affected by the deterioration of the chemical and mechanical bindings caused by de-pressurization and change of temperature in the core sampling process. These properties therefore have to be determined in situ. Isolated shear waves are not easily generated due to partial coupling into compressional waves at all interfaces. In the case of stratified, isotropic media, however, coupling can be avoided if the polarization of the shear waves is parallel to the interfaces. Here an experimental technique is described for generation and detection of horizontally polarized shear waves - or Love waves - in a horizontally stratified sea-bed. Shear velocity profiles are determined indirectly by numerical modelling of the experimental data. Results are presented for different types of marine sediments.

INTRODUCTION

The importance of the geoacoustic properties of marine sediments for low-frequency acoustic propagation is well established [1]. Geoacoustic properties also provide a major source of information for the determination of the static and dynamic characteristics of the sea-bed.

When seismic waves propagate through the marine sediments, the dynamic properties of the sediments determine the speed and the attenuation. An investigation of the seismic propagation characteristics can therefore provide accurate information on the geotechnical characteristics of the sea-bed.

Assuming that the sea-floor sediments behave like elastic media, the seismic propagation is controlled by the bulk modulus K, the shear modulus

G, and the density ρ. These parameters are related to the compressional wave velocity, C_p, and the shear wave velocity, C_s, by

$$C_p = [(K + 4G/3)/\rho]^{1/2} \quad \text{and}$$

$$C_s = (G/\rho)^{1/2}$$

If the compressional wave velocity (C_p) and the shear wave velocity (C_s) of an idealized marine sediment can be measured concurrently with a measurement of bulk density, the elastic parameters of the sediments can be completely characterized (see Tables 1 and 2).

Table 1.

BASIC WAVE TYPES AND VELOCITIES
a) BODY WAVES
-COMPRESSIONAL (longitudinal) $C_p=[(K+4G/3)/\rho]^{1/2}$
-SHEAR (transverse) $C_s=(G/\rho)^{1/2}$
b) DUCTED WAVES
- LOVE $C_L=(G_1/\rho)^{1/2}$
c) SURFACE WAVES
- SCHOLTE $C_{SCH}\sim(G/\rho)^{1/2}$

Table 2.

ELASTIC PARAMETERS IN TERMS OF WAVE VELOCITIES AND BULK DENSITY (ρ)
K: BULK MODULUS (incompressibility)
$K=\rho(C_p^2-4C_s^2/3)$
E: YOUNG's MODULUS
$E= 2C_s^2\rho(1+\sigma)$ or
$E=\rho C_p^2(1+\sigma)(1-2\sigma)/(1-\sigma)$
σ.POISSON's RATIO (transv./long. strain)
$\sigma= 1/2(C_p^2-2C_s^2)/(C_p^2-C_s^2)$
G:SHEAR MODULUS (rigidity)
$G=\rho C_s^2$
λ=LAME's CONSTANT
$\lambda=\rho(C_p^2-2C_s^2)$

Several laboratory and field methods are available to measure density and wave velocities in bottom sediment cores. However, the reliability of such measurements is degraded by sample disturbance and temperature and pressure changes. In particular, the shear properties are highly effected by the deterioration of the chemical and mechanical bindings caused by the differences in temperature and pressure between the sampling and the laboratory measurements. Also, in the laboratory, the small size of the sample does not allow direct information to be obtained about the response of these materials to low-frequency seismic/acoustic waves. Therefore the most reliable geoacoustic measurement techniques for ocean-bottom sediments are therefore in situ techniques.

The choice of an actual experimental technique is strongly influenced by the structure of the sea bed. If the bottom was homogeneous to a significant depth, the wave speeds and attenuation could be measured directly because different seismic wave types could be separated. In reality, however, recent sediments consist of a relatively thin top layer of unconsolidated clay or silty clay overlying semi-consolidated silts and sands [2,3]. This structure results from the lowering of sea levels during the glaciation of the Pleistocene epoch in which sand was deposited over wide areas of the continental shelves. The shelves were subsequently covered by unconsolidated sediments during sea level rising during the post-glacial times. Sedimentary processes such as sorting, compaction and

consolidation, also have contributed to the highly stratified structure of the sea bed.

In such a layered sea bed the compressional and shear waves couple, yielding an often complex wave field. The geoacoustic properties therefore must be determined indirectly (inversely) from the propagation characteristics. The most important attenuation mechanism of low frequency propagation in shallow water is the conversion of acoustic energy in the water column into shear waves in the bottom [1]. Because of this importance this mechanism has received special attention during the past decade. Because the propagation of seismic interface waves (also known as Scholte waves) is almost entirely controlled by their shear properties, significant effort has been applied to the analysis of these properties [4,5]. However, the inversion involves significant numerical effort not easily automated.

Here it will be demonstrated that horizontally polarized shear waves (SH), also called Love waves, can be generated by simple means in the low-velocity duct formed by the upper sediments. Because the shear waves do not couple into compressional waves in a horizontal stratification of isotropic layers, their propagation characteristics directly reflect the shear properties. The Love waves therefore form an alternative to the seismic interface waves as the basis of the shear property inversion. Further, the scalar nature of the wave equation for Love waves significantly decreases the calculations involved in the inversion compared to the requirements for the interface waves.

EXPERIMENTAL PROGRAMME

The Love wave experiments were caried out as part of a multinational research programme to measure the velocity and attenuation of seismic waves and supporting geotechnical parameters in marine sediments. The programme was initiated by SACLANT to bring together experts in geophysics, geology and acoustics to compare various measurement and analysis techniques for data gathered under identical environmental conditions.

For this program four institutes played a leading role in the specific problems related to sampling, analysis and interpretation of ocean bottom sediments. The institutes and their tasks were:

- Institute of Marine Geology (IGM-CNR), Bologna, Italy; sampling the sea-bed using different techniques, geotechnical analysis and interpretation, and geological description;

- Centro de Fisica Applicada (CENFA), Madrid, Spain; measuring reflection loss under controlled conditions in a layered sea-bed with variable sensitivity gradients, and testing a model developed by the CENFA scientists;

- US Naval Ocean Research and Development Activity (NORDA), Bay St. Louis, MS, USA; sediment sampling, laboratory analysis of the samples for compressional and shear wave velocities, sediment mass property analysis, measurements with the ELAC Sea-Bed Classifier to define high-resolution layering, and sediments classification;

- SACLANT ASW Research Centre (SACLANTCEN), La Spezia, Italy; programme coordination, measurement of seismic wave velocities and attenuation using ocean-bottom seismometers, sampling and geoacoustic analysis of sediments and site surveying (using side-scan sonar and seismic profilers); SACLANTCEN theoretical propagation models were used with seismic data to determine the sea-bed properties.

MEASUREMENT TECHNIQUES

The techniques developed by the different institutions were applied to four different sedimentary areas in the vicinity of La Spezia, Italy (Fig. 1)

Shear-wave velocity measurements

A directional energy source was developed to excite both interface and ducted Love waves. Figure 2 illustrates the techniques used by SACLANTCEN. Five ocean bottom seismometers (OBS), each with tri-axial geophones and a hydrophone, were deployed along the measurement range in each area. For the short ranges applied (<25 m), a high energy source level was not needed. The signals were generated by shooting a spear from a hydraulic gun mounted on a frame into a mass resting on the sea-bed (Fig. 3). This type of source generates a signal below the elastic limits of the sediments, thus avoiding changes in sediment properties. The direction of the gun-mount could be changed as appropriate to generate different wave types. The experiment was conducted by diving scientists [6].

Figure 4 shows examples of the signals received at a distance of 25 m from the source. For example, in Fig. 4a, the geophone received maximum energy from a transverse (shear) pulse traveling in the x-direction. The alignment of the corresponding particle-motion diagram (hodograph) also

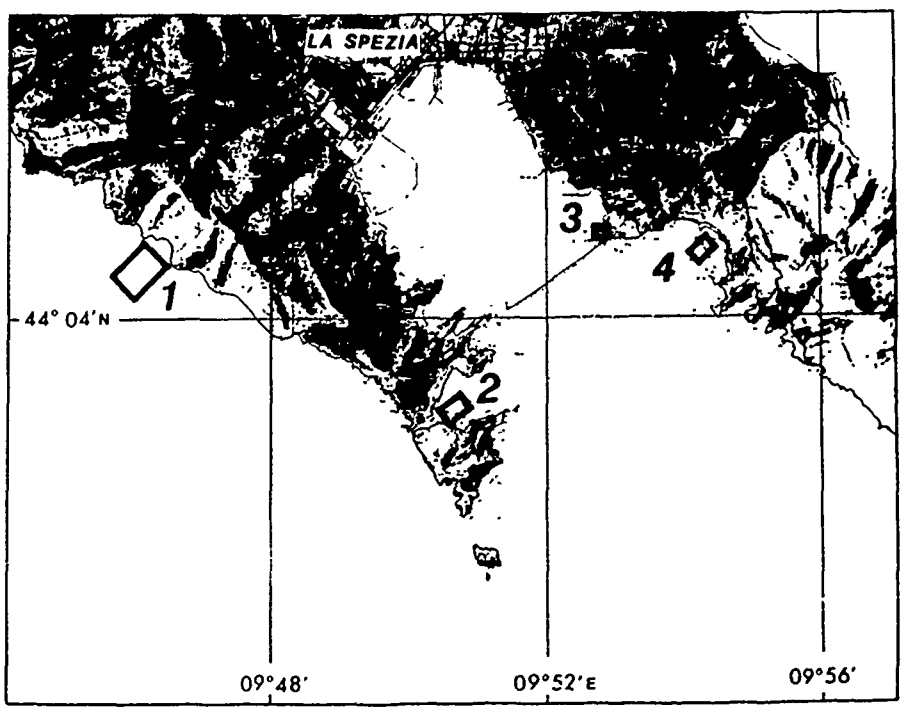

Fig. 1 Experiment areas, La Spezia, Italy.

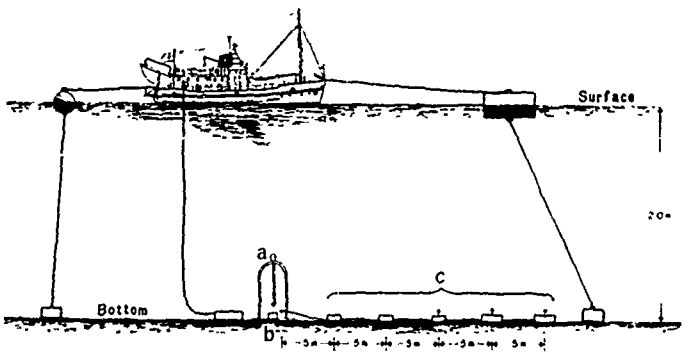

Fig. 2 Techniques used to measure Love wave velocity

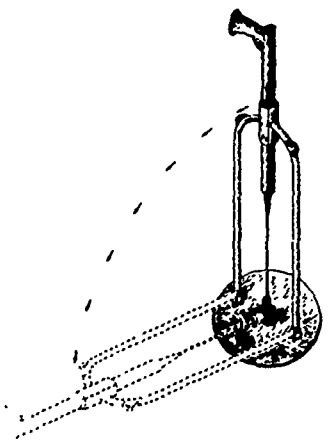

Fig. 3
SACLANTCEN technique to generate seismic signals; a gun shoots a spear against a mass coupled to the sea-bed with a heavy metal plate.

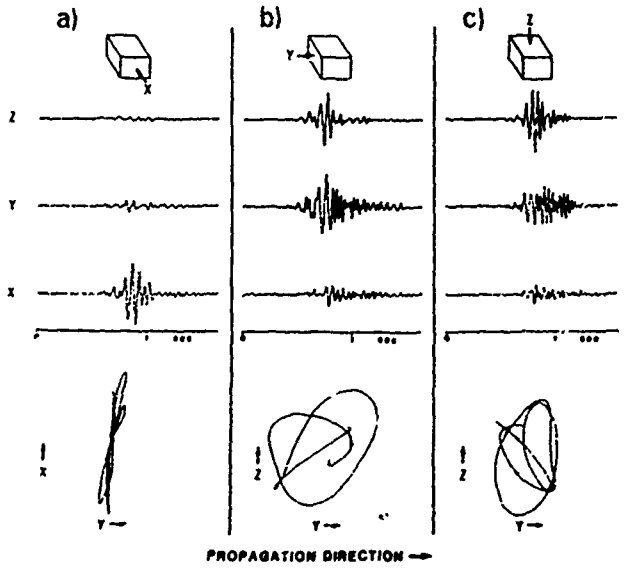

Fig. 4 Acoustic signals received at a distance of 25 m from the source, and corresponding particle motion diagrams (hodographs).

confirms that the signal is confined to the horizontal plane (x-axis). This dispersed form of the transverse signal indicates that this is no a pure body wave but a Love wave propagating within the upper sedimentary layer. This assumption was confirmed by synthetic seismograms produced by the numerical model SAFARI [7]. The radial (Fig. 4b) and vertical (Fig. 4c) signals were much more complex; the particle motions were confined to either the radial or vertical plane with very small transverse deflections, a characteristic behaviour of interface waves [4].

Bottom reflectivity measurements

Figure 5 illustrates the system used by NORDA and CENFA to measure the acoustic reflection characteristics of the bottom. NORDA's ELAC Sea-Bed Classifier (30 kHz) was used both to obtain high resolution sub-bottom layering information and high-resolution bottom reflection loss measurements. SACLANTCEN also used an EG&G UNIBOOM seismic source for bottom reflection measurements.

Sediment sampling

Figure 6 shows the techniques used to sample sea bed sediments. Samples were collected by the diver-scientists who used a grab sampler, a box corer, a gravity corer, and IGM's newly developed compressional air-powered corer.

Side-scan sonar

The site surveys, using side-scan sonar (EG&G MARK1B) provided knowledge of both the surface sediment distribution and the sea bed topography.

Continuous seismic profiling

An EG&G UNIBOOM source/receiver and a streamer were towed behind the survey ship. Resolution was poor in water depths less than 10 m.

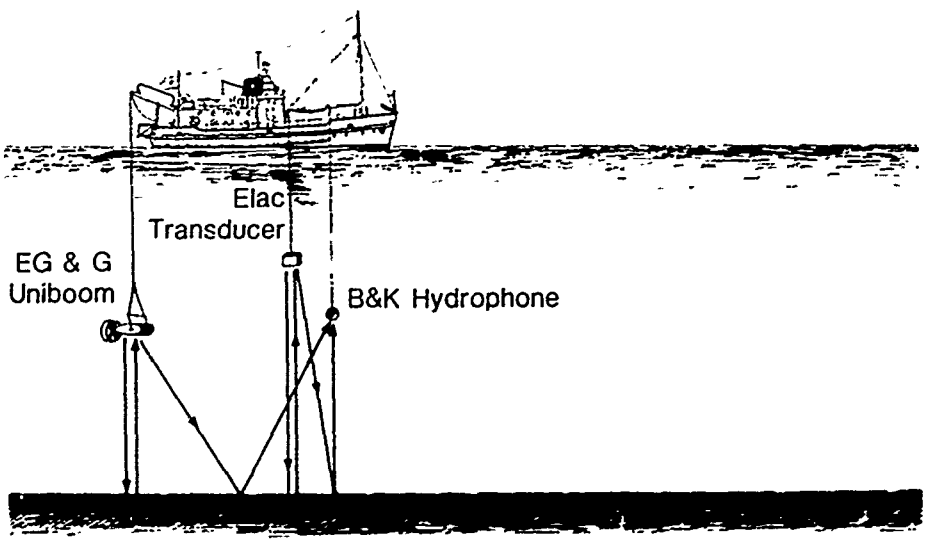

Fig. 5 NORDA and CENFA systems to measure the acoustic reflection characteristics of the bottom.

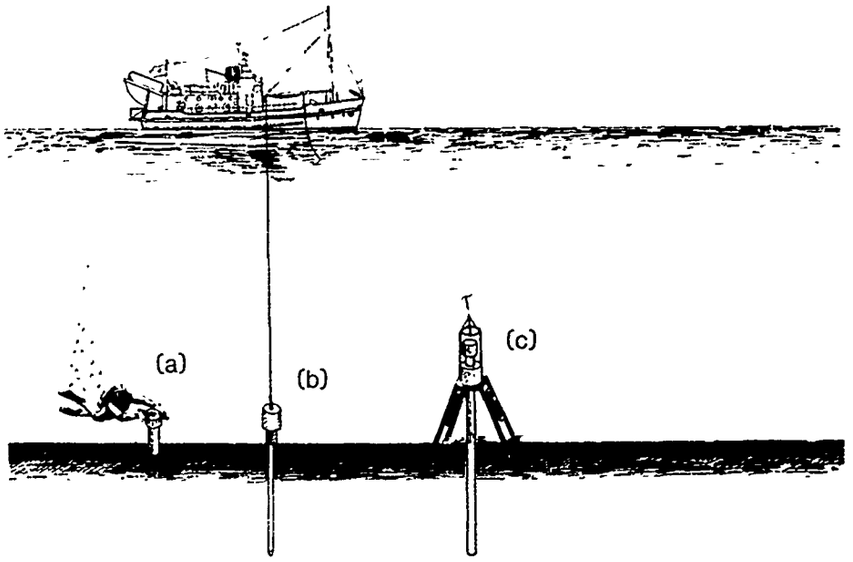

Fig. 6 Techniques used to sample sea-bed sediments
a) hand corer
b) gravity corer
c) IGM's compressional air-powered corer

Laboratory analysis

The cores were analyzed every 2 cm along their length for the following properties and characteristics:

- compressional wave velocity
- shear wave velocity
- porosity
- water content
- wet density
- dry density
- torvane and shear strength
- Attenberg limits
- grain size
- mineralogic composition

EXPERIMENTAL RESULTS

Data from two areas, 1 and 2, with different bottom conditions are presented here (see Fig. 1).

Area A is situated along the Cinque Terre coast of the Ligurian Sea; Area B is situated at the eastern entrance to the Portovenere channel of the Gulf of La Spezia.

Area 1

This study area had a water depth of 15 m. The sea-bed consisted of coarse sand and fine gravel. Side-scan sonar and observations by diving scientists indicated that the area was covered with ripples (approximately λ = 2 m) created by wave action. To avoid distorting the propagation path the axis of the measurement range was laid out parallel to the axes of the ripples. Seismic profiles (Fig. 7) show a sub-bottom reflector approximately 2 ms from the bottom. The bottom sediments apparently were derived from land slides and the reworking of sediments along the steep coastline.

Figure 8 summarizes the measured parameters along a core sample taken in this area. The high percentage of gravel in the sea bed limits the core penetration to less than 20 cm. This gravel consists mainly of limestone, slate, and sandstone, apparently derived from the adjacent mountains which have a similar lithology.

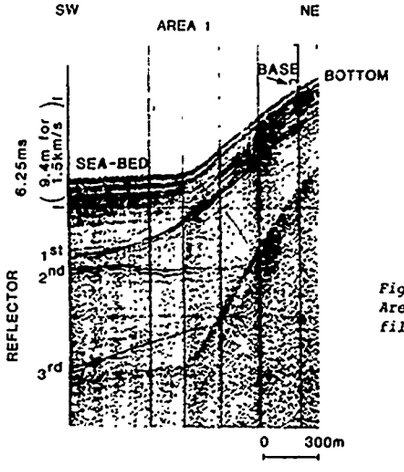

Fig. 7
Area 1. Continuous seismic profiling record and interpretation.

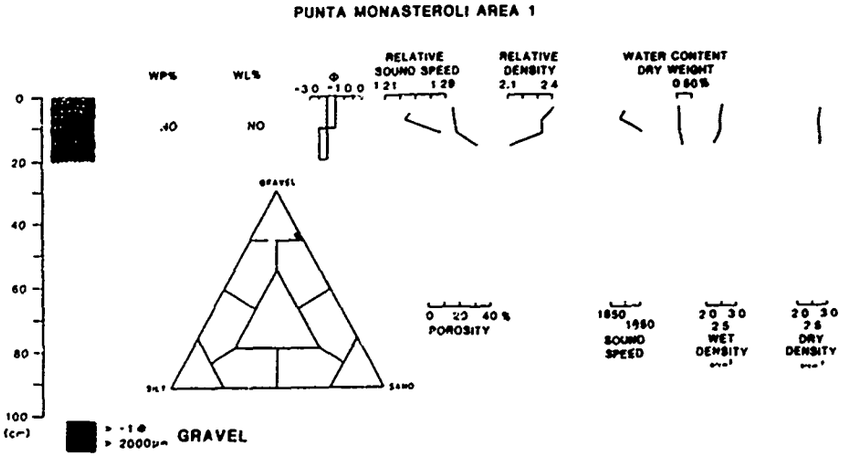

Fig. 8 Area 1. Measured parameters along a core sample.

Figure 9 is a time vs distance plot of the output of the transverse (shear) wave sensitive geophone. Distinct wavelets can be observed traveling with speeds up to 90 m/s. The inversion was performed by means of the SAFARI model [7], using trial and error. The very simple shear velocity profile shown in Fig. 10a yielded the synthetic seismograms shown in Fig. 10b, which agree well with Fig. 9.

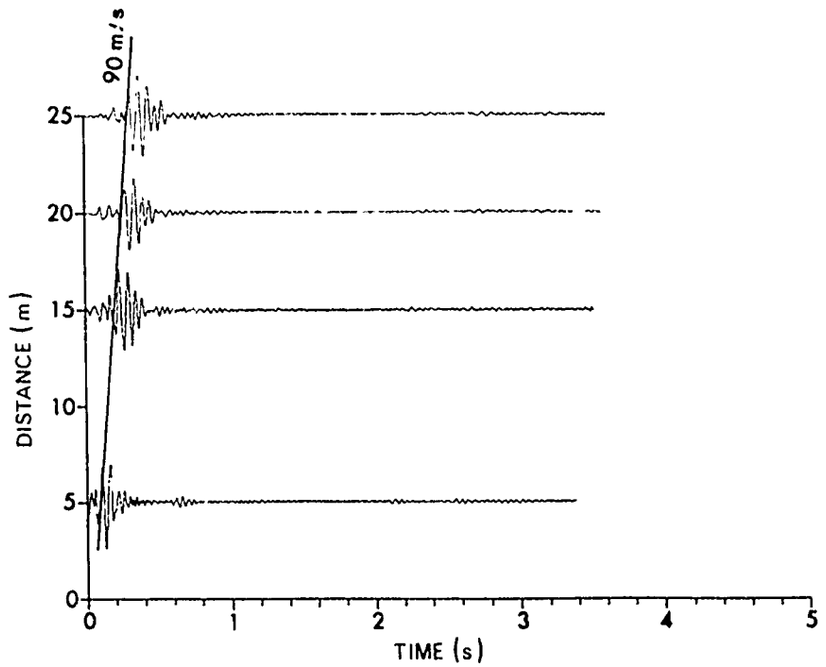

Fig. 9 Area 1. Time vs distance plot of the shear wave sensitive geophone.

Area 2

Side-scan sonar records of the eastern entrance fo the Portovenere Channel indicate a flat bottom. Sub-bottom profiles taken along the measuremen: base indicate four distinct reflectors (Fig. 11).

Figure 12 illustrates the physical parameters measured along one of the cores taken in Area 2. The material consists of silty clays and clayey silts with very small variations. The mineralogy of these sediments consists mostly of quartz and calcite with some magnesium. Of the clay minerals, 60% is illite, 10% chlorite and 30% smectite and kaolinite. The percentage of illite increases towards the bottom of the core sample with the depth in the core (and hence the sea bottom). Attenberg limits measured were 51 to 55% for the liquid limit (W_L) and about 25% for the plastic limit (Wp). The liquid limit tends to increase with depth, verifying that the sediments become finer towards the bottom of the core. Figure 13 shows the shear waves detected by transverse wave sensitive geophones. A distinct wavelet, traveling at 30 m/s, indicates Love wave speeds in the upper sedimentary layers about 1/3 of that in Area 1.

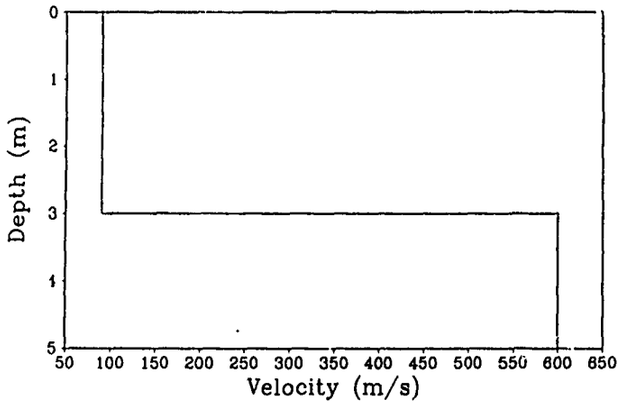

Fig. 10a Shear velocity profile.

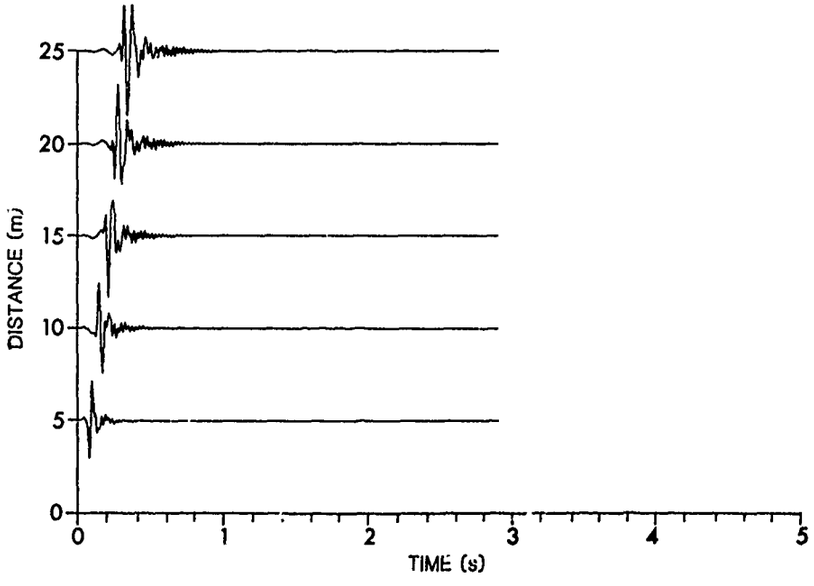

Fig. 10b Synthetic seismograms.

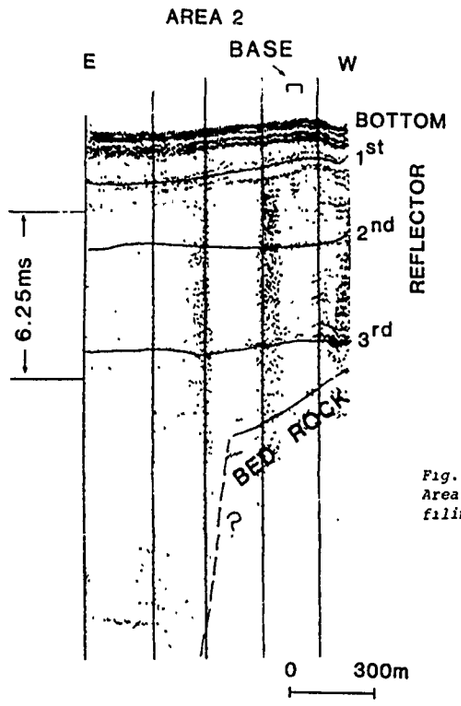

Fig. 11
Area 2. Continuous seismic profiling record and interpretation.

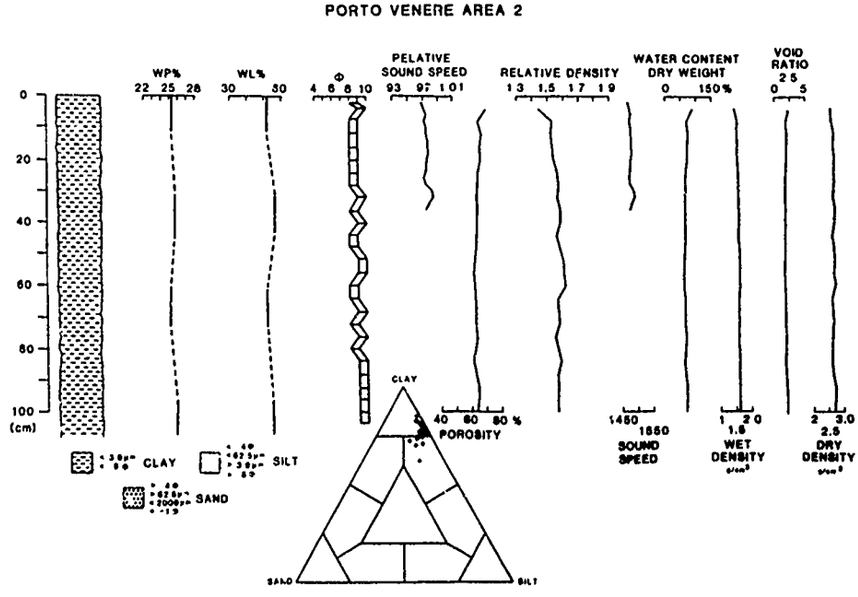

Fig. 12 Area 2. Measured parameters along a core sample taken off Porto Venere.

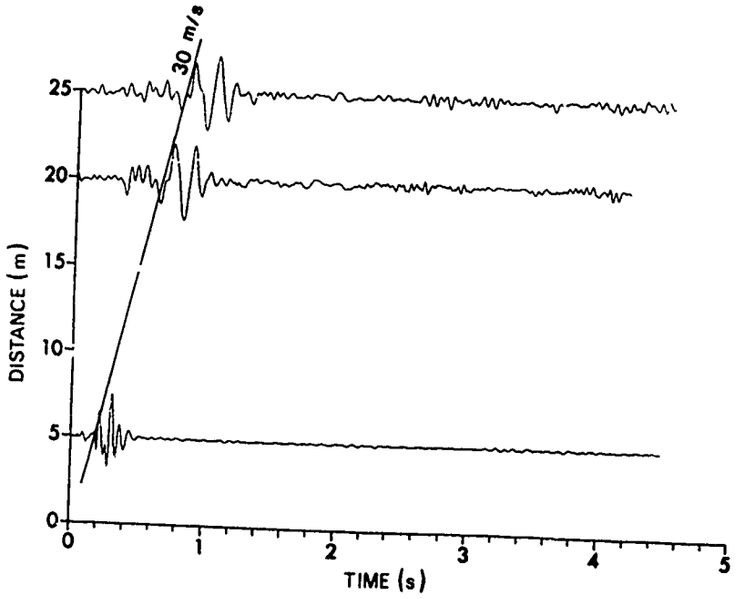

Fig. 13 Area 2. Time vs distance plots of the shear wave sensitive geophones, and shear-wave speed.

CONCLUSIONS

These simple experiments have demonstrated that Love waves can be generated in the low velocity duct formed by the uppermost unconsolidated sediment layers. The Love waves are horizontally polarized shear waves; in horizontally stratified environments they do not convert into other wave types. This property greatly simplifies theoretical modelling of their behaviour. Love waves may therefore form an alternative basis for determination of the sediment shear properties which in recent years has been based on the properties of the more complex seismic interface waves. The experiment demonstrated that two wave types (Scholte and Love) can in fact be generated and detected in a single experimental setup. The combination therefore is a realistic possibility which, if applied, can improve the prediction accuracy of deduced shear speed profiles. Further, the combination can elucidate the degree of anisotropy in the upper sedimentary layers.

REFERENCES

1. Akal, T. and Jensen, F.B. Effects of the sea-bed on acoustic propagation. In: PACE, N.R., ed. Acoustics and the Sea-Bed, Bath, U.K., Bath University Press, 1983: 225-232.
2. Akal, T. Acoustical characteristics of the sea floor: experimental techniques and some examples from the Mediterranean sea. In: HAMPTON, L., ed. Physics of Sound in Marine Sediments. New York, NY, Plenum, 1973: pp 447-480.
3. Hamilton, E.L. Geoacoustic models of the sea floor. In: HAMPTON, L., ed. Physics of Sound in Marine Sediment. New York, NY, Plenum, 1973: pp 181-222.
4. Rauch, D. On the role of bottom interface waves in ocean seismo-acoustics (this volume).
5. Jensen, F.B. and Schmidt, H. Shear properties of ocean sediments determined from numerical modelling of Scholte wave data (this volume).
6. de Strobel, F., Akal, T., and Hastrup, O.F. SACLANTCEN's use of SCUBA diving in oceanographic and acoustic research. SACLANTCEN SM-175. La Spezia, Italy, SACLANT ASW Research Centre, 1984.
7. Schmidt, H. Modelling of pulse propagation in layered media using a new fast field program. In: FELSEN, L.B. ed. Hybrid Formulation of Wave Propagation and Scattering. Dordrecht, Nijhoff, 1984: pp 337-356.

MEDIUM-INDUCED LOW-FREQUENCY FLUCTUATIONS IN ACOUSTIC TRANSMISSION LOSS: EXAMPLES FROM MEASUREMENTS IN SELECTED GEOGRAPHICAL AREAS

Hassan B. Ali, Melchiorre C. Ferla, and Sergio Fiori

SACLANT ASW Research Centre
Viale San Bartolomeo 400
19026 La Spezia, Italy

ABSTRACT

The ocean is a complex, highly variable acoustic medium. A propagating acoustic signal is affected by a host of phenomena, including the sea-surface and bottom, volume inhomogeneities, internal waves and tides, and non-stationary water masses. These effects cause fluctuations in the amplitude and phase of an acoustic signal and an accompanying loss in its coherence properties. The responsible mechanisms, and hence the acoustic effects, cover a wide range of temporal and spatial scales and, in general, can be understood only in terms of deterministic and random forces acting in concert. Although the listing of these mechanisms is generally easier than their isolation in realistic situations, it has been possible to correlate fluctuations in acoustic transmission loss with environmental variability, especially for very low acoustic frequencies. In particular, measurements conducted by SACLANTCEN in diverse geographical areas have identified semi-diurnal effects (tidal as well as heating), internal waves, inertial oscillations, and moving water masses as significant contributors to low-frequency acoustic fluctuations.

INTRODUCTION

The basic problem in using acoustics in the ocean is the complexity of the medium. The parameters controlling the propagation vary, usually unpredictably, both spatially, and, more significantly, temporally. Consequently, an acoustic signal propagating in such a medium is affected not only by interactions with the bottom and surface boundaries, but also by volume inhomogeneities caused by non-uniformities in temperature, density, and salinity distributions. The degradation of the acoustical signal is manifested by fluctuations in its amplitude and phase and by an accompanying loss in its coherence properties.

Generally, this degradation results in a decrease in performance of underwater acoustic systems, including sonar. In particular, the estimations of range and angular bearing of a sonar system can be adversely affected by temporal and spatial coherence losses. For this, and other reasons, an understanding of the causes of signal degradation is essential.

This paper will consider environmentally-induced signal fluctuations as they affect transmission loss.

Although the mechanisms leading to fluctuations in acoustic propagation are diverse, an essential common feature is an associated non-uniformity in the medium, either temporal or spatial or both. Depending on the temporal and spatial scales involved, the mechanisms can be considered either deterministic or random [1]. The general circulation of the ocean ("ocean climate") and its associated current systems (Gulf Stream, Kuroshio, etc.) are characterized by horizontal scales of variability limited only by the size of the basin, vertical scales of a few 100 m, and temporal scales from a few days to seasonal. These are deterministic structures. The intermediate scales of variability, including ocean motions such as fronts and eddies, can also be considered to be deterministic perturbations from the mean structure. The associated scales of variabilities are of the order of 100 to 1000 km in the horizontal, to ocean depth in the vertical, and days to months in time.

Internal waves, fine-structure, and microstructure comprise the smaller scales and are considered random features. The internal waves are characterized by scales from 100 m to 10 km or more in the horizontal, 1 to 100 m in the vertical, and from about 10 min to 1 day in time. Because they owe their existence to the restoring forces due to the density gradient and the Coriolis force, the frequency spectra of internal waves are bounded by the inertial frequency at the low end and by the buoyancy frequency (Brunt-Väisälä) at the high end. Variability induced by internal waves has been found to be a very significant source of sound scattering and has received considerable attention in recent years [2,3,4]. In essence, this increased activity arises from two complementary facts: on the one hand the spatial scales of internal waves match the acoustic wavelength over a broad frequency range, and thereby affect the acoustic field; on the other hand the internal wave is one of the few ocean features for which a reasonably effective statistical model (Garrett-Munk) is available. Fine- and microstructure variability involve horizontal scales from several metres to hundreds of metres, vertical scales from centimetres to about 10 m, and temporal scales of the order of milliseconds. Such variability generally affects sound propagation in the frequency range from approximately one to tens of kilohertz.

Table 1 [1] summarizes the temporal scales of environmentally-induced fluctuations often observed in acoustic propagation experiments. Of particular relevance to low frequency acoustic propagation is the information contained within the dotted area of Table 1. The remainder of the paper is devoted to a discussion of three SACLANTCEN measurements, the results of which show a clear correlation between transmission loss fluctuations and the environmental phenomena highlighted here.

In particular, long-period internal waves (inertial oscillations) and semi-diurnal, tide-related effects figure prominently in the measurements conducted in two areas of the North Atlantic Ocean and one in the Mediterranean. Moreover, although tidal forces are important at both sites, differences among the local oceanographic conditions lead to interesting contrasts between the nature and the degree to which these tidal forces affect the acoustic propagation. In particular, at the Mediterranean test site volume effects in the water column seemed to be of greater significance than in the North Atlantic test site, where acoustic interaction with the bottom was the predominant source of the fluctuations. Therefore, discussions of the results will be grouped under physical mechanisms, viz., under "volume effects" and "bottom effects", rather than under the less relevant geographical indicators.

Table 1 Temporal variation observed in acoustic data

PERIOD	PRINCIPAL ENVIRONMENTAL PARAMETERS	PRINCIPAL ACOUSTIC EFFECTS
ms	FINE AND MICROSTRUCTURE	AMPLITUDE, PHASE AND PROPAGATION PATH FLUCTUATIONS; HIGH FREQUENCY SCATTERING
5 s	SURFACE WAVE SIGNATURES	AMPLITUDE MODULATION, SCATTERING
10 min–24 h	INTERNAL WAVE SIGNATURE	AMPLITUDE AND PHASE FLUCTUATION; SIGNIFICANT REFRACTION OF NEARLY HORIZONTAL PATHS
4 h	SHALLOW WATER TIDES	PHASE AND AMPLITUDE FLUCTUATIONS OFTEN SIMPLY CORRELATED WITH TIDAL VARIATIONS.
12 h	SEMIDIURNAL TIDES	
24 h	DIURNAL TIDES	GREATEST EFFECTS IN SHALLOW WATER
4 day 15 day 1 month	MESOSCALE PHENOMENA (EDDIES, FRONTS)	FLUCTUATIONS IN PROPAGATION PATH, ACOUSTIC INTENSITY; DISTORTION OF SIGNAL SHAPE; SLOW MODULATION OF ACOUSTIC RAYS
1 year	OCEAN CLIMATE	FLUCTUATION IN AMPLITUDE, PHASE AND PROPAGATION PATH

1 MEASUREMENTS SHOWING VOLUME EFFECTS

1.1 Propagation Characteristics of the Test Environment

The acoustic propagation experiment was conducted in a shallow water region of the Mediterranean where the water depth varied from about 40 m to 85 m, as seen in Fig. 1. Although the bathymetry of the area is fairly complex, that along the propagation run is relatively simple. The water circulation in the region consists of a three-layer system: an eastward-flowing surface layer of Atlantic water, an intermediate layer in which turbulent mixing occurs, and a westward-flowing bottom layer of more saline (Levantine) water. A temperature/salinity profile of the measured data confirms this general behaviour.

For the experimental situation depicted in Fig. 1, broad-band (explosive) sources were dropped at approximately hourly intervals. A vertical array of hydrophones, 35 km distant, received the signals. Simultaneously, samplings were taken of the pertinent oceanographic parameters: sound speed, temperature, salinity and density (STD/ casts). The test was conducted during summer conditions. Figure 2 presents typical depth profiles of the environmental parameters in this area. This type of profile tends to favour downward acoustic refraction and, therefore, results in greater bottom interaction than would occur in winter. Vertical stratification and some fine-structure are evident in the profiles. A closer analysis of the sound speed profile over shorter intervals in depth and sound speed reveals more clearly the presence of fine-structure, characterized by vertical dimensions of the order of centimetres to one or two metres. As already noted, such fine-structure will tend to scatter sound of frequency ranges higher than of interest herein.

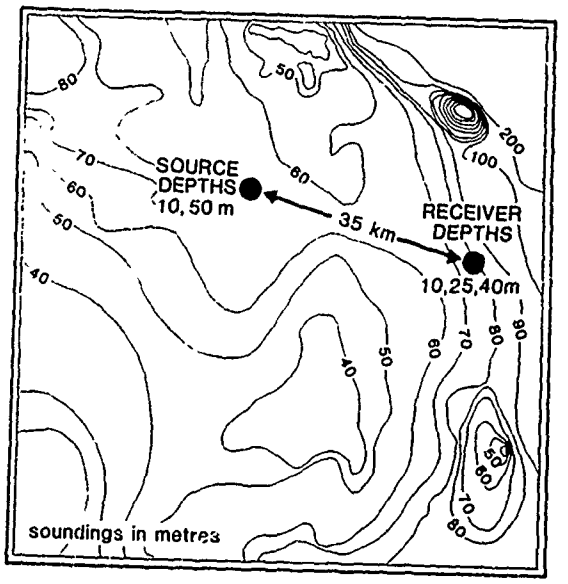

Fig. 1
Bathymetry of the experiment (Mediterranean site).

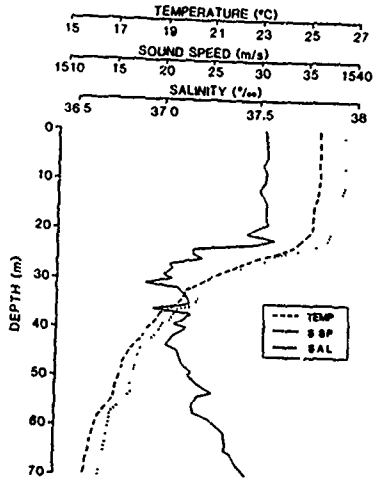

Fig. 2
Depth profiles of temperature, sound speed, and salinity (Mediterranean site).

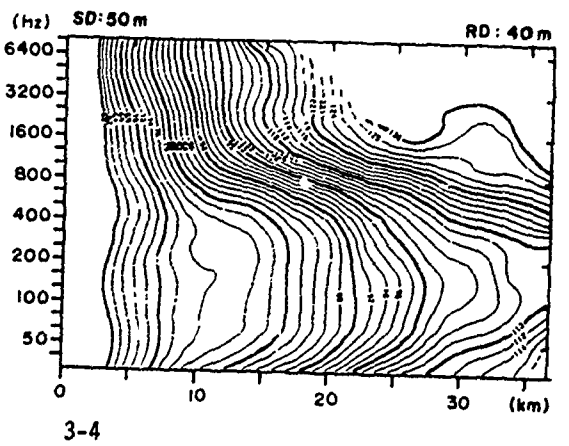

Fig. 3
Contours of measured transmission loss in 1/3 octave bands.

The effect on acoustic propagation is shown in Fig. 3 <5>, which presents contours of measured transmission loss, in 1/3 octave bands, in the frequency/range plane. The existence of an optimum frequency range (i.e. minimal transmission loss) for acoustic propagation is clearly evident. In this case, it lies between approximately 100 and 400 Hz. The explanation for this is that acoustic energy at very low frequencies suffers large attenuation as a result of bottom penetration which increases directly with wavelength. On the other hand the energy at the very high frequencies is greatly attenuated by absorption in the water column and, possibly, by scattering from fine-structure. Hence an optimum frequency range exists somewhere between the two extremes. In other words, for the conditions typefied by Fig. 3, the ocean behaves like a band-pass filter for propagating broadband acoustic signals.

1.2 Temporal Variability in the Environmental Data

Of primary interest for our purpose is the temporal variation of the relevant parameters at a fixed range, here 35 km. Figure 4 shows an example of the variation of sound speed with depth during a period of 25 hours.

The depth range from approximately 25 to 35 m comprises the steepest portion of the thermocline. The region down to 20 m or so is essentially isovelocity with a sound speed of approximately 1538 m/s. The fluctuations in sound speed are quite evident, particularly at a depth of 25 m or so within the thermocline. The plots clearly indicate an oscillation in the width of the mixed layer (surface duct). Figure 4b, in particular, indicates that typical features, e.g., "kinks" in the curve, appear to be migrating vertically with time - a behaviour often suggesting the presence of internal waves [Gregg, 6]. The frequency content of these oscillations is of particular interest because it provides clues to the responsible mechanisms. Examples of frequency spectra of the relevant environmental parameters, obtained from Fast Fourier Transforms of the corresponding normalized time series at 25 m depth, are shown in Fig. 5.

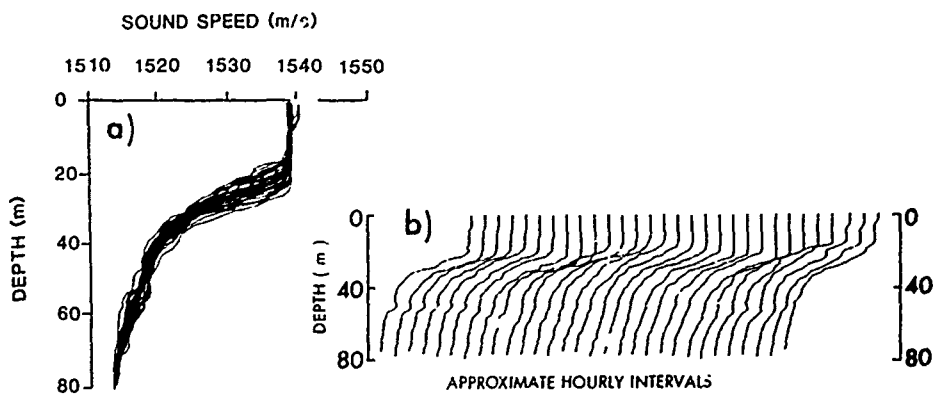

Fig. 4 Temporal variation of sound speed over approximately 25 hours.

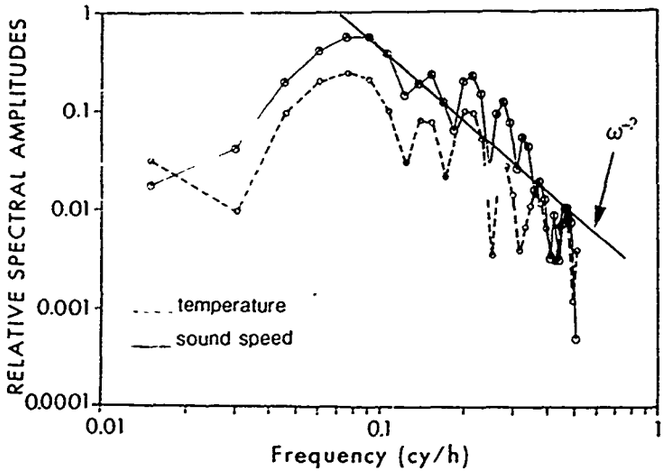

Fig. 5 Spectra of sound speed and temperature at 25 m.

The dominant fluctuations occur in the frequency range from 0.08 to 0.06 cycle/h, or for periods from 12 to 17 hours. This is a broad response and includes both the semi-diurnal period and inertial period (approximately 17 hours here). The time series was too short to allow for the spectral separation of the two responses. From the results obtained at other depths it does appear, however, that the relative significance of the semi-diurnal tidal and inertial effects depends on depth. In particular, from the analysis of the depth-dependent frequency spectra it appears that there are fluctuations of inertial period in the surface layers, and that as the depth increases the dominant fluctuations are semi-diurnal.

Inertial oscillations may occur in connection with a sudden change of the wind (i.e. a wind impulse of short duration) and changes in barometric pressure [7]. The whole of the Mediterranean is dominated by meteorological forcing; therefore it is likely that inertial oscillations are present in the study area. That they dominate the surface waters is probably related to their meteorological origin. The local water stratification retains most of this energy in the surface layers, so that at depth the semi-diurnal components are discernible.

In the spectra of Fig. 5 there also appear to be higher-frequency phenomena, with periodicities of about 2,4,5, and 7 h. These may be associated with internal wave activity. Note that the drop-off rate (sloping line) of the sound speed spectrum is approximately ω^{-2}, a slope consistent with that predicted by the Garrett-Munk model of internal waves.

1.3 Fluctuations in Acoustic Transmission Loss

Figure 6 shows the contours of measured transmission loss (1/3 octave bands) in the frequency/time plane for source and receiver depths of 50 m and 40 m, respectively. The higher frequencies (>1.6 kHz) exhibit far more pronounced fluctuations than the lower frequencies. This may indicate that the responsible environmental phenomena have physical dimensions that are comparable to the acoustic wavelengths of the higher frequencies. In order to demonstrate this selective frequency effect more clearly, the spectra of transmission loss at 200 Hz and 1600 Hz were compared (Fig. 7).

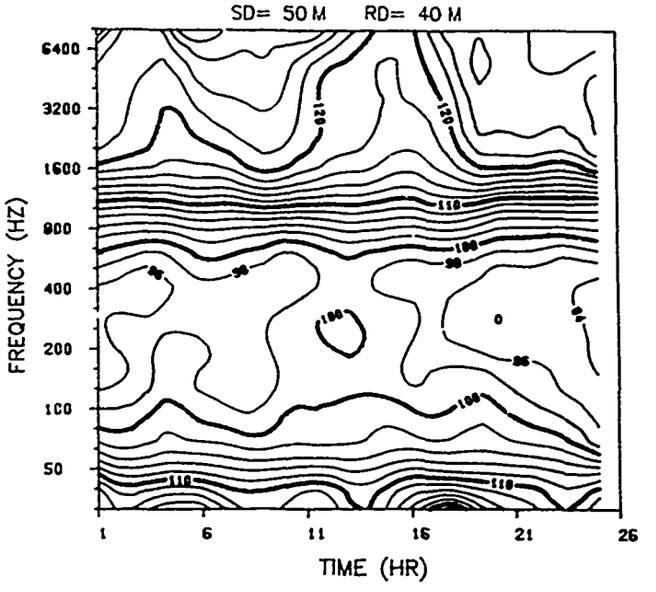

Fig. 6 Contours of measured transmission loss fluctuations at a fixed range (35 km).

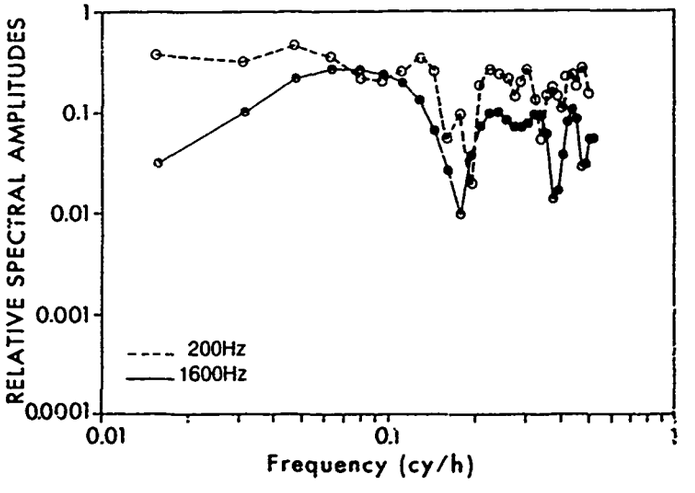

Fig. 7 Spectra of transmission loss for two selected frequencies.

The spectra, obtained for the same source/receiver as those in Fig. 6, emphasize the difference in the effect of variability. These results suggest that the optimum frequency range is less susceptible to environmental variability than other frequency ranges. A comparison of these spectra with those shown in Fig. 5 reveals a good correlation between the spectra of environmental variability and the higher frequency transmission loss spectrum.

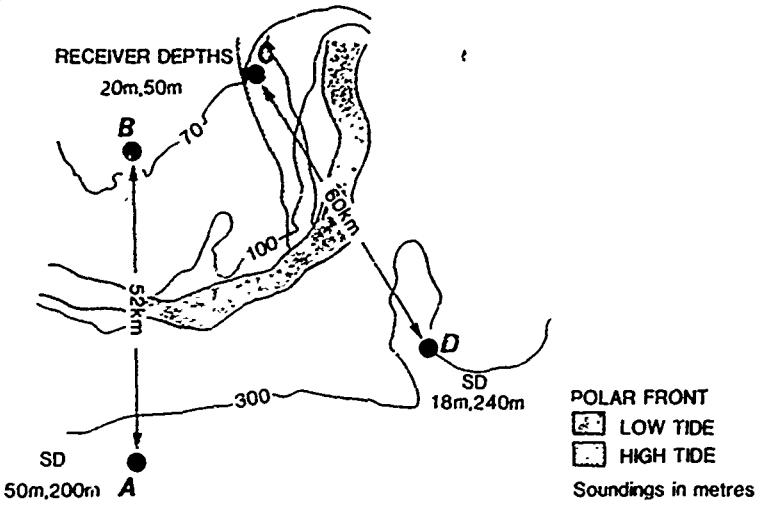

Fig. 8 Geometry of the North Atlantic measurements.

2 MEASUREMENTS SHOWING BOTTOM EFFECTS

2.1 Propagation Characteristics of the Test Environment

The North Atlantic test site is a very complex geological, oceanographic, and biological province and has been the object of many investigations [8]. The test site is located in an area affected by a large-scale permanent front resulting from the convergence of two water masses. In particular, at this location, cold, less saline Arctic water meets warmer Atlantic water to form the Polar oceanic front. The substantial differences in salinity and temperature of the two water-types (35‰ and 6° to 7°C for the Atlantic vs 34.6‰ and about 0°C for the Arctic) cause the Polar front to be characterized by steep gradients in these parameters, with significant implications for sound propagation. An added complication arises from the changing position of the front, which oscillates with semi-diurnal tidal periodicity.

The geometry and relevant details of the measurements are provided in Fig. 8. The two tracks, A-B and D-C, represent the propagation paths for measurements conducted one year apart. The environmental conditions along the two paths were somewhat different. Although both tracks A-B and D-C cross the Polar front, in water changing from deep to shallow, track A-B is over a generally hard bottom (sand) while track D-C is over a generally soft bottom (sand, silt, clay). From the point of view of temporal variability, however, a more fundamental difference between the two receiver locations arises from their relative proximity to the Polar front. In particular, station C is directly affected by movements of the front, the water above 20 m changing from Polar to Atlantic with an approximately 12-h periodicity, while the waters below 20 m remain of the Polar type. In comparison, station B remains in virtually isothermal Polar water, north of the front, as shown schematically in Fig. 8.

In effect, the Polar front serves as a demarcation line between two different propagation areas. To the north of the front, in isothermal water, an important part of the propagation will be in shallow water under upward-refracting conditions, resulting in small total transmission losses as a result of less bottom-interaction. On the other hand, in waters affected by the front, propagation will be under strong downward refracting conditions, as a result of the steep gradients, and thereby subject to higher losses, particularly at low frequencies. As noted, measurement site B was always in isothermal waters, whereas C was periodically subject to the effects of the front. From this one would expect the transmission losses measured at site B to be both lower in magnitude and subject to less temporal fluctuation than those at site C. Though generally valid, this conclusion is nevertheless based on an oversimplification of the propagation conditions. In particular, the propagation depends not only on the front, but also on frequency, source and receiver depths, bottom conditions (which are different for the two tracks), and, possibly, other features such as currents and inertial oscillations.

2.2 Selected Examples of Temporal Variability

In the following, typical results of measurements made over a 48-h period will be presented, emphasizing the data obtained at position C. The experimental procedure was essentially the same as that for the Mediterranean measurements, described previously.

Figure 9 provides a typical example of the fluctuations in measured transmission loss at site C for several frequencies, along with the predicted tidal curve for the area. It is clear that the fluctuations in transmission loss correlate well with tidal periodicity, particularly for the lower frequencies. This is consistent with the assumption that the lower frequencies are more affected by the tidally-induced change in downward-refracting conditions. Both diurnal and semi-diurnal periodicities are evident, the former seemingly the more significant. Further,

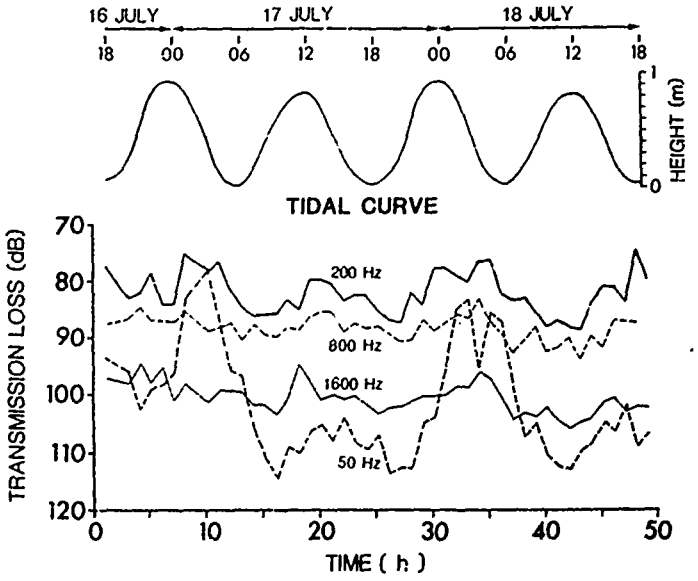

Fig. 9 Temporal variation of transmission losses and predicted tidal curve at site C.

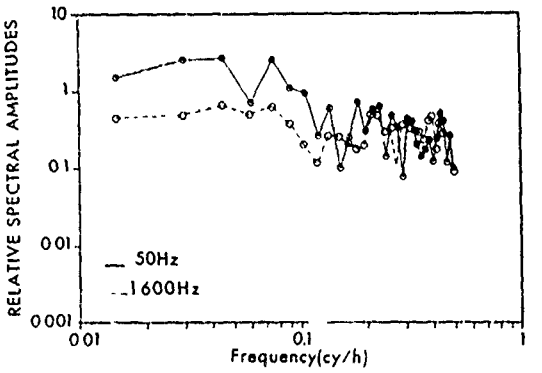

Fig. 10
Spectral composition of transmission loss at site C for two selected frequencies (SD 240 m / RD 50 m).

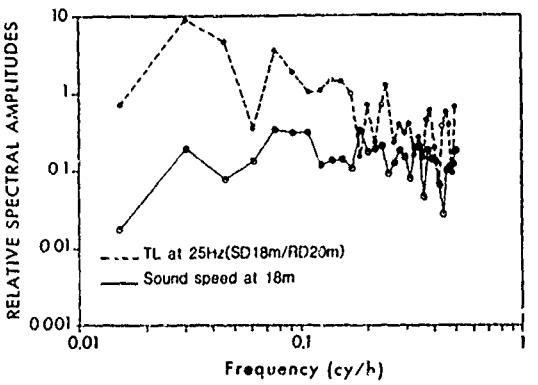

Fig. 11
Comparison of spectra of transmissi loss at 25 Hz and sound speed.

there is a correspondence, albeit inexact, between high tide and high transmission loss, consistent with the fact that the front reaches site C during periods of high tide. Although the curves shown are for a particular source/receiver combination (240 m / 50 m) the observed trends are fairly representative of all the data obtained at this site. The spectral composition of the 50 Hz and 1600 Hz signals is shown in Fig. 10, again demonstrating the more marked fluctuations at the lower frequency, as well as the conspicuous presence of diurnal and semi-diurnal periodicities.

Figure 11 provides a comparison between the 25 Hz transmission loss spectrum at a depth of 20 m (source depth = 18 m) and the sound speed spectrum at a depth of 18 m. As seen the correlation between the two spectra is quite good.

It is instructive to compare the variability for the two positions B and C. An example of the fluctuations in temperature is shown in Fig. 12. Several features are immediately evident from the figure. First, it is clear that the amplitudes at C are greater than those at B and, in addition, show a definite dependence on depth. Further, although both data sets reveal tidal effects, they are more conspicuous at position C, particularly at 18 m depth. This behaviour no doubt reflects the position of the stations with respect to the Polar front, station C being directly affected by the movements of the front, while station B is constantly in isothermal waters, as discussed earlier. The significant differences in results between the two locations suggest that tidally advected changes in water masses, as at C, are more important than the indirect tidal effects (changes in water depth, currents, etc.) that are evident at B. The greater energy measured at 18 m (for site C) seems to confirm this conclusion since the transition zone between the Atlantic and Polar waters occurs at this depth.

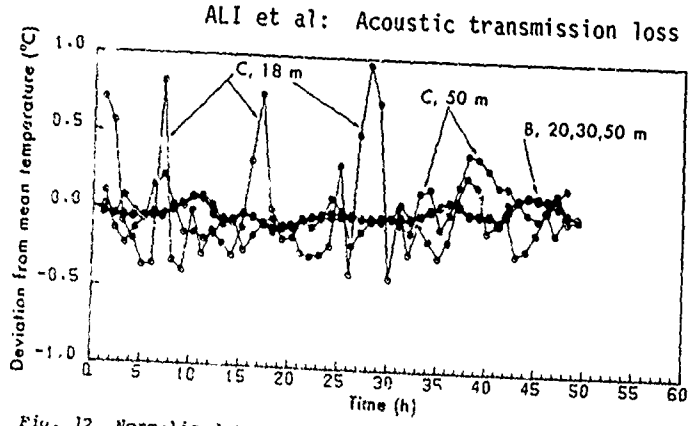

Fig. 12 Normalized temperature fluctuations at the two sites.

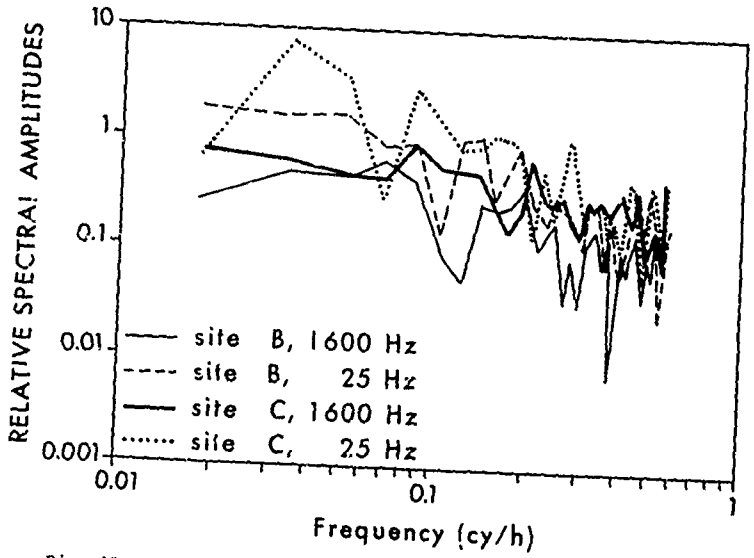

Fig. 13 Transmission loss spectra at receiver sites B and C (North Atlantic).

Finally, the comparison of the transmission loss spectra at the two sites is shown in Fig. 13. Note the fluctuations in low frequency transmission loss are greater at site C than at B; but there is little difference between the sites vis-a-vis the higher frequency transmission loss. This is consistent with the stronger downward refracting conditions at site C.

CONCLUSIONS

The measurements conducted in the Mediterranean and the North Atlantic indicate that fluctuations in acoustic transmission loss correlate well with the diurnal, semi-diurnal, and inertial periodic variability of the environmental parameters. However, the nature and extent of the causal phenomena differ for the two areas. At the Mediterranean test site volume effects appear to be the principal cause of the fluctuations, while at the N. Atlantic test sites bottom effects predominate. Both types of effects are described below:

Volume Effects

- Inertial effects dominate in the surface layers, whereas the semi-diurnal effects are of greater importance at greater depths. This suggests a meteorological forcing function.
- The fluctuations in the magnitude of acoustic transmission loss are greatest for the higher frequencies (1.6 kHz and above) and least for an optimum frequency range from approximately 100 to 400 Hz.

Bottom Effects

- At the N. Atlantic site the inertial period coincides with the semi-diurnal period and cannot be resolved by spectral analysis.
- The transmission loss oscillations correlate with tidal movements of the Polar front and are more marked at the lower frequencies. The effects on acoustic propagation are associated more closely with the tidally-advected changes in water masses than with the more subtle, indirect tidal effects.

ACKNOWLEDGMENT

The authors gratefully acknowledge the contribution made by Mr. S. Mari of SACLANTCEN.

REFERENCES

1. H.B. Ali. Spatial and temporal variabilities in underwater acoustic transmission: an analytical review, SACLANTCEN SM-166. La Spezia, Italy, SACLANT ASW Research Centre, 1983. [AD A 129 959].
2. Y. Desaubies. Statistical aspects of sound propagation in the ocean. In: Adaptive Methods in Underwater Acoustics, H. Urban, ed. Dordrecht, Reidel, 1985.
3. S.M. Flatte, R. Dashen, W.H. Munk, K.M. Watson and F. Zachariasen, eds. Sound Transmission through a Fluctuating Ocean. Cambridge, Cambridge University Press, 1979.
4. B.J. Uscinski, C. Macaskill and T.E. Ewart. Intensity fluctuations, part I: theory, part II: comparison with the Cobb experiment. J. Acoust. Soc. Am., Vol. 74, 1474-1499, (1983).
5. T. Akal. Sea floor effects on shallow-water acoustic propagation. In: W.A. Kuperman and F.B. Jensen, eds. Bottom Interacting Ocean Acoustics, New York, NY, Plenum, 1980.
6. M.C. Gregg. Finestructure: Oceanic "kinks and wiggles." Naval Research Reviews, Vol. 34, 52-72 (1982).
7. R.T. Pollard. On the generation of inertial waves in the ocean. Deep Sea Res., Vol. 17, 795-812, (1970).
8. J. Pietrzak, and H.B. Ali. Fluctuations in environmental parameters observed during acoustic measurements in the Barents Sea and the Strait of Sicily. La Spezia, Italy, SACLANT ASW Research Centre. (SM- in preparation).

DIRECTIONAL MEASUREMENTS OF LOW-FREQUENCY ACOUSTIC BACKSCATTERING FROM THE SEAFLOOR

J.M. Berkson, T. Akal, H.J. Kloosterman*, and J.L. Berrou+

SACLANT ASW Research Centre
Viale San Bartolomeo 400
I-19026 La Spezia, Italy

*Present Address:
Laboratory of Seismics and Acoustics
Delft University of Technology
Delft, The Netherlands

+Present Address:
Thomson-CSF
ASM Division
06802 Cagnes-sur-Mer, France

ABSTRACT

Long-range, low-frequency directional measurements of acoustic backscattering from the seafloor were made in the Tyrrhenian Sea using explosive sound sources. The signals were received by a horizontal towed array of hydrophones and were processed by a beamforming procedure to obtain the directional distribution of the scattered field as a function of time. These data are used to form images of scatterers and to estimate the backscattering strength of specific physiographic features. From the data obtained the scattering strengths were estimated to range from -25 dB to -35 dB and did not exhibit strong dependence on frequency.

INTRODUCTION

Low-frequency acoustic backscattering from the seafloor has often been studied using omnidirectional measurement techniques [1-4]. Generally, omnidirectional sources and receivers are used. The calculation of scattering strength assumes uniform scattering in a ring-shaped area on the seafloor for a given element of travel time. Such measurements can be contaminated by non-bottom returns having the same travel time as the scattering ring [5] or by non-uniform roughness within the scattering ring [6]. Although careful measurements using omnidirectional geometries will yield proper estimates of scattering strength, these techniques are more limited than directional methods in application. Directional methods make it possible to obtain images of the scattering features and to estimate the scattering strength of specific physiographic features such as seamounts and continental slopes. Images of seafloor topography from long-

range directional measurements of acoustic backscattering have been obtained by various methods: broad-side beam, side-scan mode with towed array [7], full beamforming with a towed array [8,9], and full beamforming with two-dimensional arctic arrays [10]. Backscattering values have been reported for some of these measurements [9,10].

Previously the authors have reported beamforming methods applied to sensors of a towed array receiving backscattered sound [11] and aspects of resolution of seafloor images that were obtained [12]. In this paper we further describe the technique used for processing broadband data received from an explosive source and report additional measurements of bottom backscattering strength for the Tyrrhenian Sea.

EXPERIMENTAL METHODS

An omnidirectional explosive source (broadband) is deployed near a hydrophone array. The sounds reflected and scattered back to elements of the array are processed to form beams, as in Fig. 1. For processing, the hydrophone signals are split into time increments. For each time increment, a beamforming procedure is used to obtain the angular distribution of energy over a given frequency band of the source.

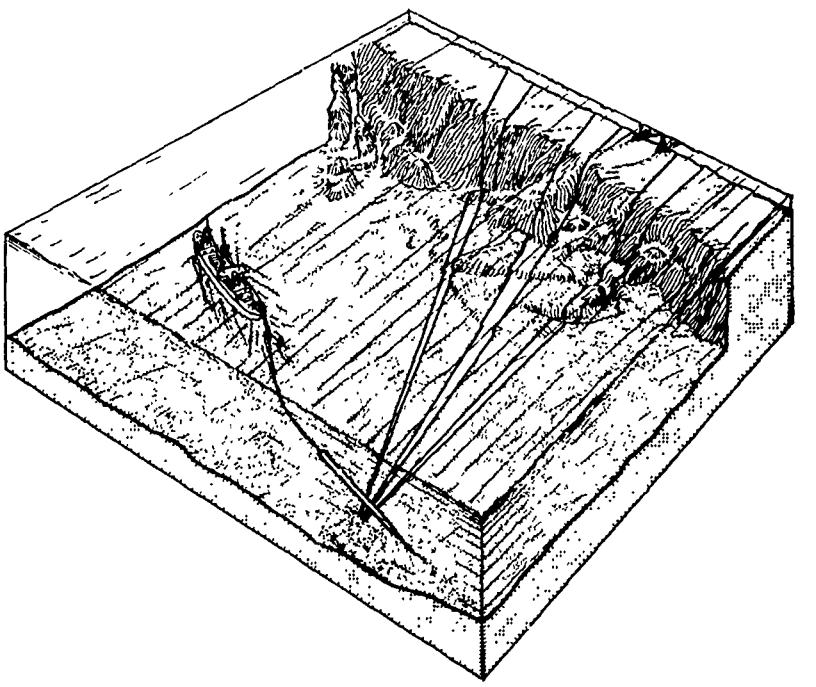

Fig. 1
Experimental geometry for backscattering measurement (not to scale): returns from an omnidirectional sound source (not shown) are received on directional receiving beams. The beams, which actually scan a vertical section of the volume, are indicated by their wedge-shaped areas on the seafloor. For simplicity only three beams on the right-hand side of the array are shown in their far field and the complementary (ambiguity) beams on the left-hand side of the array are omitted.

The beamforming procedure has been described in Refs. [11] and [12] and is based on the assumption of plane-wave sound signals of uniform velocity and is an application of frequency-domain beamforming based on the Fast Fourier Transform [13]. The procedure applied to sensors of a line array results in the estimation of beam power values equally spaced in spatial wavenumber, k_x, for the different acoustic frequencies, f, of the analysis band. With the assumption of uniform sound velocity, we can discriminate plane waves with different beam-pointing angles, α, where

$$k_x = (\omega/c) \sin \alpha. \qquad (1)$$

in which c is the speed of sound and ω is the angular acoustic frequency, $\omega = 2\pi f$. The method of processing broadband data is shown graphically in Fig. 2. For each k_x value at the central frequency of the band, a set of interpolated beam powers is determined for the other frequencies. This is

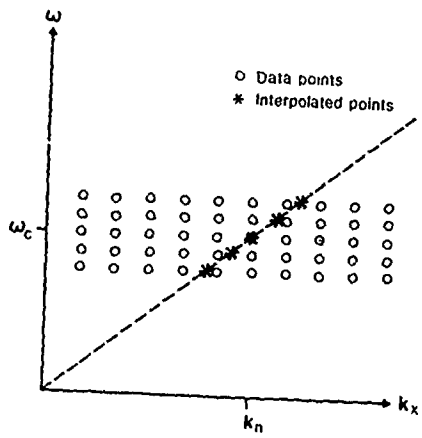

Fig. 2
Beam-power interpolation for wavenumber k_n: beam-power levels are interpolated for the points indicated by stars from the data at the points indicated by circles. The interpolated points fall along the azimuth line (dotted) of the central frequency of the band ω_c.

done by linearly interpolating between the appropriate beam-power values in such a way that the beam azimuth equals the beam azimuth that corresponds to the central frequency of the band. An average beam-power value over a given frequency band is obtained at each k_x value by averaging the interpolated powers. This procedure corresponds in k_x-ω space to averaging data points along a line.

The scattering area is defined by the intersection of the beam and the scattering ring boundaries for the particular travel time and processing-time window, as in Fig. 3. Assuming a process of totally incoherent scattering, the scattering strength S, for a given frequency band may be

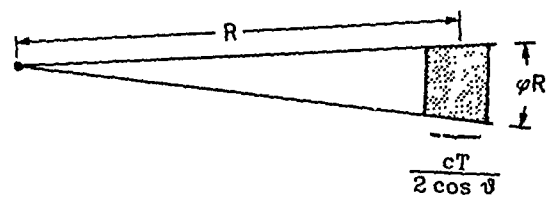

Fig. 3 Plan view of scattering area at seafloor: approximate dimensions of scattering area for small grazing angles;
c is the sound speed in seawater;
T the processing time;
ϕ the 3-dB beamwidth (rad);
θ the grazing angle at the bottom; and
R the range.

expressed in terms of the sonar equation as

$$S = RL - SL + TL1 + TL2 - 10 \log A \ , \qquad (2)$$

where S is the scattering strength in dB/m^2; RL and SL are respectively the equivalent reverberation level and source level in dB re 1 μPa; TL1 and TL2 are the one-way transmission losses in dB; and A is the effective scattering area of the bottom in m^2. If the process involves a combination of scattering, reflection, and diffraction, then the estimated scattering strength may have errors or may be inappropriate. However, if the process is entirely that of specular reflection for an area of the seafloor greater than a Fresnel zone, a reflection loss parameter would be more appropriate.

MEASUREMENTS

Measurements were made in the Tyrrhenian Sea at the locations shown in Fig. 4; the same figure also indicates the major scattering features. Explosive SUS sources (0.8 kg TNT) were set at a depth of 245 m near a receiving array towed at a depth of 100 m. The hydrophone signals were split into increments that were processed by the beamforming technique described above and implemented in the processing system presented schematically in Fig. 5. Repetition of the beamforming procedure for adjacent

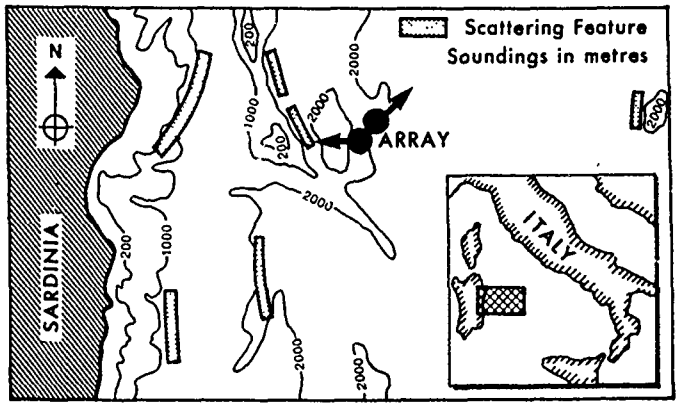

Fig. 4 Location of experiment: estimated positions of major scattering features are shown in shading.

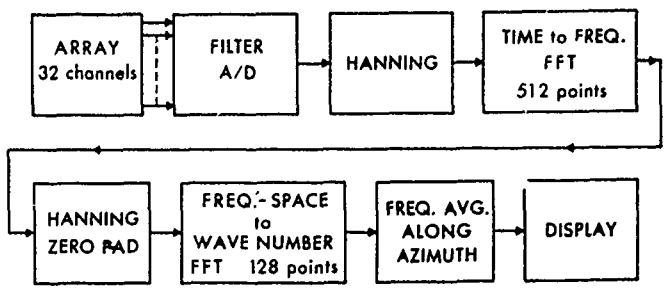

Fig. 5 Acquisition and processing system..

time segments gave a display of the beam-time history of features of the seafloor that scattered sound back to the array. Examples of beam-time histories are shown in Figs. 6 and 7. It can be seen that the direct arrival is followed by arrivals due to multiple reflection from the seafloor at high grazing angles. These appear strong on all beams because of sidelobe reception of the overloaded signals. Later arrivals are primarily due to backscattering from the seafloor at low grazing angles. The records also

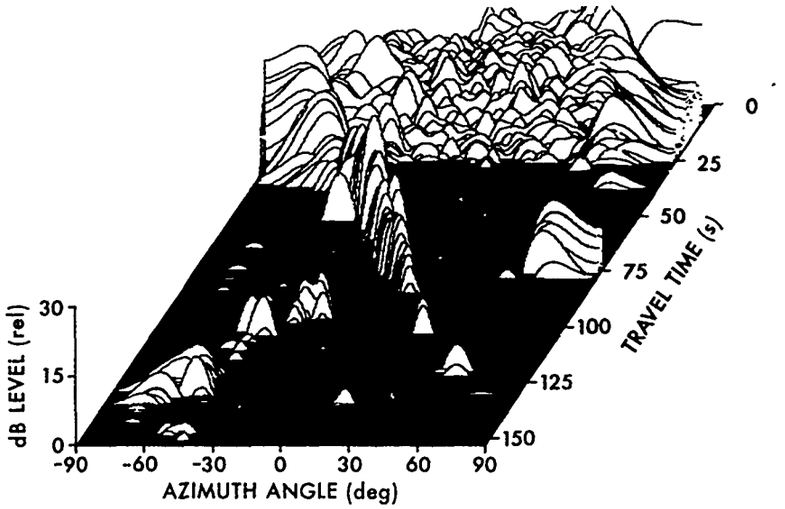

Fig. 6
Beam-time history at 600 Hz: 50-Hz bandwidth and array orientation 45°; positive azimuth toward ship; explosive source occurs at t = 6 s.

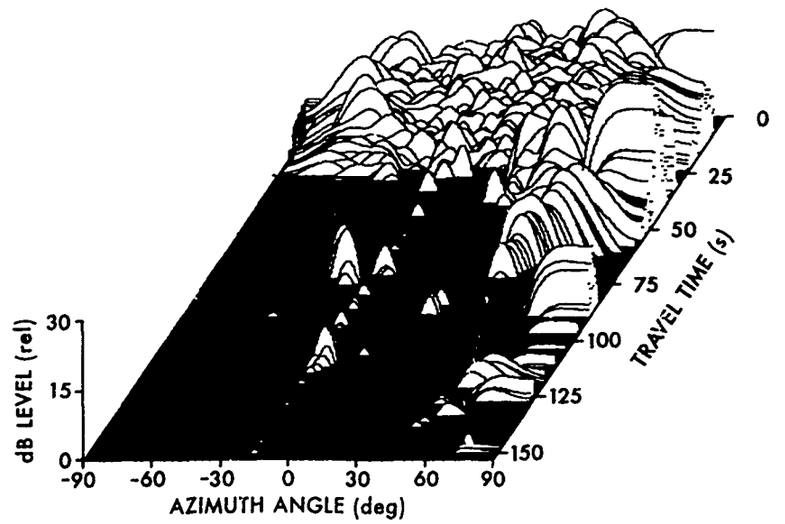

Fig. 7
Beam-time history at 700 Hz: 50-Hz bandwidth and array orientation 270°; positive azimuth toward ship; explosive source occurs at t = 6 s.

show continuous arrivals (artifacts) that are unrelated to returns from the explosive source and are comprised of towship and shipping noise. The major features are caused by backscattering from major physiographic features, e.g. island slope of Sardina and the Baconi Seamounts.

Scattering strengths were calculated using Eq. (1) and are shown in Fig. 8 as a function of frequency. Also shown are other scattering strength values calculated from directional measurements at low frequency [9,10]. The frequency dependence of the scattering strengths of these data is apparently weak. This is in agreement with most measurements of scattering from the seafloor at frequencies of 2 kHz to 100 kHz [14]. More data are required before the relationship at low frequencies can be established. However, at this point these limited data certainly do not suggest the very strong frequency dependence (about 1.6 power dependence, or 4.8 dB per octave) found in some of the high-frequency (13 to 290 kHz) data of McKinney and Anderson [15].

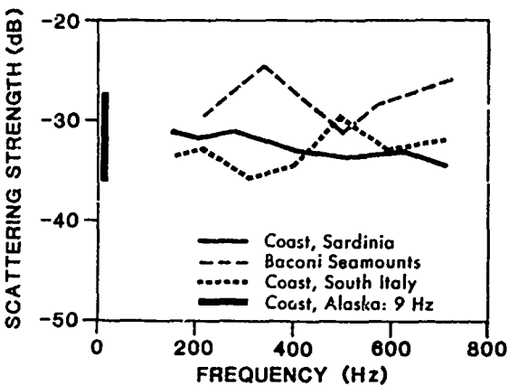

Fig. 8
Scattering strength versus frequency: data for coasts of South Italy and Alaska taken from Refs. 9 and 10 respectively.

CONCLUSION

Directional measurements of backscattering were made with an omni-directional explosive source and a linear towed receiving array. The hydrophone signals were processed to form receiving beams and the data are displayed as images of the scattering features of the seafloor. The scattering strengths obtained exhibit weak frequency dependence, but more data are required before the frequency dependence of the seafloor features can be established.

REFERENCES

1. K.V. Mackenzie, Bottom reverberation for 530- and 1030 cps sound in deep water, J. Acoust. Soc. Am. 33:1498-1503 (1961).

2. R.J. Urick and D. S. Saling, Backscattering of explosive sound from the deep sea-bed, J. Acoust. Soc. Am. 34:1721-1724 (1962).

3. P.B. Schmidt, Monostatic and bistatic backscattering measurements from the deep ocean, J. Acoust. Soc. Am. 50:326-331 (1971).

4. H.M. Merklinger, Bottom reverberation measured with explosive charges fired deep in the ocean, J. Acoust. Soc. Am. 44:508-513 (1963).

5. R.R. Goodman, Comment on two papers concerning reverberation from the ocean floor, J. Acoust. Soc. Am. 37: 174 (1965).

6. J.M. Berkson, C.S. Clay, and T.K. Kan, Mapping the underside of Arctic sea ice by backscattered sound, J. Acoust. Soc. Am. 53:778-781 (1973).

7. R.C. Spindel and J.R. Heirtzler, Long-range echo ranging, J. Geoph. Res. 77:7073-7088 (1972).

8. D.E. Schifter, E.R. Franchi, J.M. Griffin, and B.B. Adams, Hydrographic reconnaissance of large undersea topography using scattered acoustic energy, Rec. IEEE Electronics and Aerospace Systems Conventions 270-274 (1980).

9. J.M. Berkson, T. Akal, and J.L. Berrou, Techniques for measuring backscattering from the seafloor with an array, In: Adaptive Methods in Underwater Acoustics, H. Urban, ed., Reidel, Dordrecht, (1985).

10. I. Dyer, A.B. Baggeroer, J.D. Zittel, and R.J. Williams, Acoustic backscattering from the basin and margins of the Arctic Ocean, J. Geoph. Res. 87:9477-9488 (1982).

11. J.M. Berkson, H.J. Kloosterman, T. Akal, and J.L. Berrou, Application of beamforming techniques to measurements of acoustic scattering from the ocean bottom, IEEE J. Oceanic Engineering, in press (1985).

12. J.M. Berkson, H.J. Kloosterman, T. Akal, and J.L. Berrou, Aspects of spatial resolution for long-range, low-frequency imaging of the seafloor, In: "Acoustic Imaging, Vol. 14," A.J. Berkhout, J. Ridder, and L. VanderWal, eds., in press, (1985).

13. J.R. Williams, Fast beamforming algorithm, J. Acoustic. Soc. Am. 44:1454-1455 (1968).

14. A.V. Bunchuk and Y.Y. Zhitkovskii, Sound scattering by the ocean bottom in shallow-water regions (review), Sov. Phys. Acoustic 26:363-370 (1980).

15. C.M. McKinney and C.D. Anderson, Measurements of backscattering of sound from the ocean bottom, J. Acoust. Soc. Am. 36:158-163 (1964).

SHEAR PROPERTIES OF OCEAN SEDIMENTS DETERMINED FROM NUMERICAL MODELLING OF SCHOLTE WAVE DATA

Finn B. Jensen and Henrik Schmidt

SACLANT ASW Research Centre
Viale San Bartolomeo 400
19026 La Spezia, Italy

ABSTRACT

Recently it has become apparent that shear properties of ocean sediments are most easily determined from measured propagation characteristics of seismic interface waves. We use a newly developed numerical model of wave propagation in horizontally stratified viscoelastic media to reconstruct from Scholte-wave records the shear-speed and shear-attenuation profiles in the upper sediment layers of a shallow-water test area. For an unconsolidated sand-silt bottom we find the shear speed to increase with depth from 85 m/s at the sea floor to 300 m/s at 60 m depth. On the other hand, the shear attenuation at 3 Hz decreases with depth from 0.45 dB/λ at the sea floor to 0.15 dB/λ at 60 m depth, with an approximately quadratic frequency dependence.

INTRODUCTION

It is well established that shear rigidity of the ocean bottom affects propagation of waterborne sound through the conversion of acoustic energy into shear waves. This energy conversion is of particular importance in low-frequency shallow-water acoustics, in which the excitation of shear waves in the bottom often becomes the dominant loss mechanism for waterborne sound [1]. Under these circumstances a realistic physical model of the ocean bottom is a viscoelastic solid described by compressional and shear-wave velocities, by the attenuation factors associated with these waves, and by the material density.

While density and the compressional-wave properties (speed and attenuation) in sediments can be determined by direct methods, the shear-wave properties are difficult to measure. This is because of the usually high attenuation of these waves and because it is difficult to generate a wave that consists of predominantly transverse particle motion. The shear speed and attenuation can be indirectly determined, however, through the measured propagation characteristics of the ocean-bottom interface wave. The existence of this wave is intrinsically related to the shear properties of the sediments.

We shall review the characteristics of seismic interface waves and give some simple formulas that relate their speed and attenuation to those

of shear bulk waves. We shall also provide examples from the literature of indirectly determined shear speeds in sediments. Finally, we will demonstrate how the use of a sophisticated numerical model of seismic-wave propagation allows us to reconstruct from seismic records the shear speed and shear attenuation profiles in the upper sediment layers.

SEISMIC INTERFACE WAVES

This particular wave type - sometimes named a boundary, surface, or interface wave - is a guided wave propagating along the interface between two media with different shear speeds [2,3]. The wave is generally given different names according to the media of propagation involved [4]. Hence, if propagating on a free surface of a solid, it is called a Rayleigh wave, if propagating along a liquid/solid interface, it is called a Scholte wave and if associated with a solid/solid boundary, it is called a Stoneley wave. Note that at least one of the media must be a solid for the interface wave to exist. In the case of a water/sediment interface, the pertinent wave type is a Scholte wave with the following characteristics:

- The wave propagates along the sea floor with exponentially decaying amplitude away from the guiding interface (the wave is evanescent in both media).
- Its particle motion is elliptical in the depth/range plane.
- There is no low-frequency cutoff.
- Its propagation speed and attenuation are closely related to the shear properties of the sediment.

For a simplified environment consisting of two homogeneous media in contact, the Scholte wave is non-dispersive. Its propagation speed (V_{sch}) and attenuation (Δ_{sch}) then relate in an extremely simple manner to the sediment shear properties as:

$$V_{sch} \approx 0.9\ V_s \qquad (1)$$

and

$$\Delta_{sch} \approx 1.1\ \Delta_s, \qquad (2)$$

where the attenuation is in decibels per unit length. Using numerical simulation these formulas were determined to be accurate to within a few percent for unconsolidated sediments (clay, silt, sand) with low shear speeds. The formulas indicate that the Scholte wave properties are virtually independent of densities and compressional wave properties in the two media [5]. Consequently the Scholte interface wave is ideal for determining the shear properties of ocean sediments.

In a realistic environment with sediment layering, the Scholte wave becomes dispersive. In addition, a finite number of ducted shear modes will be present. Figure 1 shows dispersion curves for a solid layer of low shear speed on a high-speed solid substratum. The fundamental mode (M_0) is an interface wave that in the low-frequency limit, $kH \to 0$, propagates as a Rayleigh wave on the substratum, and in the high frequency limit, $kH \to \infty$, propagates as a Rayleigh wave on the surface of the upper layer. The higher-order modes are ducted shear modes in the upper layer. They all have a cutoff frequency at which they propagate with the shear speed of the substratum. In the high-frequency limit these modes propagate with the shear speed of the upper layer. In this case there is no

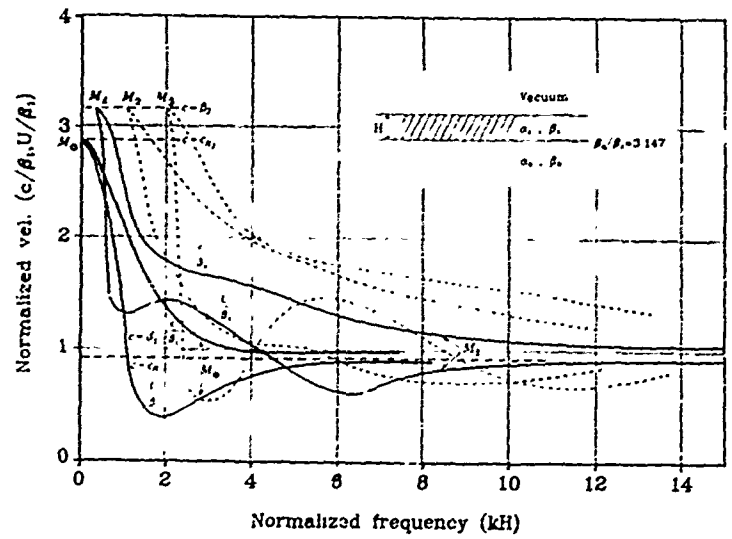

Fig. 1 Dispersion curves for elastic layer on a semi-infinite elastic substratum (Tolstoy and Usdin [2]).

Stoneley wave due to the stringent conditions necessary for the existence of this type of wave. A Stonely wave exists only when the change in shear speed across a solid/solid boundary is less than 10%.

In the following section we show how the complex information contained in experimentally determined dispersion curves similar to those of Fig. 1 can be used to extract shear information about the ocean bottom. Such an analysis generally requires the use of a numerical model. However, if experimental results show negligible dispersion, we can use simple formulas (Eqs. 1 and 2) to determine shear properties for the upper sediment layer. No dispersion means that the sediment is homogeneous to a depth of 1 to 2 wavelengths, the approximate penetration depth of the Scholte wave.

SEDIMENT SHEAR PROPERTIES

Over the past 20 years various investigators [6-17] have used Scholte waves to determine the shear properties of unconsolidated sediments. Their experimental results are summarized in Table 1. Note that experiments were done in water depths ranging from 1 to 5260 m, over sandy or silty bottoms, and for frequencies between 3 and 35 Hz. The measured Scholte wave attenuations (with geometrical spreading removed) vary more than three orders of magnitude, with the highest attenuation being associated with the highest centre frequency. The inferred shear speeds are between 25 and 260 m/s and in excellent agreement with the values quoted by Hamilton [18].

Assuming the shear attenuation to be linear with frequency [18], we can conveniently express it in decibels per wavelength. This has been done in the last column of Table 1, using the simple formulas of Eqs. (1) and (2) to relate measured attenuation of the Scholte wave with the bulk shear-wave attenuation. We obtain values that still vary more than two orders of magnitude (0.02 - 2.3 dB/λ_s), whereas Hamilton [18], based on

Table 1 Interface wave experiments

Investigators	Year	Water depth (m)	Bottom type	Centre freq. (Hz)	Measured att. (dB/km)	Inferred shear speed (m/s)	Inferred shear att. (dB/λ_s)
Bucker, Whitney, Keir[6]	1964	70	sand sand	20 75	300 200	100 195	1.4 1.4
Davies[7]	1965	4419	-	6	-	50-190	-
Herron, Dorman, Drake[8]	1968	5	silt	5	-	40-115	
Hamilton et al.[9]	1970	390 985	silt silt	- -	-	100 90	- -
Schirmer[10]	1980	130	sand	4.5	7	120	0.2
McDaniel, Beebe[11]	1980	32	sand	10	-	200	-
Essen et al.[12]	1981	1	silt	4	-	75-250	-
Tuthill et al.[13]	1981	7	mud	4.5	-	25-50	-
Whitmarsh, Lilwall[14]	1982	5260	-	4.5	-	25-170	-
Holt, Hovem, Syrstad[15]	1983	-	sand	35	600	135-195	2.3
Brocher et al.[16]	1983	67	sand	5	0.43	260	0.02
Schmalfeldt, Rauch[17]	1983	20 30	- -	3 3	10 2	100 150	0.3 0.1

sparse in situ measurements for silt and sand sediments, quotes attenuation values around 0.5 - 2 dB/λ_S. Note, however, that the very low attenuation values are all associated with low-frequency experiments (3 to 5 Hz).

There are two possible explanations for the observed large variation in shear attenuation with frequency. First, that the shear attenuation in sediments decreases with depth as reported by Hamilton [18]. This leads to lower attenuation values for the low-frequency experiments, since the Scholte wave here penetrates deeper into the bottom. The second explanation is that the attenuation does not depend on the first power of frequency as assumed above, but rather follows a power law (f^n) where the exponent is between 1 and 2. Some experimental evidence for this latter assumption does exist [18]. In particular, Stoll in a recent paper [19] has strongly advocated the hypothesis of a marked frequency dependence of attenuation in fluid-saturated sediments, based both on recent field and laboratory data, and on theoretical results from the Biot model. However, more experimental work is needed in order to definitely resolve the depth and frequency dependence of shear-wave attenuation in marine sediments.

NUMERICAL MODELLING OF SCHOLTE WAVES

Figure 2 displays the Scholte wave data from which shear speed and shear attenuation profiles can be determined using a sophisticated propagation model. Stacked time signals for both the vertical and horizontal (radial) particle velocities are shown as recorded by a geophone on the ocean bottom [17]. The source was an explosive charge detonated near the sea floor in 20 m of water. The charge size was increased with range as indicated by the black dots in Fig. 2. We clearly see the dispersed low-frequency Scholte-wave arrivals with group velocities between 78 and 235 m/s.

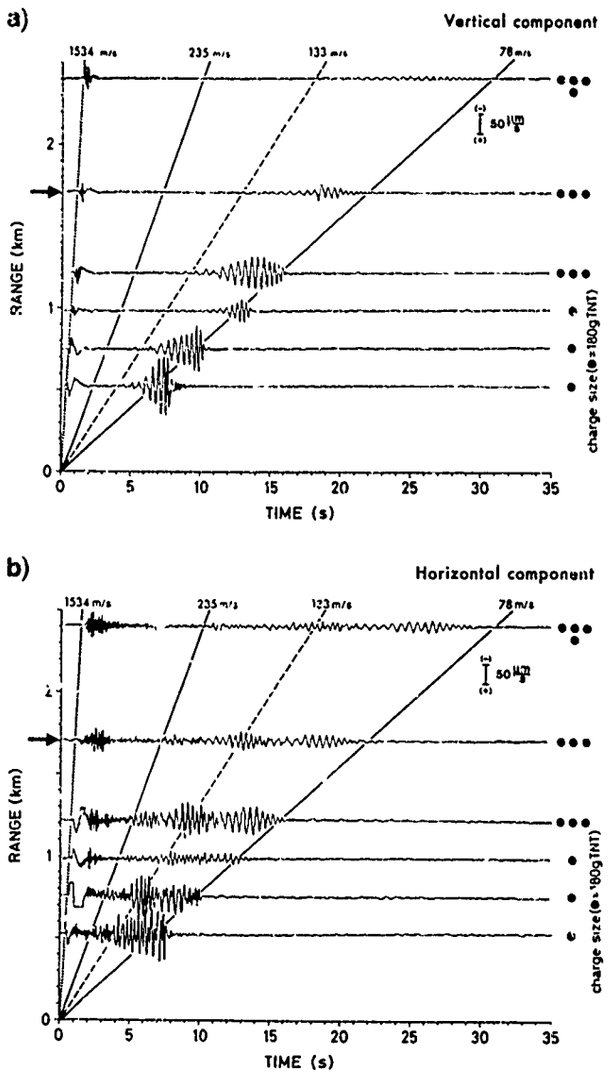

Fig. 2 Stacked time signals for vertical (a) and horizontal (b) particle velocities as recorded by a geophone on the sea floor.

Before performing detailed modelling of this propagation situation, it is convenient to carry out a dispersion analysis of the experimental data. By applying the multiple filter technique [17] to the recorded time series at range 1.7 km, we obtain the dispersion diagrams shown in Fig. 3. The contours indicate energy levels in arbitrary decibels (max level = 99 dB). It is evident that the radial component of the particle velocity gives more information about the propagation situation than does the vertical component. Thus Fig. 3b shows that energy is arriving in three discrete modes, of which the slowest arrival is the Scholte mode (M_0) with its energy centred around 2 Hz. The first shear mode (M_1) is strongly excited, with maximum energy around 2.8 Hz, while the second shear mode (M_2) is only weakly excited.

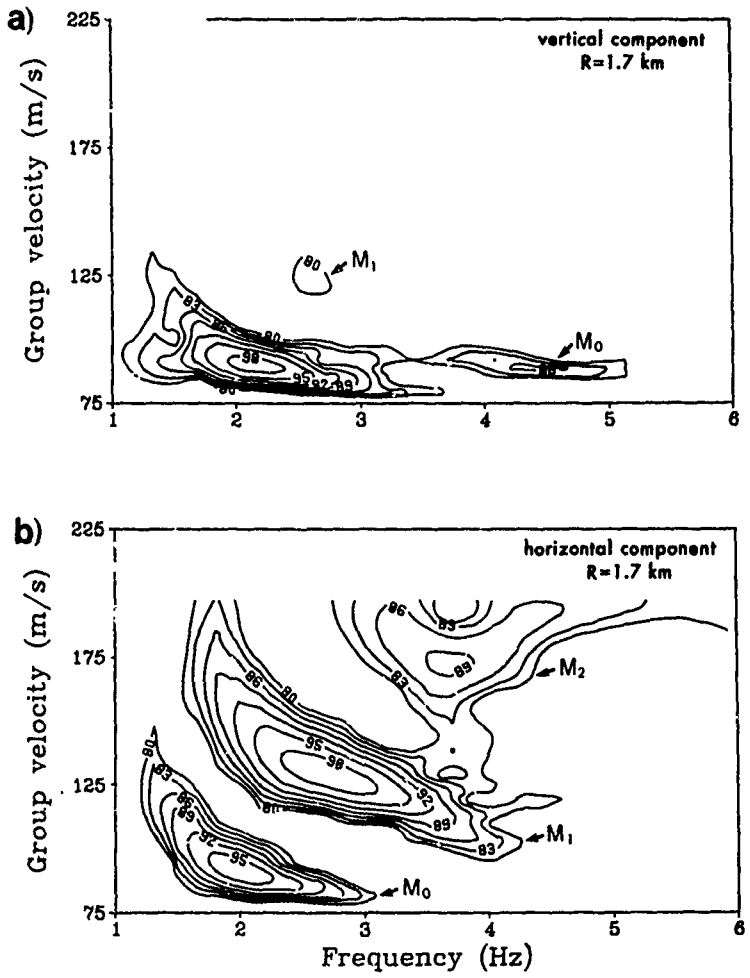

Fig. 3 Dispersion curves obtained by applying a multiple filter technique to the experimental records at range 1.7 km. Energy is seen to be propagating in three discrete modes: M_0 , M_1 , and M_2 .

The modelling is done with a newly developed numerical model of seismic wave propagation in horizontally stratified media [20,21]. The aim is to construct a model environment leading to computed dispersion characteristics that agree with the experimental results of Fig. 3. The modelling is done in a trial-and-error fashion, in which environmental parameters are changed in a systematic way until acceptable agreement is obtained between theory and experiment. Since we are interested in determining the shear properties for an unconsolidated sediment, we can fix, a priori, the compressional-wave properties and densities, which are known to have negligible effect on the propagation characteristics of bottom interface waves [5]. The compressional-wave properties (C_c,β_c) and densities (ρ) used as input to the seismic model are shown in Fig. 4. Also shown are the final choices of shear-speed (C_s) and shear-attenuation (β_s) profiles for the bottom.

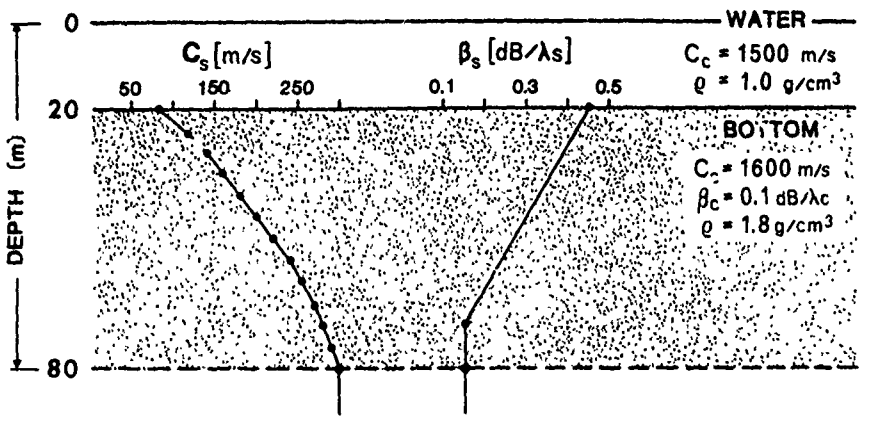

Fig. 4 Model environment used for generating synthetic seismograms.

The computed low-frequency dispersion curves for the model environment are shown in Fig. 5. In Fig. 5a we have superimposed the theoretical dispersion curves (dashed lines) on the experimental data. Clearly there is good agreement between theory and experiment for the modal arrival structure, particularly for the two lower-order modes. This, in turn, means that we have chosen an appropriate shear-speed profile. Figure 5b shows the relative energy distribution in the first three modes as determined from the numerical model. Again there is good agreement with the experimental results in Fig. 5a, indicating that the choice of shear-attenuation profile is also appropriate. It should be pointed out, however, that it was necessary to assume a quadratic frequency dependence of shear attenuation in order to get agreement on energy levels over the entire frequency band.

The inferred shear speeds (85 to 300 m/s) and shear-speed gradients (< 6 m/s/m) agree well with values given by Hamilton [18] for sand-silt bottoms. Reported data concerning the shear-attenuation profiles are so sparse that no comparison with those in the literature can be made.

As a final confirmation of the validity of this modelling exercise, we have created synthetic seismograms for both the vertical and horizontal (radial) particle velocities (Fig. 6). We notice a good overall agreement with the experimental results in Fig. 2, the main difference being fast, low-frequency arrivals present in the synthetic seismograms but filtered out in the experimental data.

CONCLUSIONS

Direct measurements of shear properties of ocean sediments are difficult to perform. However, both shear-speed and shear-attenuation profiles can be inferred from measured dispersion characteristics of bottom interface waves through the use of a sophisticated propagation model. The modelling is considerably simplified because the propagation characteristics of Scholte waves depend entirely on the sediment shear properties and have only negligible dependence on the compressional-wave properties and the density. For a shallow water test area we find sediment shear speeds (85 to 300 m/s) and shear attenuations (0.15 to 0.45 dB/λ at 3 Hz) that are in good agreement with values reported in the literature. Moreover, in accordance with recent sediment studies, we find the shear attenuation to have an approximately quadratic frequency dependence.

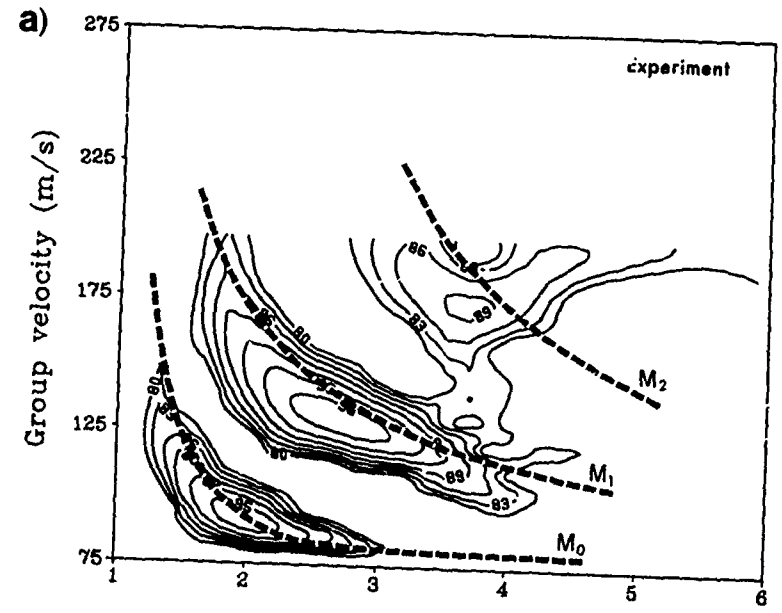

Fig. 5 Experimental (a) and theoretical (b) dispersion curves associated with the horizontal particle velocity of the sea floor at range 1.7 km.

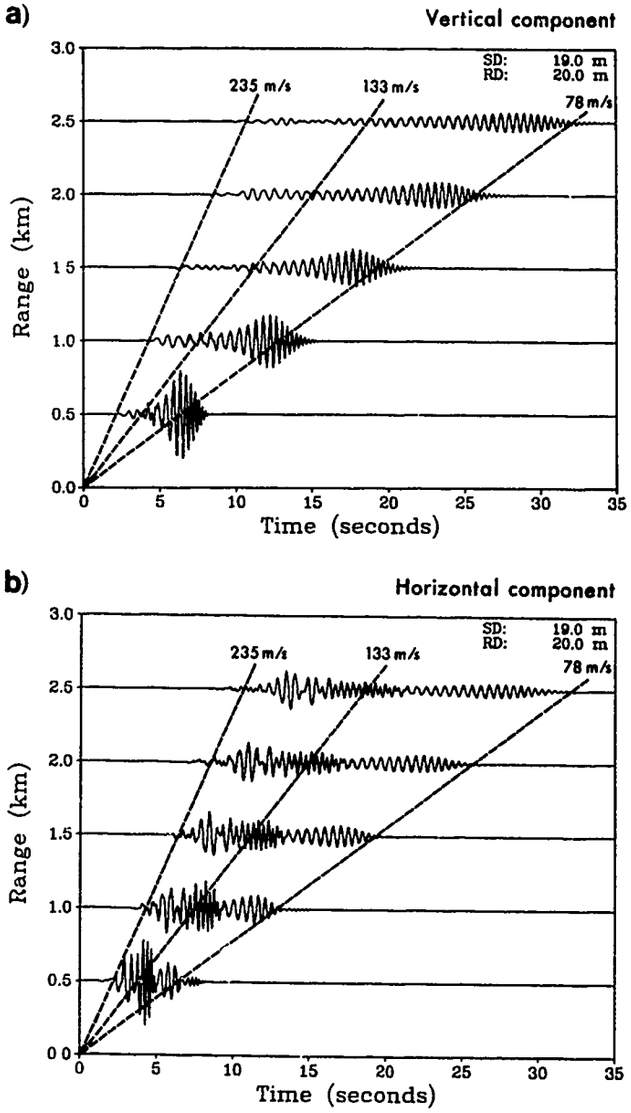

Fig. 6 Synthetic seismograms for vertical (a) and horizontal (b) particle velocities at the sea floor.

REFERENCES

1. T. Akal and F.B. Jensen, Effects of the sea-bed on acoustic propagation. In: "Acoustics and the Sea-Bed," N.G. Pace, ed., Bath Univ. Press, Bath, UK (1983): 225-232.
2. W.M. Ewing, W.S. Jardetzky and F. Press, "Elastic Waves in Layered Media," McGraw-Hill, New York, NY (1957).

3. I. Tolstoy and C.S. Clay, "Ocean Acoustics: Theory and Experiment in Underwater Sound," McGraw-Hill, New York, NY (1966).
4. D. Rauch, Seismic interface waves in coastal waters: a review, Rep. SR-42, SACLANT ASW Research Centre, La Spezia, Italy (1980). [AD A 095 018]
5. E. Strick and A.S. Ginzbarg, Stoneley-wave velocities for a fluid-solid interface, Bull. Seis. Soc. Amer. 46: 281-292 (1956).
6. H.P. Bucker, J.A. Whitney and D.L. Keir, Use of Stoneley waves to determine the shear velocity in ocean sediments, J. Acoust. Soc. Amer. 36: 1595-1596 (1964).
7. D. Davies, Dispersed Stoneley waves on the ocean bottom, Bull. Seis. Soc. Amer. 55: 903-918 (1965).
8. E.M. Herron, J. Dorman and C.L. Drake, Seismic study of the sediments in the Hudson River, J. Geophys. Res. 73: 4701-4709 (1968).
9. E.L. Hamilton, H.P. Bucker, D.L. Keir and J.A. Whitney, Velocities of compressional and shear waves in marine sediments determined in situ from a research submersible, J. Geophys. Res. 75: 4039-4049 (1970).
10. F. Schirmer, Experimental determination of properties of the Scholte wave in the ocean bottom at the North Sea. In: "Bottom-Interacting Ocean Acoustics," W.A. Kuperman and F.B. Jensen, eds., Plenum, New York, NY (1980): 285-298.
11. S.T. McDaniel and J.H. Beebe, Influence of semiconsolidated sediments on sound propagation in a coastal region. In: "Bottom-Interacting Ocean Acoustics," W.A. Kuperman and F.B. Jensen, eds. Plenum, New York, NY (1980): 493-505.
12. H.H. Essen, H. Janle, F. Schirmer and J. Siebert, Propagation of surface waves in marine sediments, J. Geophysics 49: 115-122 (1981).
13. J.D. Tuthill, B.R. Lewis and J.D. Garmany, Stoneley waves, Lopez Island noise, and deep sea noise from 1 to 5 Hz, Marine Geophys. Res. 5: 95-108 (1981).
14. R.B. Whitmarsh and R.C. Lilwall, A new method for determination of in-situ shear-wave velocity in deep-sea sediments, Proceedings of Oceanology International 82, Spearhead Publications, Kingston-upon-Thames, UK (1982).
15. R.M. Holt, J.M. Hovem and J. Syrstad, Shear modulus profiling of near bottom sediments using boundary waves. In: "Acoustics and the Sea-Bed," N.G. Pace, ed., Bath Univ. Press, Bath, UK (1983): 317-325.
16. T.M. Brocher, B.T. Iwatake and D.A. Lindwall, Experimental studies of low-frequency waterborne and sedimentborne acoustic wave propagation on a continental shelf, J. Acoust. Soc. Amer. 74: 960-972 (1983).
17. B. Schmalfeldt and D. Rauch, Explosion-generated seismic interface waves in shallow water: experimental results, Rep. SR-71, SACLANT ASW Research Centre, La Spezia, Italy (1983). [AD A 134 551]
18. E.L. Hamilton, Geoacoustic modelling of the sea floor, J. Acoust. Soc. Amer. 68: 1313-1340 (1980).
19. R.D. Stoll, Marine sediment acoustics, J. Acoust. Soc. Amer. 77: 1789-1799 (1985).
20. H. Schmidt and F.B. Jensen, Efficient numerical solution technique for wave propagation in horizontally stratified ocean environments, Rep. SM-173, SACLANT ASW Research Centre, La Spezia, Italy (1984). [AD A 148 537]
21. H. Schmidt, Excitation and propagation of interface waves in a stratified sea-bed, In: "Acoustics and the Sea-Bed," N.G. Pace, ed., Bath Univ. Press, Bath, UK (1983): 327-334.

EVALUATION OF LOW-FREQUENCY BOTTOM BACKSCATTERING STRENGTH VS GRAZING ANGLE BY MEANS OF MULTIPLE BEAMFORMING

D. Marandino and T.G. Goldsberry
SACLANT ASW Research Centre
Viale San Bartolomeo 400
I-19026 La Spezia, Italy

ABSTRACT

Bottom backscattering strength was measured in deep water as a function of grazing angle in the Balearic Abyssal Plain of the Mediterranean. The measurements were made with a towed, narrowband low-frequency omnidirectional source and a towed, horizontal linear array. The method takes advantage of the multiple beamforming capability of the receiving array and processor to accurately discriminate returns at given grazing angles from interfering returns. Approximations for the evaluation of the backscattering area are described and discussed. The results are presented and compared with previously reported measurements. At the higher grazing angles, specular reflection from normal incidence dominates the returns. However at medium and small grazing angles data have a large plateau region, with small variations. A Lambert's rule relationship, with a coefficient of -33 dB, can approximate results for grazing angles as low as about 20°.

INTRODUCTION

Low-frequency bottom backscattering strength values have been previously measured and reported by several authors [1 to 5]. These results refer to experiments with broad-band sources (explosives) and omnidirectional receivers. However the data presented herein were collected using narrowband sources and directional receivers. By taking advantage, on reception, of the directional properties of a towed linear array, it was possible to accurately discriminate returns at various grazing angles. Indeed, it is well known that beams formed by a linear array have conical symmetry around the array's axis. This property was exploited to discriminate returns in the vertical plane and to estimate arrivals from progressively longer times and thus smaller grazing angles.

Measurements were made in a deep water area in the Balearic Abyssal Plain. While the results are pertinent only to a similar environment the evaluation criteria can be generally applied to horizontal towed arrays.

The next section provides a description of the experiment and is followed by a discussion on the measurement criteria that emphasizes the evaluation of the backscattering area. Finally, the results are presented and discussed.

1 DESCRIPTION OF THE EXPERIMENT

The experiment was conducted in an area of the Balearic Abyssal Plain which is typical of Mediterranean-type abyssal plains. The water depth at the site is 2800 m. Cores, 6 m long that were previously collected in the same area, show layers of sand interspersed with thin layers of clayey and silty deposics. An isothermal water column was present, giving rise to typical Mediterranean winter propagation conditions characterized by a totally upward refracting profile. Wind speed was less than 7 kn and sea state was 1 to 2, with a moderate swell.

The experimental set-up for the collection of monostatic reverberation used the SACLANTCEN R/V Maria Paolina to tow a sound source and a linear array receiver at constant speed, course and depth. During the run, the source generated pulses at regular intervals, and the bottom echoes were received by the towed linear array and subsequently processed on board. Both the source and array depth were 100 m.

Figure 1 shows a simplified block diagram of the data acquisition and processing system. The array has 32 hydrophones with half wavelength spacing. Hamming shading is applied to the hydrophone data. The filtered and digitized returns are beamformed via a time-domain, programmable multiple beamformer, and subsequently match-filtered in the array processor. Figure 2 depicts the beamformer file that was used during the experiment and indicates both a plan and side view of the beam-pointing directions, as determined by conical symmetry and assuming a constant sound speed profile.

The transmitted waveform was a linear frequency modulated (LFM) pulse with a one second duration and 10 Hz swept bandwidth at a centre frequency of 365 Hz. The received signals were processed through a quadrature replica correlator with Hanning shading; the final equivalent slant range resolution is approximately 120 m.

2 BOTTOM SCATTERING STRENGTH EVALUATION METHOD

2.1 The Data Base

Returns from a number of pings were ensemble-averaged to determine a mean reverberation envelope. Reverberation at initial ranges is dominated by bottom backscattering that affects returns in two distinct ways:

- The first is referred to as the "fathometer effect", and is caused by the energy that is radiated by the omnidirectional source in the vertical direction and that propagates vertically in the water column, repetitively bouncing off the bottom and the surface. This is evidenced in the processed beam output time series as a sequence of peaks of the received power, which are regularly spaced at a distance equal to twice the water depth.

- The second effect is the progressive decay of the received power which is caused by backscattering from the bottom at progressively longer ranges, and thus smaller grazing angles.

Both effects can be seen in Fig. 3 where the ping-to-ping (ensemble) average of the returns received at the broadside beam over a limited set of ranges is shown on a logarithmic scale in an A-scan format. Also shown is the measured ambient noise level in the processed band (noise floor). The lower half shows the standard deviation of the averaging procedure of

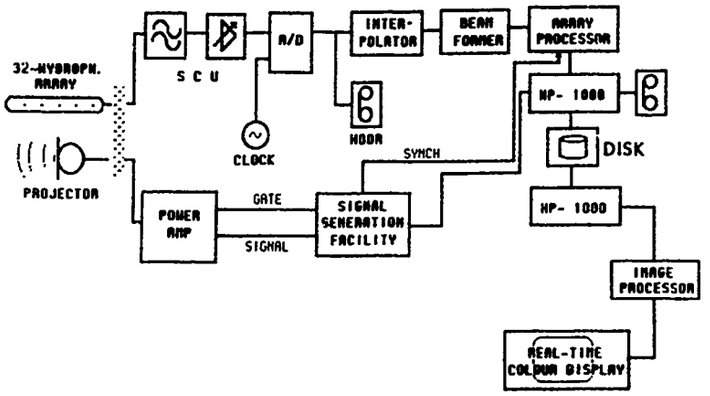

Fig. 1 Block diagram of SACLANT's data acquisition and processing system for reverberation measurements.

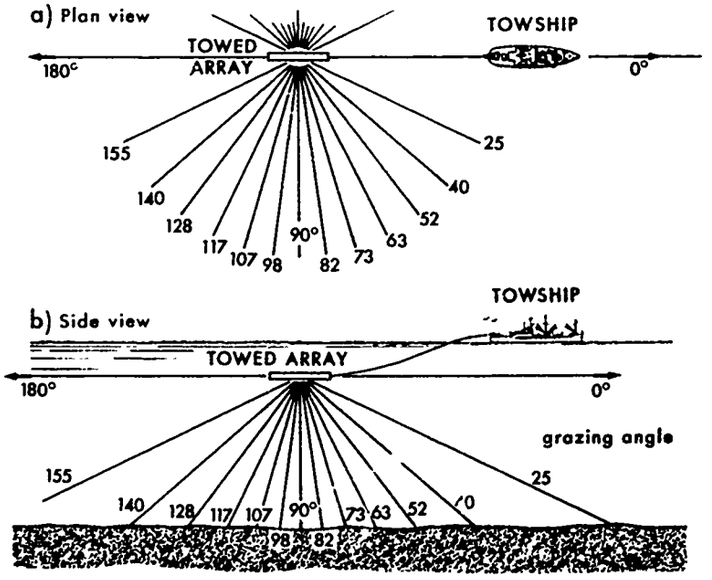

Fig. 2 Beam geometry of low frequency bottom backscattering experiment.

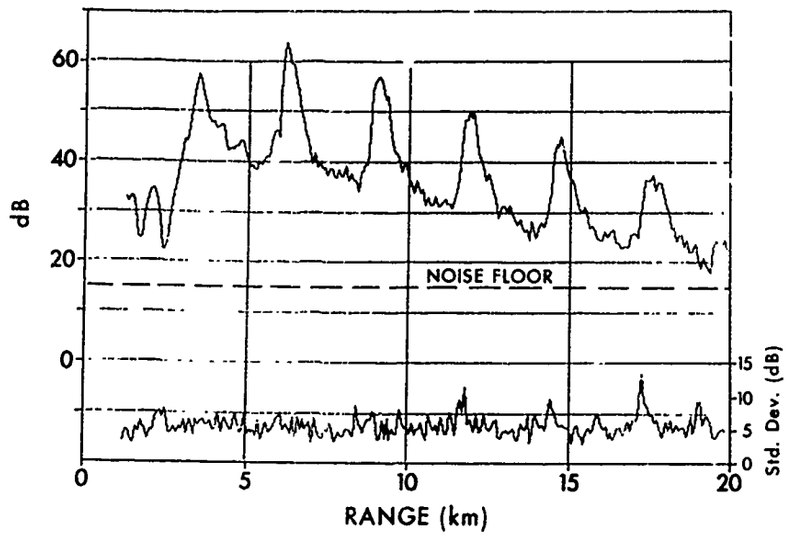

Fig.3 Average of reverberation returns received at the 90° beam, ambient noise floor, and standard deviation. (water depth: 2800 m; centre frequency: 365 Hz).

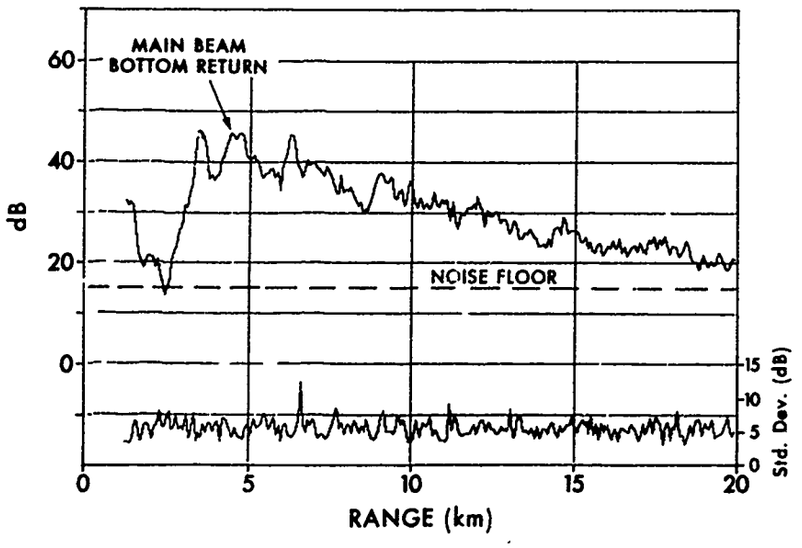

Fig. 4 Average of reverberation returns at the 38° from broaside beam, ambient noise floor, and standard deviation. (water depth: 2800 m; centre frequency: 365 Hz).

the figure which has a mean value of 5.5 dB, as expected from the averaging of Rayleigh distributed log normalized data. The fathometer peaks and the regular decay of bottom reverberation vs range are evident. However, broadside beam data cannot be used to accurately determine bottom backscattering strength because of the high sidelobes associated with the fathometer returns. To overcome that, the data from the off-broadside beams have been used. In this case, the fathometer effect is attenuated because vertically propagating energy is picked up through the angular sidelobes of the various beam patterns. Also, the beam power time series shows a local maximum corresponding to the onset of the bottom returns at the grazing angle related to the main beam pointing direction. This correspondence confirms the hypothesis of the predominance of bottom reverberation.

This is illustrated in Fig. 4 which show the time series associated with the beam pointing at 38° from broadside, which corresponds to a 52° grazing angle. An arrow marks the main beam bottom return. The advantages of evaluating backscattering strength in this manner are that: a) a (local) maximum of the signal-to-noise ratio is used; b) the influence of the fathometer effect can be considered negligible; c) the propagation loss can easily be estimated by assuming spherical spreading.

Bottom backscattering strength vs grazing angles can then be determined by direct application of the sonar equation, using the power output time series of the various beams.

2.2 Evaluation of the Backscattering Area

In order to determine scattering strength by means of the sonar equation, an estimate of the backscattering area (A_b) must be obtained. The evaluation of A_b is determined by three factors: propagation mechanism, the characteristics of the waveform and the beam shape at reception.

Figure 5 provides a plan and side view of the geometry of the experiment which is applicable to the evaluation of A_b and defines the pertinent axes and parameters. The y-axis is orientated along the array axis direction. In the figure,

A_{bM} is backscattering area at medium to small grazing angles

A_{bm} is backscattering area at high grazing angles

d_w is water depth

h is water depth less source depth

γ is the grazing angle (angle between bottom and propagation path)

γ_{eq} is the "equivalent" grazing angle, at small grazing angles

d_r is the annular width related to the signal range resolution

d_b is the annular width related to the mainbeam intersection and

d_{cr} is the "cross-range" dimension of A_b.

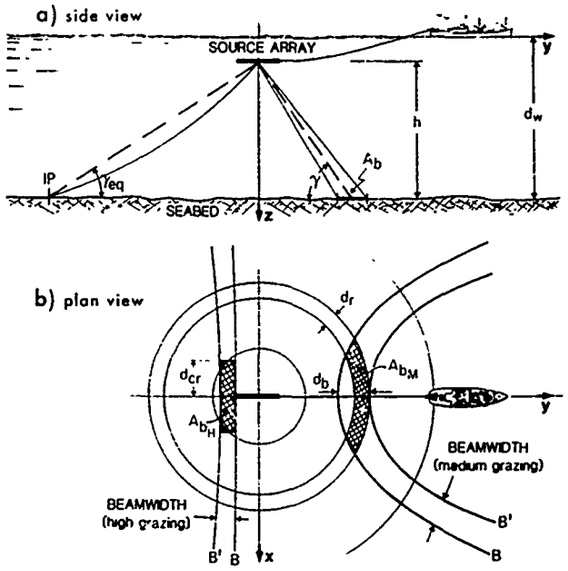

Fig. 5 Geometry for the backscattering area.

The energy radiated by the source propagates spherically and intersects the (flat) bottom along circles, whereas the various beams, which define cones around the array axis, intersect the bottom along hyperbolic curves B and B' in Fig. 5. However, such representation is only applicable to high and medium grazing angles (> 20°) where ray bending caused by the true sound speed profile are negligible. In this case the grazing angle is also equal to the complementary angle of the ray at the source/receiver. For smaller grazing angles, say below 20°, it has been assumed that the geometry remains approximately valid, provided that the actual grazing angle is replaced by an "equivalent" angle obtained by the straight-line approximation to the actual intercept point (IP in the figure) as determined by the actual sound speed profile. For this experiment, the ray at 13.86° at the source grazed the bottom at 0° with an equivalent grazing angle of 6.93° and slant range of 22370 m.

For an omnidirectional receiver, power comes from a circular annulus with a width (d_r) expressed by:

$$d_r = d_s \,/\, \cos(\gamma) \qquad (1)$$

where d_s = slant-range signal resolution (here, 120 m).

Since the receiver is directional, only that part of the annulus which is included in the mainbeam contributes to backscattering, under the assumption that contributions from the beam's sidelobes are negligible. The intersection of the mainbeam with the bottom (hyperboli' curves B and B' in Fig. 5) is expressed by:

$$y_i^2 = \frac{x^2+h^2}{\cdot^2} \quad ; \; i = 1, 2 \qquad (2)$$

where γ_1 and γ_2 are the grazing angles corresponding to the 3 dB beamwidth.

This area has a minimum radial width, d_b, along the trace of the array axis on the bottom, expressed by

$$d_b = h * b_w(90°) / (\sin(\gamma))^3 \qquad (3)$$

where $b_w(90°)$ = array beamwidth at broadside, with the assumption that the beamwidth for any beam pointing direction is given by

$$b_w(\gamma) = b_w(90°) / \sin(\gamma).$$

The backscattering area can then be estimated through the rectangular approximation:

$$A_b = D_r * D_{cr} \qquad (4)$$

where D_r is the radial dimension, and

D_{cr} is the cross-range dimension.

Two cases may thus be distinguished:

- $d_r > d_b$. This is valid at high grazing angles (A_{bH} in Fig. 5). In this case the width of the transmission annulus is larger than the width of the hyperbolic annulus generated by the mainbeam intersection; therefore, in Eq. 4 it is:

$$D_r = d_b \qquad (5)$$

- and, for the cross-range dimension, simple geometrical considerations on returns included between R and R+d_s, where R is the slant range in the mainbeam give:

$$D_{cr} = 2\, d_s \sqrt{\left(1 + \frac{2h}{d_s \sin\gamma}\right)} \qquad (6)$$

- $d_r < d_b$. This is valid at medium to small grazing angles. The backscattering area (A_{bM} in Fig. 5) is that part of the circular annulus that is delimited by the intersection with the beam hyperbola. For a given range, the area can then be expressed by the rectangular approximation (4), where the radial dimension is

$$D_r = d_r\ , \qquad (7)$$

and the cross-range dimension D_{cr} is the arc of circle generated by the intersection of the lowermost hyperbola and the circle related to that range. Then:

$$D_{cr} = \frac{2h}{\tan\gamma_R} \cdot \arcsin \sqrt{\frac{\tan^2\gamma_L - \tan^2\gamma_R}{1 + \tan^2\gamma_L}}$$

where γ_L = higher grazing angle, which corresponds to the 3 dB beamwidth boundary

γ_R = grazing angle corresponding to the given range.

At small grazing angles, however, ray bending increases the distance at which the rays intercept the bottom and the beam intersections with the seabed are not expressed as hyperbolas. However the evaluation of A_b is still based on formulas (7) and (8), in which equivalent grazing angles that correspond to the linear approximation to the actual rays are used.

The relationship between the actual and the equivalent grazing angle can easily be established since the experiment was carried out in isothermal water and thus with a constant velocity gradient. In this case the rays are arcs of circles whose centers lay at a fixed distance

$$R_o = C_{REF} / \zeta \tag{9}$$

where

C_{REF} is the reference sound velocity (1500 m/s), and

ζ is the velocity gradient (0.017 s^{-1})

It is then:

$$\cos \gamma = (1 + \frac{h}{R_o}) \cos \gamma_{RAY} \tag{10}$$

and

$$\gamma_{eq} = \frac{1}{2} (\gamma_{RAY} + \gamma) \tag{11}$$

where

γ is the angle of the grazing ray

γ_{RAY} is the angle of the (monostatic) ray at the source/array and

γ_{eq} is the equivalent grazing angle.

The approximations used in the evaluation of A_b at small grazing angles can be considered satisfactory because d_r is much smaller than the other dimensions.

The behaviour of the bottom backscattering area for beams off broadside, as a function of the true grazing angle, is indicated in Fig. 6 along with the two-way propagation loss at the pertinent ranges. A_b is expressed in dB relative to one square meter and is evaluated with the parameter values applicable to the experiment.

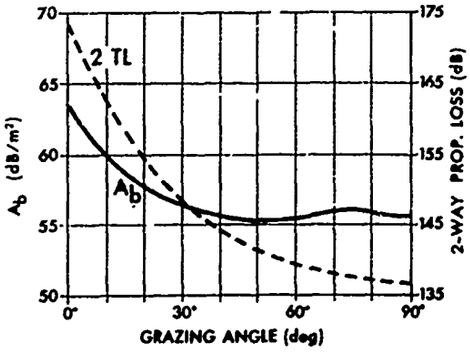

Fig. 6
Bottom backscattering area and two-way propagation loss as a function of the true grazing angle.

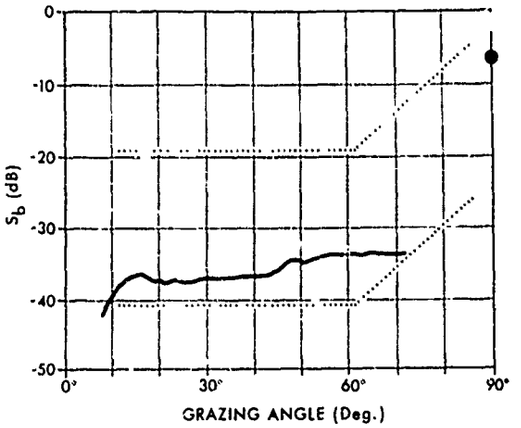

Fig. 7
Backscattering strength coefficient S_b, versus grazing angle, at a centre frequency of 365 Hz. The dotted lines show the limits of reported values for low frequency bottom backscattering strength.

3 RESULTS AND CONCLUSIONS

By applying the sonar equation [6] and using the appropriate curves for the backscattering area and the propagation loss, a point estimation of the backscattering strength coefficient versus grazing angles is obtained (see solid line in Fig. 7).

Two cases must be distinguished:

- At high grazing angles, because of the signal slant-range resolution returns from 73° to 90° cannot be separated and are merged into the fathometer peak and sidelobes. Nevertheless, the fathometer peak itself can be regarded as high grazing angle backscatter. Therefore, an estimation of S_b at near incidence can be obtained by measuring the power at the peak of the fathometer return. However, since the first-bounce fathometer return saturates the hydrophones, it is impossible to determine S_b reliably. Instead the second-bounce fathometer return was used with the addition of the estimated bottom loss incurred at the first bounce (6 dB). The applicable backscattering area here is that of the broadside beam at 90°. The result is given in Fig. 7 by the value at the 90° grazing angle.

- The evaluation of S_b for medium to small grazing angles is outlined in Sect. 2.2. Both rear and forward beam pointing directions were used; however forward beams have a higher noise level due to the towship contributions and are not suitable for estimates at small grazing angles. The estimate is quite accurate for angles above 30° because the backscattering area has small variations and, more importantly, because the measurements are made before the onset of the second fathometer return and are thereby free of multiple bounce scattering. At smaller grazing angles, the estimate of S_b becomes more difficult because the output ratio of signal-to-ambient noise is lower, small variations of the array tilt cause large variations of the intercept area and contributions from multiple-bounce scattering are more likely. However measurements can still be made and an approximate, upper bound for S_b can be obtained for these smaller grazing angles.

The overall behaviour of the bottom backscattering strength indicated in Fig. 7 shows that S_b has high values in that region where backscattering is dominated by specular reflection. The range of angles of high backscattering is determined by the system geometry and the type of

waveform such that the coherent (specular) component dominates incoherent (diffuse) scattering.

For decreasing angles, S_b quickly decays by about 30 dB. Then, for medium and small grazing angles, it has a plateau region where the variations are small. Values of -33 to -37 dB are measured for medium angles (60° to 30°) and of -40 to -42 dB for smaller angles (around 10°).

A comparison with Lambert's rule for diffuse backscattering shows that a value of -33 dB for the Lambert coefficient is reasonable for medium grazing angles. The limits of reported data for low-frequency bottom backscattering strength range from -20 to -40 dB, and are shown in Fig. 7 by the dotted lines (see, for instance, Ref. 6, page 246). These include results at various frequencies and for different types of bottom. As can be seen, the range of previously reported data spans the present measurements, although similar types of seafloor are usually assumed to have slightly higher S_b values.

In conclusion, a method has been presented to evaluate low frequency bottom backscattering strength which takes advantage of the multiple beamforming capability of a towed linear array. The intrinsic system directivity confines backscattering to small, homogeneous seafloor patches and suppresses interference from other directions.

REFERENCES

1. K.V. Mackenzie, Long range shallow-water bottom reverberation, J. Acoust. Soc. Amer. 34: 62-66 (1962).
2. R.J. Urick and D.S. Saling, Backscattering of explosive sound from the deep-sea bed, J. Acoust. Soc. Amer. 34: 1721-1724 (1962).
3. A.W. Burstein and J.J. Keane, Backscattering of explosive sound from ocean bottoms, J. Acoust. Soc. Amer. 36: 1596-1597 (1964).
4. P.B. Schmidt, Monostatic and bistatic backscattering measurements from the deep ocean bottom, J. Acoust. Soc. Amer. 50: 327-331 (1971).
5. H.M. Merklinger, Botton reverberation measured with explosive charges fired deep in the ocean, J. Acoust. Soc. Amer. 44: 508-513 (1968).
6. R.J. Urick, Principles of Underwater Sound, 2nd ed. New York, NY, McGraw-Hill (1975).

SPATIAL VARIABILITY OF SURFICIAL SHALLOW WATER SEDIMENT GEOACOUSTIC PROPERTIES

Michael D. Richardson

SACLANT ASW Research Centre
Viale San Bartolomeo 400
I-19026 La Spezia, Italy

ABSTRACT

Variability of surficial sediment geoacoustic properties was determined from cores collected at eight shallow-water continental shelf regions in the U.S., Italy and Australia. Highly porous muds found in low energy environments exhibited the lowest range of values in physical and acoustic properties; mixtures of sand and shell found in higher energy environments exhibited the highest range of values. Compressional wave attenuation consistently exhibited the highest variability followed by mean grain size, porosity and compressional wave velocity. Vertical variability was generally greater than horizontal variability for all properties measured. Sediment geoacoustic properties of most coastal marine sediments are controlled by the interaction of biological and hydrodynamic processes. Biological processes tend to dominate in finer sediments, whereas hydrodynamic processes control sediment geoacoustic properties in sandy substrates. Understanding these processes in various environments not only explains the spatial distribution of sediment geoacoustic properties but leads to improvement of predictive geoacoustic models.

INTRODUCTION

Knowledge of the spatial variability of surficial sediment geoacoustic properties is important to the prediction of acoustic scattering from the sediment-water interface and to the prediction of propagation of acoustic energy through the sediment[1]. It is within this surficial zone (upper 50 cm of sediment) that the most active and rapid diagenic changes in sediment properties are found. Gradients and variability of geoacoustic properties result from dewatering caused by overburden pressure, as well as active chemical, sedimentological, biological and hydrodynamic processes which mix and alter sediment properties[2,3].

For high frequency (>10 kHz) acoustic applications, geoacoustic properties of the upper tens of centimeters must be known, whereas for low frequency applications surficial geoacoustic properties provide the initial conditions used for prediction of depth gradients of sediment physical properties[1]. Accurate values, including variability, of surficial sediment geoacoustic properties are therefore required for geoacoustic

models covering the wide range of frequencies of interest to those studying underwater acoustics, marine sedimentology, geophysics and marine geotechnique.

In this paper I compare data on the spatial variability of sediment geoacoustic properties among eight shallow-water continental shelf regions in the U.S, Italy and Australia. I also discuss the relative importance of biological, hydrodynamic and sedimentological processes in determining spatial distribution of these geoacoustic properties. Results are then compared to a similar study of geoacoustic properties of three sedimentary provinces in the Venezuela Basin (3500 to 5050 m water depth).

MATERIALS AND METHODS

Replicate sediment samples were collected from eight sites along the continental shelves of the United States, Italy and Australia (Table 1). Sediment types ranged from clayey-silts found in Long Island Sound and the Arafura Sea (off northern Australia) to coarse sands off San Diego, California. All sediments were collected with 6.1 cm (inside diameter) cylindrical cores either in situ by scuba divers or from relatively undisturbed 0.25 m^2 USNEL box core samples collected from deeper sites (Washington coast and Arafura Sea). Collection, measurement and handling procedures were designed to minimize sampling disturbance and maintain an intact sediment water interface with overlying sea water. Sediment compressional wave velocity and attenuation were measured after sediments equilibrated with laboratory temperature, usually one-half to two days after collection. Temperature and salinity of the overlying water were measured with a YSI model 43TD temperature probe and an AO Goldberg temperature-compensated salinity refractometer. Compressional wave velocity and attenuation were measured at 1 cm intervals on sediments in 129 subcores using a pulse technique.

*Table 1. Collection sites, including mean values of porosity, mean grain size, compressional wave velocity (V_p-ratio) and attenuation (dB/m at 400 kHz) (*unpublished data).*

Site	Date	Water Depth (m)	Substrate type	Porosity (%)	Grain Size (φ)	V_p-ratio	Attenuation (dB/m)	References
Long Island Sound	XIII 80							3,4
FOAM		10	clayey-silt	73.2	7.4	0.99		
NWC		16	clayey-silt	77.2	8.4	0.99	-	
San Diego,CA	IV - V 82							5
fine sand		18	very fine sand	-	3.5	1.10	188	
coarse sand		18	coarse sand	-	1.0	1.15	116	
Montauk Point,NY	V 82	35	fine sand	36.6	2.1	1.04	88	6
Quinault, Washington	IV 83	49	fine sand	41.2	2.9	1.11	160	7
Charleston S.C.	VI 83	18	medium sand	37.9	1.6	1.12	292	8,*
La Spezia, Italy	XI 83							8,9
MT		17	gravel	-	-1.6	1.20	-	
ST		8	silty-clay	69.8	8.9	0.98	104	
PV		13	silty-clay	67.6	9.4	0.98	64	
AV		5	very fine sand	43.3	3.6	1.10	136	
Arafura Sea	V 84	47	clayey-sand	69.2	5.3	0.99	336	*
Panama City, Florida	IX 84							10
pre-site		18-33	fine, medium sand	39.3	1.8	1.14	216	
experimental		33	fine sand	39.0	2.6	1.13	228	

Time delay measurements were made through sediments and a distilled water reference with a Hewlett-Packard 1743A dual time interval Oscilloscope. Signals were generated by driving a Underwater Systems, Inc. (Model USI-103) transducer-receiver head with a 400 kHz, 20 volts p-p sine wave triggered for 25μs duration every 10 ms with a Tektronic FG 501 Pulse Generator and FG 504 Function Generator. Differences in time delay between distilled water and sediment samples were used to calculate sediment compressional wave velocity (Vp). Compressional wave velocity was expressed as the dimensionless ratio of measured sediment velocity divided by the velocity in the overlying water that was calculated for the same temperature, salinity and depth[11]. This ratio is independent of sediment temperature, salinity and depth and therefore ideal for comparison to other geoacoustic properties. Attenuation measurements were calculated as 20 log of the ratio of received voltage through distilled water to received voltage through sediment[12]. Values of attenuation were extrapolated to a 1 m pathlength and expressed as dB/m.

After completion of the acoustic measurements, core samples were extruded and sectioned at 2 cm intervals for determination of sediment porosity and grain size distribution. Porosities were determined by weight loss of sediment dried at 105°C for 24 hours. Values were not corrected for pore water salinity. Salt-free porosity may be obtained by multiplying values by 1.012. Sediment grain size distribution was determined on disagregated samples by dry sieving for sand-sized particles and with a Micromeritics Sedigraph and/or pipette for silt and clay-sized particles. Grain size statistics were determined using the graphic formula of Folk and Ward[13].

RESULTS

Sediment geoacoustic data were measured on 129 cores that were collected for this study at eight different sites. I have restricted the data presentation to a summary of sediment geoacoustic properties from each site together with selected graphical representations of the spatial variability of sediment geoacoustic properties. Detailed data presentation can be found elsewhere[3-10].

Sediment samples were collected from two sites in Long Island Sound. Both sites were characterized by high porosity, fine grained, low velocity sediments. At the deeper (18 m) NWC site sediments, were characterized by a uniform distribution of geoacoustic properties (Table 2) on scales of centimeters to meters with no apparent depth gradients in the upper 20 cm. Richardson et al.[3] attributed this low variability to sediment mixing by macrofaunal animals that feed on bottom deposits (bioturbation). At the shallower FOAM site (10 m) sediments exhibited a much higher variability in sediment geoacoustic properties (Table 2). This higher variability was a result of storm induced erosional and depositional events creating laminations within the upper 35 cm of sediment. These laminations, each with different values of geoacoustic properties, were preserved because sediment mixing by macrofaunal animals at the FOAM site rarely extended below the upper few centimeters of sediment[3].

The shallow water samples collected off San Diego came from two distinct sediment types: a fine sand that had lower compressional wave velocity and higher attenuation than the coarser sand over which it was migrating. Of particular interest were the significant positive gradients in compressional wave velocity and attenuation with depth (Fig. 1) for both substrate types without a concordant change in mean grain size. These gradients probably resulted from increased packing and compaction of sands with depth in the sediment.

*Table 2. Coefficient of variation (CV) of porosity, mean grain size, compressional wave velocity ratio (Vp-ratio) and attenuation, calculated for eight shallow water and one deep-sea location (*data from the upper 2 cm of sediment only).*

Site	Porosity	Grain Size	V_p-ratio	Attenuation
Long Island Sound				
FOAM	7.33	11.53	0.82	-
NMC	1.50	1.91	0.35	-
San Diego				
fine sand	-	11.75	1.16	16.41
coarse sand	-	7.42	0.97	25.73
Montauk Point, NY	3.36	6.45	0.93	15.72
Quinault, Washington	4.98	3.63	1.19	33.08
Charleston S.C.	6.28	18.84	1.03	37.76
La Spezia, Italy				
ST	6.07	3.89	0.31	36.63
PL	6.86	1.80	0.34	36.11
AV	3.11	5.42	0.85	10.05
Aritura Sea	5.81	14.56	0.51	47.26
Panama City				
prosite	5.60*	36.51*	1.07	33.03
experimental	3.72	6.14	0.87	15.59
Venezuela Basin				
carbonate	2.82	11.23	0.45	19.75
turbidite	9.88	16.22	1.67	105.88
hemipelagic	3.41	4.51	0.25	23.68

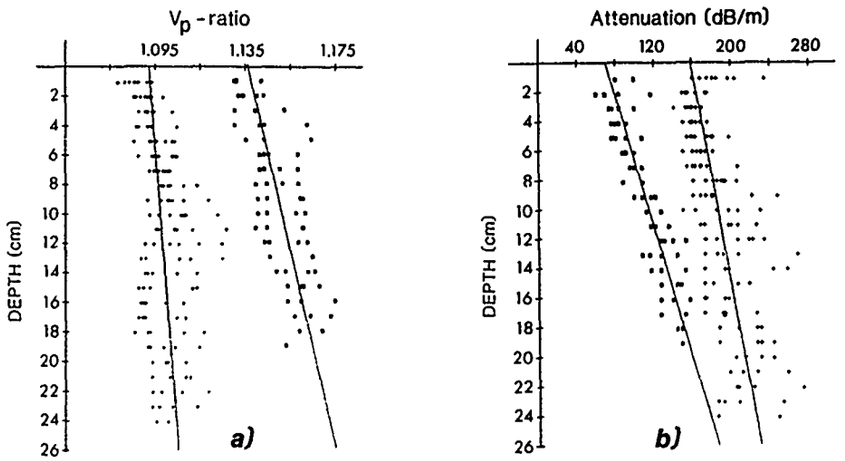

Fig. 1 Regressions of compressional wave velocity ratio (V_p-ratio) and attenuation (dB/m at 400 kHz) with depth for fine (+) and coarse (□) sand substrates found off San Diego, California.

The fine sand sediments collected in 35 m of water 25 km east of Montauk Point, Long Island, New York exhibited relatively low variability in sediment geoacoustic properties, especially attenuation. This low variability was attributed to mixing of sediments by an abundant population of sand dollars[6]. The positive gradient of compressional wave velocity with depth with little change in mean grain size was similar to gradients found in sediments from San Diego. Porosity generally decreased with depth supporting the argument that, for sand, positive gradients in compressional wave velocities can result from increased compaction. Surficial sediment samples collected within a 0.5 km^2 area around the prime collection site exhibited considerable variability in mean grain size (CV=108) because the study site was located at the base of a drowned barrier spit. At this site coarse grained lag deposits formed during the last glacial advance were covered intermittently by fine-grained sediments which were in equilibrium with current hydrodynamic conditions.

Fine sand surficial sediments collected in 50 m water depth on the continental shelf off Washington State exhibited little variation in values of geoacoustic properties from the surface to 12 cm depth (Fig. 2). Below 12 cm, the sediments had higher percentages of silt-sized particles that resulted in higher values of porosity, mean grain size, and attenuation as well as lower values of compressional wave velocity. Variability of geoacoustic properties was also highest below 12 cm depth. A high abundance of molluscan shells below 12 cm also contributed to higher variability of geoacoustic properties, especially attenuation.

Scuba divers observed two surficial substrate types in a one km^2 study area off the Charleston, S.C. coast. Fine to medium sand (mean grain size

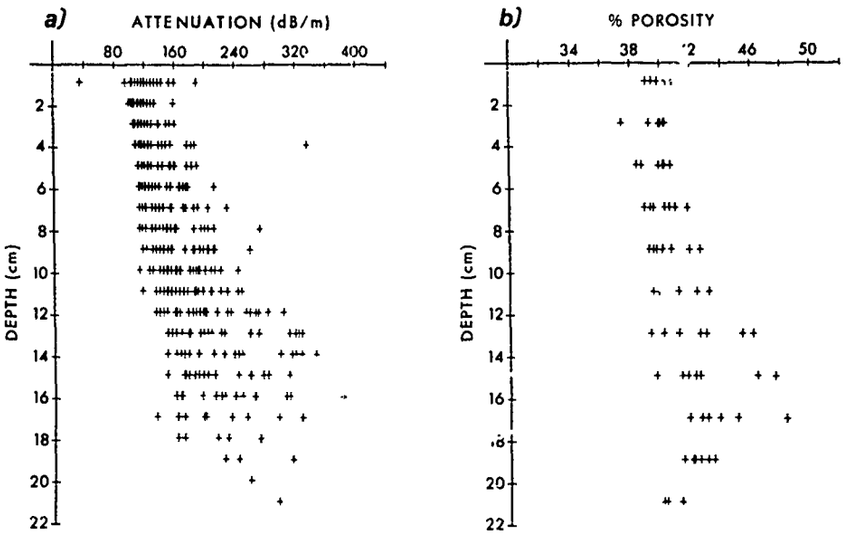

Fig. 2 Depth distribution of values of compressional wave attenuation (dB/m at 400 kHz) and porosity (%) for sediments collected in the Quinault acoustic tracking range - Washington.

1.8 to 2.2ϕ) with porosity values of 37 to 42% were found in troughs of shallow sand waves. The coarser (0.9 to 1.7ϕ) sediments on crests contained abundant shell material and generally had lower values of porosity (30 to 40%). Below 6 to 10 cm, shell material was abundant in all cores. Coefficients of variation for geoacoustic properties of the Charleston samples were higher than at most other locations (Table 2). Most of the variability at the Charleston site was associated with samples that had greater than 2% gravel-sized particles. If these samples are excluded, coefficients of variation are reduced to 0.72% for compressional wave velocity; 23.25% for attenuation; 5.19% for grain-size; and 2.20% for porosity.

Sediment samples were collected from four locations in the vicinity of La Spezia, Italy as part of an international program to compare various acoustical, geotechnical and geophysical measurement techniques[9]. Locations were chosen to include a wide spectrum of sediment types (Table 1). The Monasteroli site (MT) was located in a high energy environment next to the Ligurian coast. Sediments were composed of gravel-sized particles (75% by weight) making it difficult to collect adequate samples.

The coarser sediments (mean grain-size -1.57ϕ) probably originated from erosion of the nearby steep coastline[9]. Frequent storms winnowed finer material from the gravel sediments leaving only 0.17% silt-and clay-sized particles. Compressional wave velocity ratio (mean 1.20) and its coefficient variation (3.45%) were higher than at any other location. Porosity, mean grain size and attenuation were not accurately measured to permit the calculation of coefficients of variation. Sediments from the PV site located at the eastern entrance of the Portovenere channel were protected from physical disturbance, e.g. storms. Sediments were composed of silt and clay mixed with up to 5% gravel-sized shell particles. Compressional wave velocity and mean grain size values varied little (Table 2). However, the high coefficient of variation for porosity reflected 10 to 15% higher values of porosity found in the uppermost 4 cm of sediment. Both biological (bioturbation) and hydrodynamic processes probably maintained this higher surficial porosity. The Santa Teresa site (ST) was located in a small protected harbor on the eastern side of the Gulf of La Spezia. Samples consisted of very soft muds. Compaction of the upper 6 cm produced a negative gradient of porosity with depth without apparent change in sediment acoustic properties. The lack of vertical gradients in compressional wave velocity resulted in a low coefficient of variation. The Venere Azzurra site (AV) was located on a shallow (6 m), flat, hard-packed sandy bottom off Lerici in the Gulf of La Spezia. These well sorted and hard packed sediments had the lowest coefficient of variation for values of attenuation of any site listed in Table 2.

Twelve sediment cores were collected from a one km^2 area in the central Arafura Sea. The clayey-sand sediments contained an abundant quantity of both whole and broken gravel-sized molluscan shells (2 to 23%). The lack of orientation of shells suggested considerable biological mixing had occurred. Variability of mean grain size was a function of the patchy distribution of shells whereas variability of porosity was related to vertical gradients caused by bioturbation and by strong currents which resuspend sediments. Very high values of attenuation measured at 400 kHz (mean 336 dB/m) were a direct result of scattering of the high frequency signal from shell material. Even at 125 kHz values of attenuation were high (mean 65 dB/m) and highly variable (45.7%). Compressional wave velocity ratio appeared to be much less affected by shell material, and was controlled primarily by the clayey-sand matrix (0.989 at 125 kHz vs 0.988 at 400 kHz).

As part of a pre-site survey, 27 sediment cores were collected from a variety of sandy sites (18 to 33 m water depth) off Panama City, Florida. The upper 2 cm of sediments ranged from coarse to fine sand (0.42ϕ to 2.75ϕ) with a relatively narrow range of porosities (36.3 to 43.9%). The coefficient of variation for attenuation and compressional wave velocity were approximately the same as other sandy sites (see Table 2). As part of the acoustic experiment 15 cores were collected from a one km^2 area that had uniform surficial sediment properties[10]. As expected the coefficient of variation for all geoacoustic properties was lower than that calculated from the pre-site survey (Table 2, Fig. 3).

DISCUSSION

The data in Table 2 demonstrate that shallow-water geoacoustic properties of sediment can be quite variable on scales of a kilometer or less. Not evident from Table 2 are the spatial sources of this variation (either vertical or horizontal), the scales (cm to km) or the processes that create this variation. Understanding these relationships can increase the predictability of sediment geoacoustic properties in time and space.

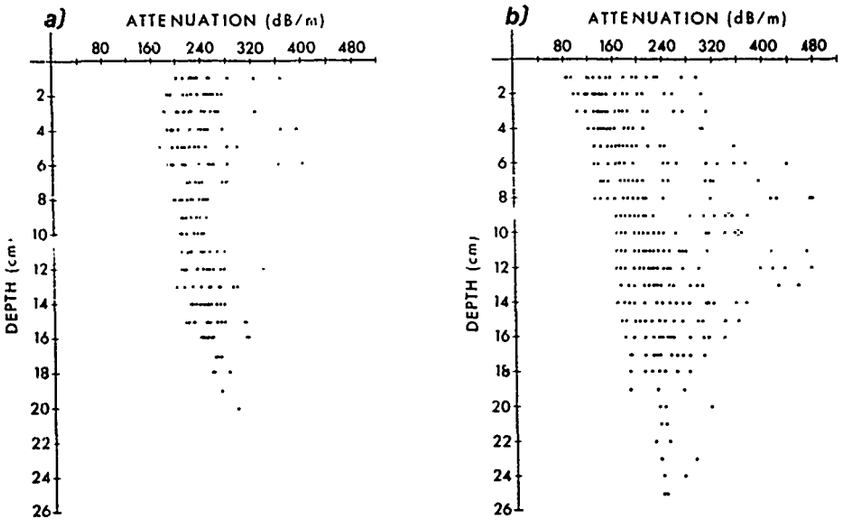

Fig. 3 Comparison of the variability and depth distribution of attenuation (dB/m at 400 kHz) for a one km² experimental site (a) and a larger presite survey area (b) off Panama City, Florida.

Several general observations can be made from the data presented in Table 2. Compressional wave attenuation consistently had the highest values of variation, and velocity the lowest. These results were expected given the previously reported range of values for compressional wave velocity and attenuation[12,14,15]. The coefficient of variation for mean grain size was generally higher than for porosity. The lowest coefficients of variation for mean grain size and compressional wave velocity were found at muddy sites, whereas attenuation and porosity exhibited the lowest coefficients of variation in fine hard packed sands. The highest variability of attenuation was found at sites with an high percentage of shell material.

Depth gradients in geoacoustic properties at several sites (FOAM, San Diego, Montauk Point, Washington and Charleston) accounted for a considerable percentage of variation of sediment geoacoustic properties. At the San Diego site compressional wave velocity and attenuation significantly correlated with depth (F-test, >0.001) for both fine and coarse sand substrates (see Fig. 1). The coefficients of variation for these properties after correction for depth gradients were 11.59 to 11.79 for attenuation and 0.72 to 0.79 for velocity. Depth gradients in geoacoustic properties at the San Diego and Montauk Point sites were the result of increased packing of sand-sized particles with depth[5,6]. At the FOAM site sediment laminations produced by storm induced erosional and depositional events resulted in the higher values of mean grain size and porosity and lowest values of compressional wave velocity between 5 to 15 cm depth in the cores[3,4]. Increased percentages of silt with depth at the Washington continental shelf site resulted in higher values of porosity and lower values of compressional wave velocity below 12 cm depth in the cores[7]. At both the Washington and Charleston sites the higher abundance of shell material with depth resulted in higher values of attenuation with depth[7,8]. Knowledge of the depth distribution of values of sediment geoacoustic properties can greatly increase predictability of these properties.

The magnitude of horizontal variation in geoacoustic properties varied considerably among sites. At the FOAM site in Long Island Sound horizontal patchy distribution of animals resulted in considerable variation in geoacoustic properties on scales of 10 to 100 meters[4]. At San Diego, sediments were classified as fine and coarse sands based on a mosiac created from overlapping tracks of side-scan sonar records[5]. Knowledge of the distribution of these two substrate types greatly reduced coefficients of variation of geoacoustic properties used in correlations with the values of acoustic bottom backscatter[16]. Side-scan mosaics from the Charleston, S.C. and Panama City sites also indicated considerable spatial variability in sediment types. The improved predictability of sediment geoacoustic properties for the Panama City site is clearly demonstrated in Table 2. At the Charleston site both horizontal and vertical variations in sediment geoacoustic properties must be taken into account to improve the predictability of sediment properties. Large scale horizontal variation, such as found in data collected from the Gulf of La Spezia, can usually be accounted for by utilizing detailed sediment distribution maps which are available for many continental shelf regions.

Table 3. Dominant factors affecting geoacoustic properties of sediment (xx = very important; x = important).

Experiment	Hydrodynamic Processes	Biological Processes	Relict (Inherited) Features
Long Island Sound	x	xx	
San Diego CA	xx		x
Montauk Point	x	x	xx
Quinault, Wash	xx		
Charleston S.C.	xx	x	x
La Spezia, Italy	xx		xx
Arafura Sea	x	xx	x
Panama City, Fl.	xx	x	

Sediment geoacoustic properties of many coastal marine sediments are controlled by the interaction of biological and hydrodynamic processes[3]. Table 3 presents the relative importance of these processes as well as that of relict (inherited) features in determining values and variability of sediment geoacoustic properties. Bioturbation (mixing of sediment by deposit-feeding animals) tends to reduce horizontal variation in sediment physical properties especially in fine grained sediments (NWC, Arafura Sea). The vertical gradients created by bioturbation are usually restricted to the upper 10 cm and are predictable on a seasonal basis given knowledge of biological processes present. A high abundance of tube dwelling species tends to stabilize the sediment surface, thus preserving the spatial variability of geoacoustic properties (FOAM). In fine sediment where the dominance of hydrodynamic and biological processes alternate horizontal and vertical variability is great and predictability poor (FOAM).

In sandy substrates, surface deposit feeding species, such as sand dollars, tend to reduce horizontal variability[5]. Feeding also reduces packing in the upper few centimeters increasing porosity and decreasing compressional wave velocity (Montauk Point, Panama City). At Montauk Point sand dollars were so abundant that they acted as surface point scatterers of acoustic energy[17]. The presence of surface and buried shell material contributes to considerable fine scale variation of geoacoustic properties (Quinault, Charleston, Arafura Sea and Panama City sites). The high values and variability of compressional wave attenuation associated with shell material are due to scattering from the shells as opposed to the intrinsic absorption described by Hamilton[12]. The distribution of shells in the sediment is controlled by both biological and hydrodynamic processes.

The random distribution and lack of preferred orientation of shells at the NWC and Arafura Sea sites suggests biological mixing processes were dominant, whereas hydrodynamic mixing processes control the distribution of shells at sandy sites (Charleston, Quinault and Panama City).

Large scale variability is generally controlled by hydrodynamic processes acting on given relict features. At the San Diego site a recently deposited fine-grained sand was found to be migrating over a coarser-grained offshore Pleistocene deposit[5]. At the Montauk Point site a light colored fine grained sand of modern origin discontinously covered a reddish granular sediment which was a lag deposit formed by the erosion of a drowned Pleistocene barrier spit[6]. At both locations the sand of modern origin was in dynamic equilibrium with recent storm events, whereas the coarser Pleistocene deposits were in equilibrium with winter storm events.

Hamilton and Bachman[14] presented data on geoacoustic properties from 340 sediment samples collected on the continental shelf and slope. They classified sediments into nine groups based on grain size. The coefficient of variation for porosity (range 5.0 to 13.8%; mean 10.3%) and compressional wave velocity ratio (0.7 to 3.2%; mean 2.3%) were much greater within those nine sediment classes then for the individual sites included in this study (Table 2). Direct measurements of geoacoustic properties are therefore preferred to predictions based on sediment type despite considerable fine-scale variability of geoacoustic properties demonstrated in this paper.

Briggs et al[18], using the same techniques employed here, characterized sediment geoacoustic property variability for three sedimentary provinces in the Venezuela Basin (3450 to 5050 m water depth) (see Table 2). Most of the variability was associated with vertical gradients of geoacoustic properties (cm) as opposed to horizontal variability (on scales of cm to km)[18]. As would be expected in the deep sea coefficients of variation for the carbonate and hemipelagic sites were lower than at most shallow-water sites, whereas the turbidite site had very high coefficients of variation. This variability resulted from the presence of alternating layers of pelagic and terrigeneous sediments. This study indicates the importance of considering the variability of geoacoustic properties for geoacoustic modelling of both deep-sea and shallow water sediments.

ACKNOWLEDGMENTS

I wish to thank Kevin Briggs and Ricky Ray of NORDA for their assistance in data collection, laboratory analysis and data preparation. I also thank Dave Young for his encouragement and support during field exercises and report preparation. Data collection and analysis were conducted while the author was at the Naval Ocean Research and Development Activity and was supported by NAVSEA Program Element 62759N (Bob Martin, Program Mgr) and NORDA Program Element 61153N (Herb Eppert, Program Mgr). The paper was written at the SACLANT ASW Research Centre (R.R. Goodman, Technical Director).

REFERENCES

1. E.L. Hamilton, Geoacoustic modelling of the sea floor, J. Acoust. Soc. Am. 68: 1313-1340 (1980).
2. M.D. Richardson and D.K. Young, Geoacoustic models and bioturbation, Mar. Geol. 38: 205-218 (1980).
3. M.D. Richardson, D.K. Young, and K.B. Briggs, Effects of hydrodynamic and biological processes on sediment geoacoustic properties in Long Island Sound, USA, Mar. Geol. 52: 201-226 (1983).
4. M.D. Richardson, D.K. Young, and K.B. Briggs, Acoustical, physical and biologial properties of surface sediment cores collected from Long Island Sound, August 27-28, 1980, NORDA TN 150. NSTL, MS, Naval Ocean Research and Development Activity, (1982). [AD A 118 183]
5. M.D. Richardson, D.K. Young, and R.I. Ray, Environmental support for high frequency acoustic measurements at NOSC Oceanographic Tower, 26 April - 7 May 1982; Part I: Sediment geoacoustic properties, NORDA TN 219. NSTL, MS, Naval Ocean Research and Development Activity, (1983).
6. M.D. Richardson, J.H. Tietjen, and R.I. Ray, Environmental support for Project Weapons Environmental Acoustic Program (WEAP) East of Montauk Point, New York, 7-28 May 1982, NORDA Report 40. NSTL, MS, Naval Ocean Research and Development Activity, (1983). [AD A 139 800]
7. M.D. Richardson, K.B. Briggs, R.I. Ray, and W.I. John, Environmental support for high frequency acoustic experiments conducted at the Quinault Range off the Washington Coast, 28 April - 1 May 1983. NORDA Report. NSTL, MS, Naval Ocean Research and Development Activity, (1985).
8. M.D. Richardson, Environmental bottom characterization required for modeling and prediction of high-frequency acoustic bottom scattering, J. Acoust. Soc. Am. 75: S50-S51 (1984).
9. T. Akal, P. Curzi and E. Michelozzi, Geoacoustic measurements: physical property variations and sedimentary processes. In: Convegno sul tema: La Geologia Marina — aspetti di ricerca pura ed applicata. S. Benedetto del Tronto, 16-18 aprile 1984, Ascoli Piceno, Societa' Geologica Italiana (to be published).
10. S. Stanic, M.D. Richardson, P. Fleischer and B.E. Eckstein, High frequency acoustic bottom scattering experiments conducted off Panama City, Florida. NORDA Report. NSTL, MS, Naval Ocean Research and Development Activity, (1985).
11. E.L. Hamilton, Prediction of in-situ acoustic and elastic properties of marine sediments, Geophys. 36: 266-284 (1971).
12. E.L. Hamilton, Compressional-wave attenuation in marine sediments, Geophys. 37: 620-645 (1972).
13. R.L. Folk and W.C. Ward, Brazos River bar, a study in the significance of grain size parameters, J. Sediment. Petrol. 27: 3-26 (1957).
14. E.L. Hamilton and R.T. Bachman, Sound velocity and related properties of marine sediments, J. Acoust. Soc. Am., 72: 1891-1904 (1982).
15. T. Akal, The relationship between those physical properties of underwater sediments that affect bottom reflection, Mar. Geol., 13: 251-266 (1972).
16. H. Boehme, N.P. Chotiros, L.D. Rolleigh, S.P. Pitt, A.L. Garcia, T.G. Goldsberry, and R.A. Lamb, Acoustic backscattering at low grazing angles from the ocean bottom. Part I. Bottom backscattering strength, J. Acoust. Soc. Am., 77: 962-974 (1985).
17. W.I. Roderick and R.K. Dullea, High resolution bottom backscatter measurements, NUSC Tech. Document 7181. New London, CT, Naval Underwater Systems Center, (1984).
18. K.B. Briggs, M.D. Richardson, and D.K. Young, Variability in geoacoustic and related properties of surface sediments from the Venezuela Basin, Caribbean Sea. Mar. Geol. (in press).

EVALUATION OF EXPERIMENTAL TECHNIQUES FOR DETERMINING THE PLANE WAVE REFLECTION COEFFICIENT AT THE SEA FLOOR

Henrik Schmidt and Finn B. Jensen
SACLANT ASW Research Centre
I-19026 La Spezia, Italy

ABSTRACT

One of the most commonly used techniques for determination of the geoacoustical properties of the sea bed is the measurement of plane wave reflection coefficients at the ocean bottom. An incident field is produced by either an explosive source or a beam generating device and the reflected field is then detected by means of an array of hydrophones. The associated angles of incidence have traditionally been determined by simple geometrical considerations. However such simple interpretations give results that in some cases depend on the actual experimental geometry. For example critical angles can appear far away from the correct values or not be present at all. Here an exact numerical model is used to examine the different experimental techniques. The observed discrepancies are explained, both for the point and beam source experiments. In addition, guidelines are given for interpretation of results obtained by the different experimental techniques.

INTRODUCTION

The importance of the sea bed geoacoustic properties for shallow water sound propagation is well established, and reliable transmission loss predictions obtained by means of numerical propagation models therefore require accurate knowledge of the sea bed properties. The traditional raytrace propagation models require a plane wave reflection coefficient at the bottom in order to account for the bottom loss. More recent wave theory models like those based on normal modes, the full wavefield fast field programs (FFP) and the parabolic equation models (PE), require a more detailed knowledge of the wave speeds, attenuations and densities in the sea bed. These parameters could in principle be obtained from samples, but due to the fact that the low-frequency acoustic waves penetrate deeply, very deep and expensive boreholes would be required. Further, and often more important, the de-pressurisation and change of temperature, unavoidable in the core sampling process, tend to deteriorate the mechanical and chemical bondings in the sediment material, and thus heavily influence the properties, shear in particular.

The geoacoustic properties therefore primarily have to be determined from in-situ propagation experiments. One of the most common experimental

techniques is the determination of the plane wave reflection coefficient at the sea floor. This approach has two advantages: the results can be used directly by the raytrace models, and the plane wave reflection coefficient is needed as an input parameter in most inverse schemes for the determination of bottom properties [1].

Several experimental techniques have been devised with the objective of determining the reflection coefficients directly. They are all based on the detection, by hydrophones, of the bottom reflected part of the field produced by a sound source placed in the water column. The source has been either an omnidirectional explosive source or a device producing a narrow beam of sound directed towards the sea floor at a variable angle of incidence. However, several authors have shown that the results obtained are usually not directly interpretable as plane wave reflection coefficients.

Here we will use the full wavefield SAFARI model [2,3], to demonstrate how these discrepancies arise, and to show how numerical models are not restricted to interpretational purposes, a traditional application in underwater acoustics, but can also be used for the design and planning of experimental setups.

EXPLOSIVE SOURCE EXPERIMENTS

The most common experimental technique for determination of plane wave reflection coefficients uses an explosive omnidirectional source to generate a transient field. The hydrophone array used as a detector may be either horizontal or vertical, moving or fixed (Fig. 1).

By assuming that the source and receivers are so far apart that the bottom-interfering eigenrays can be considered plane waves when hitting the bottom, a very simple interpretation technique has been used. First the nominal specular reflection angle at the bottom is determined for each receiver by means of simple raytracing. Then the received signals are split into a direct part and a bottom reflected part by inspection. After correction for different travel paths, the reflection coefficient is found simply by dividing the frequency spectrum of the reflected signal by that of the direct signal.

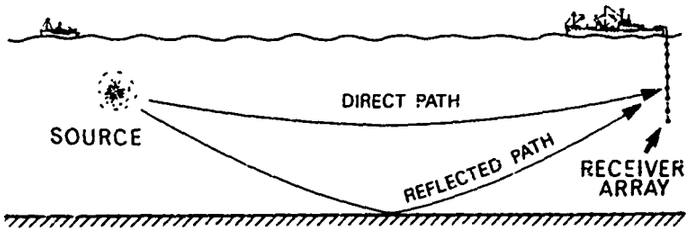

Fig. 1 Experimental set up for bottom reflection-loss measurements by means of an explosive source and a vertical hydrophone array.

The obvious advantage of the explosive source experiments is the possibility of separating the different arrivals in the time domain, and hence to eliminate unwanted surface multiples. Further, the experiments are cost-effective because they do not require any specialized equipment. As pointed out by several authors, however, the simple interpretation technique outlined above is only rarely applicable. Stickler [4] and Santaniello et al [5] demonstrated that the simple interpretation technique will give wrong reflection coefficients when the bottom is upward refracting or has deeper, reflecting interfaces, because of the interference between the different arrivals. Non-physical effects like negative bottom loss and source/receiver position-dependent results arise. The critical angle shift pointed out by Stickler [4] is due to the same effect. Even in the case of an isovelocity bottom with a sound speed higher than that of the ocean, the headwave formation will give rise to the same phenomenon. The simple interpretation technique can be applied only in the rather unusual case of a purely downward refracting or homogeneous bottom with a sound speed less than that of water.

We will here illustrate the limitations of the simple interpretation principle by simulating an explosive source experiment in a very simple ocean environment by means of the SAFARI full-wavefield model. The sound speed profile is shown in Fig. 2. The water is characterized by an upward refracting profile close to the bottom, and surface multiples of no present interest are avoided by replacing the ocean above -800 m by an isovelocity halfspace. The fluid bottom is upward refracting to 30 m below the seabed. Below this depth it is represented by an isovelocity halfspace. In order to more clearly illustrate the phenomenon, the bottom is considered lossless. Thus the reflection loss is identically zero for grazing angles less than the critical 14.6° onto the water-bottom interface.

An explosive source is assumed to be placed 400 m above the bottom and the radiated pressure pulse has a duration of 10 ms and a centre

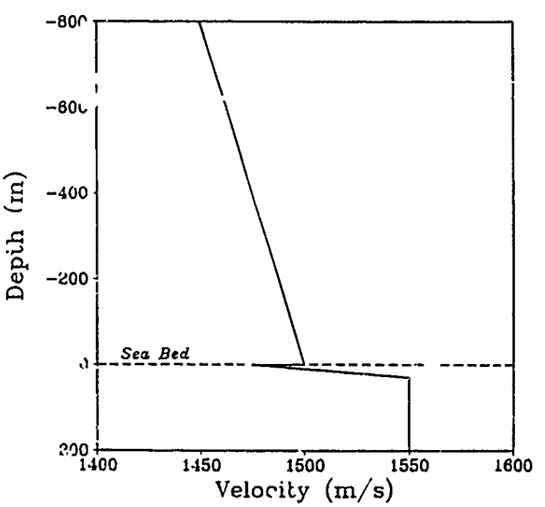

Fig. 2 Sound speed profile for simulation of experiment. Depth 0 m refers to the sea bed.

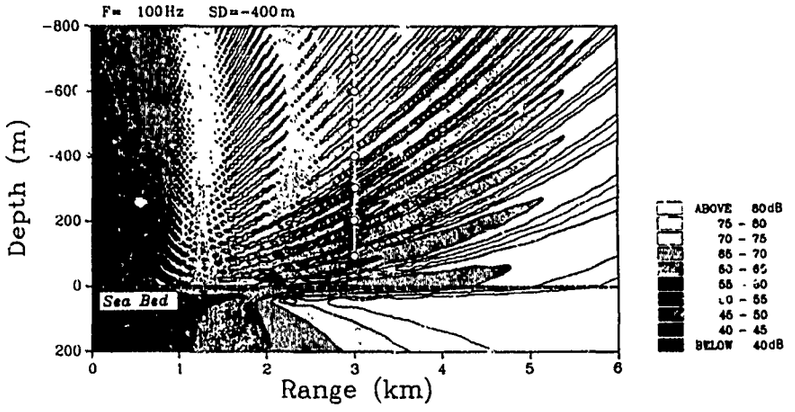

Fig. 3 Transmission loss contours at 100 Hz for a point source 400 m above the bottom. Hydrophone array used for pulse calculations is indicated by o.

frequency of 100 Hz. Figure 3 shows the transmission loss contours in depth and range at the centre frequency (black indicating highest intensity). The Lloyd-mirror pattern due to the interference between the direct and the bottom reflected fields is evident and illustrates the complexity of the sound field even in this very simple case.

A vertical array of 7 hydrophones with 100 m spacing is placed 3 km from the source as indicated in Fig. 3. The synthetic hydrophone signals for this array are shown in Fig. 4, with each trace being identified by the nominal specular angle of the reflected signal at the ocean bottom, as separated from the reflected parts, which, however, do not clearly

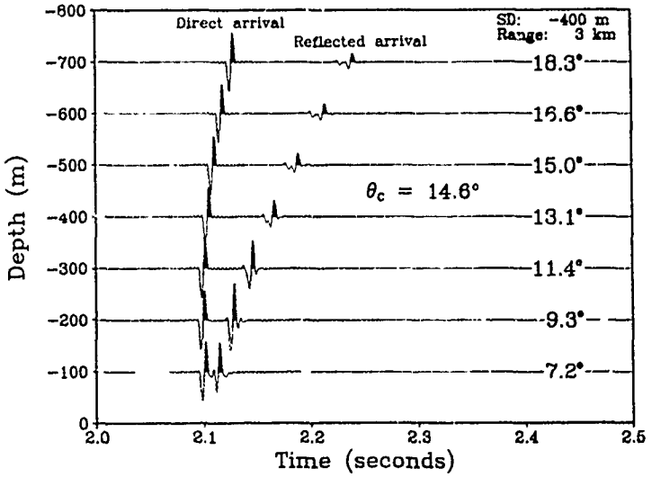

Fig. 4 Synthetic hydrophone signals for vertical array at 3 km range. Each trace is identified by its corresponding nominal specular reflection angle.

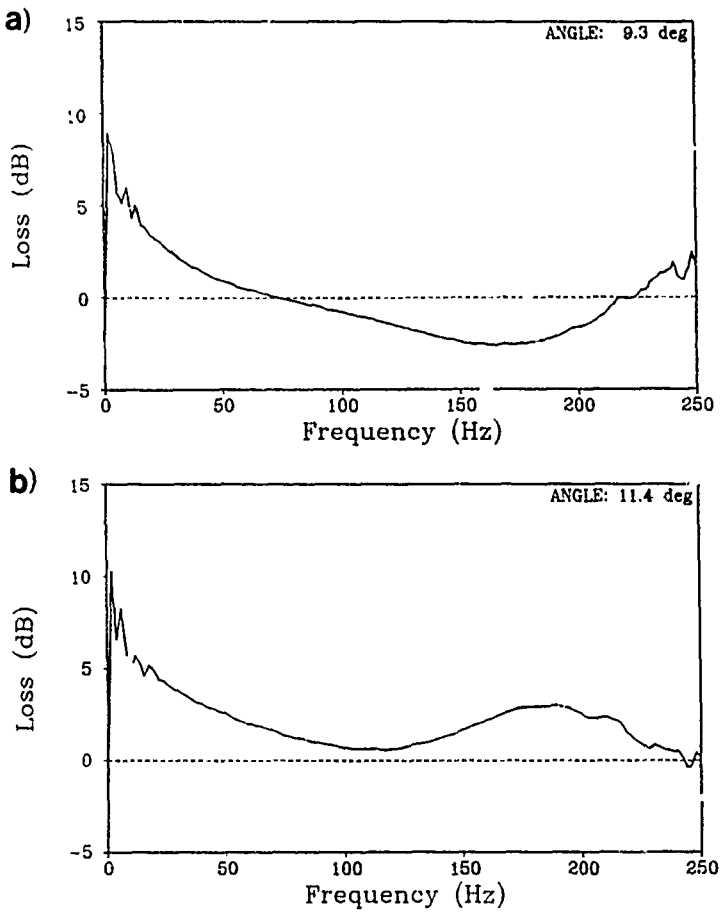

Fig. 5 Reflection coefficients determined by deconvolution of synthetic signals: a) 9.3°, b) 11.4°

indicate the critical angle of 14.6°. Further, the trace corresponding to 9.3° indicates an apparent negative bottom loss. These properties are also indicaced by the reflection coefficients obtained by the simple deconvolution principle for the grazing angles 9.3° (Fig. 5a) and 11.4° (Fig. 5b) respectively. Both angles are less than critical; therefore the reflection loss should be zero in both cases. The "ringing" at low and high frequencies is due to the very low energy content of the source pulse at these frequencies, but even in the central frequency interval errors of several dB are obtained.

Figure 6 outlines the different travel paths yielding errors in the reflection coefficients obtained by the simple technique. The possibility of multiple paths, due to headwaves (1), upward refracting profiles (2) or reflecting interfaces (3), yields results which are dependent on whether the different arrivals are interfering constructively or destructively, which is again dependent on the source-receiver positions. As is also clear from Fig. 6, the multiple arrivals do not correspond to the same angle as the nominal specular reflection angle at the water-bottom

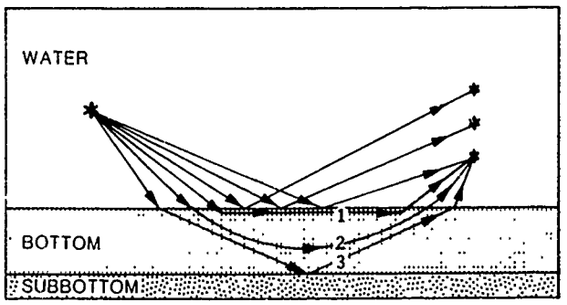

Fig. 6 Additional arrivals obstructing simple deconvolution. 1) Headwaves, 2) Upward refracted arrivals, 3) Deep reflection.

interface. The field detected by each hydrophone is therefore not a single plane wave component, as is assumed when the simple interpretation technique is used, but a complicated interference between several different components.

This phenomenon directly leads to the conclusion that in order to obtain the plane wave reflection coefficient from explosive source experiments, some kind of beamforming, or plane wave decomposition, has to be applied to the received signals. In principle this could be done by using towed arrays. However, at the low grazing angles, often of main interest, this technique requires very long arrays because the bottom refracted signals travel a long distance before re-entering the water column, and the whole reflected field has to be covered by the array. Therefore, a synthetic aperture technique, as proposed by Frisk et al [6], is often more convenient than the use of a towed array.

BEAM EXPERIMENTS

In contrast to the omnidirectional explosive source described above, a source that generates an approximate plane wavefield would provide the opportunity to directly measure the plane wave reflection coefficients. This is the philosophy behind the use of beamed sources, as shown schematically in Fig. 7. A beam is directed towards the water-sediment interface at a nominal angle of incidence, and the reflected beam is measured in the specular direction by means of a hydrophone.

It is well known, however, that very wide beams are required in order to simulate plane wave behaviour. This is due to the fact that a beam of finite width has a finite angular spectrum, whereas for a plane wave the angular spectrum is infinitely narrow [3]. For practical reasons this technique has therefore not been a realistic alternative to the explosive source experiments until the development of the parametric transducer [7]. In principle, this transducer generates a virtual endfire-array that is the source of a highly directional beam which can be used for measurement of plane wave reflection coefficients [8]. In practice, however, the virtual array will have a finite length, and thus results in the beam having a finite angular spectrum.

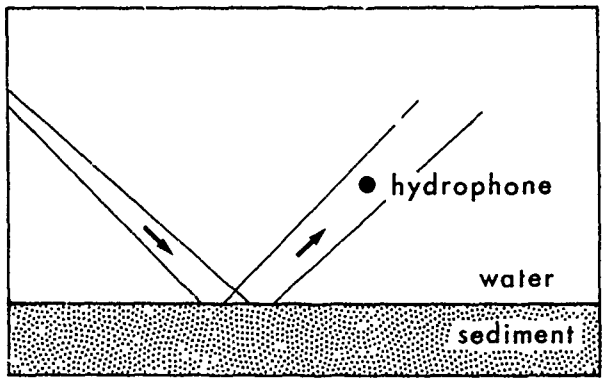

Fig. 7 Reflection of a narrow beam from the sea bed.

We will here use the SAFARI model to demonstrate how a velocity profile in the ocean close to the bottom influences the reflection of a realistic, narrow beam at low grazing angles. The environment shown in Fig. 2 is also used for this study. A vertical source array of 61 elements at half-wavelength spacing, placed 400 m above the bottom is used to generate a narrow beam, 6 wavelengths wide at the sea bed, measured between the 3-dB down points. The array is phased to yield a nominal grazing angle of 2.5°, 5° and 10° at the sea bed.

The resulting fields are shown in Fig. 8 (black indicating highest intensity). The contour interval is 2 dB, but the actual dB values are arbitrary. Obviously the beams are not specularly reflected. At the two smallest grazing angles, Figs. 8a and 8b, a clear beam splitting occurs, and the reflected beam with highest amplitude has a much smaller grazing angle than the incident beam. A comparison with Fig. 3 shows that the directions of the split beams correspond to those of the lowermost lobes of the Lloyd-mirror pattern in the point source field. This indicates that the angular spectrum of the beam is apparently so wide that the interference between the direct, but upward refracted, purely waterborne arrivals and those reflected off the bottom is important. This assumption is supported by the calculated angular spectrum of the 5° beam at the bottom, shown in Fig. 9. The beam is seen to contain significant energy at grazing angles in the interval of 1° through 12°. Figure 8c indicates that the splitting effect due to the interference decreases for higher grazing angles, as expected, but although the energy is here concentrated in a single beam, a significant widening of the beam cross-section has occured. Even at this relatively high grazing angle, a single hydrophone in the specular direction would not yield the right value of the reflection coefficient; instead it would indicate too high a reflection loss.

Even in the ideal case of an isovelocity water column over a homogenous bottom, it was shown by Muir et al [8], that narrow parametric beams could penetrate into the bottom at grazing angles less than critical. This problem has been treated theoretically by several authors. Tjotta and Tjotta [9] presented a wide beam approximation showing the effect qualitatively. Schmidt and Jensen [3] used the SAFARI model to simulate the experiments in which extremely narrow beams, not covered by the approximate theory, were used. The reported beam cross-section at the bottom interface was simulated by means of a focusing linear array.

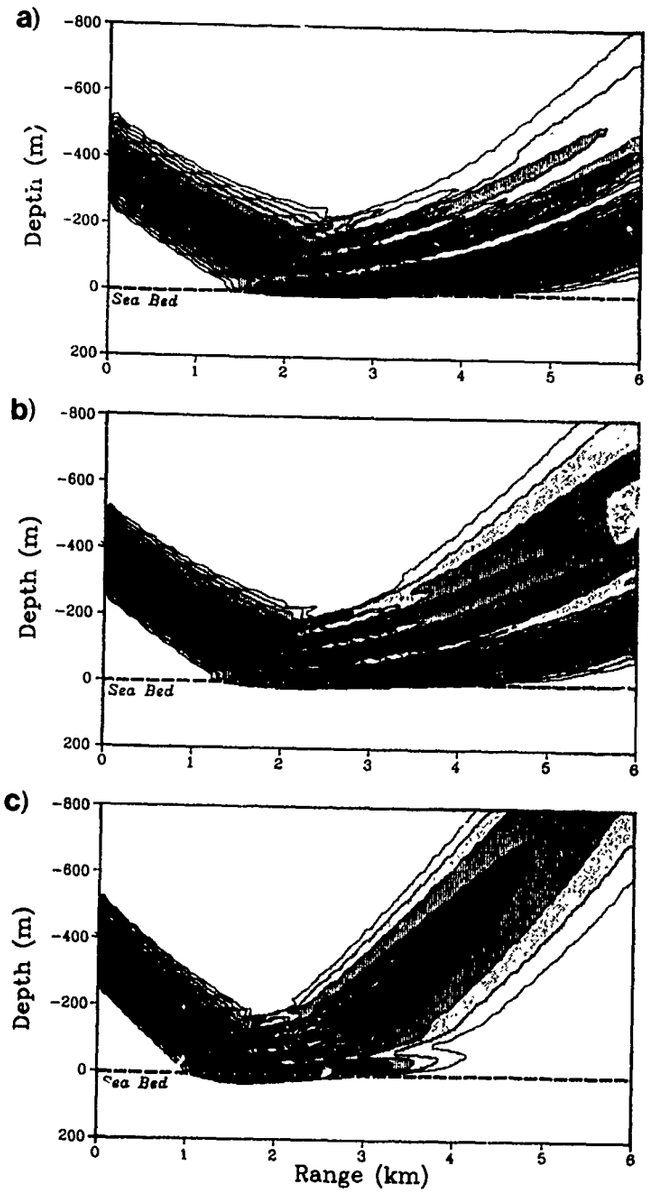

Fig. 8 Field contours at 100 Hz for an incident beam of 6 wavelengths width at 3 nominal grazing angles: a) 2.5°, b) 5° and c) 10°. (Contour interval = 2 dB).

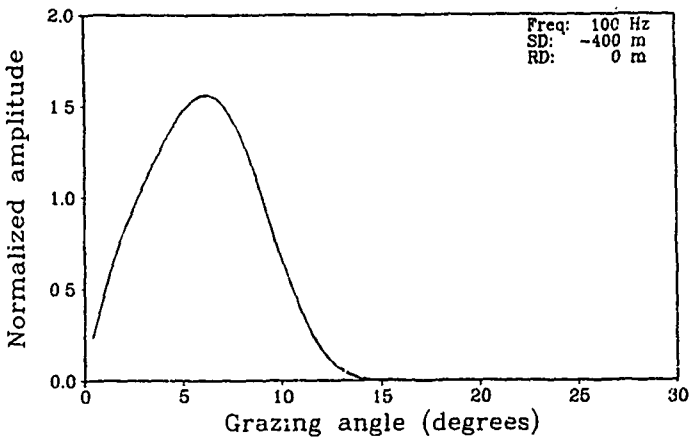

Fig. 9 Angular spectrum of beam at the ocean bottom for nominal grazing angle of 5°.

The results demonstrated that subcritical penetration is a simple consequence of the basic physical principle that a narrow beam has a wide angular spectrum. Thus the narrow beam may contain energy that propagates at grazing angles greater than critical although the nominal angle of incidence is subcritical. The results further showed that, for the same reason, the reflected beam was not specular, but shifted towards a smaller grazing angle. In conclusion, the parametric beams in practice are narrow and not highly directional as often stated, and hence they are a poor approximation to a plane wave.

To summarize, the use of beam sources does not yield the possibility of measuring the plane wave reflection coefficients directly by means of a single hydrophone. As was the case for the explosive sources, plane wave decomposition has to be applied to the reflected field. However, the advantage of using beam sources is that smaller arrays or synthetic apertures can be used because only a limited part of the angular spectrum is activated by the beam.

CONCLUSION

A full wavefield numerical model has been used to demonstrate that neither explosive source techniques nor narrow beam techniques yield the plane wave reflection coefficients directly. It has been demonstrated, that the narrow beams are not highly directional, and thus do not behave like plane waves. Therefore, both experimental techniques require the application of either plane wave decomposition or beamforming to the reflected field in order to correctly determine the plane wave reflection coefficients.

REFERENCES

1. D.J. Thomson, The determination of material properties of the sea-bed from the acoustic plane-wave reflection response, In: Acoustics and the Sea-Bed, Ed. N.G.pace, Bath University Press, Bath, UK, 41-50, (1983).

2. H. Schmidt and F.B. Jensen, A full wave solution for propagation in multilayered viscoelastic media with application to Gaussian beam reflection at fluid-solid interfaces, J. Acoust. Soc. Am. 77(3), 813-825, (1985).

3. H. Schmidt and F.B. Jensen, Efficient numerical solution technique for wave propagation in horizontally stratified ocean environments, Rep. SM-173, SACLANT ASW Research Centre, La Spezia, Italy, (1984).

4. D.C. Stickler, Negative bottom loss, critical-angle shift, and the interpretation of the bottom reflection coefficient, J. Acoust. Soc. Am. 61(3),707-710, (1977).

5. S.R. Santaniello, F.R. DiNapoli, R.K. Dullea and P.D. Herstein, Studies on the interaction of low-frequency acoustic signals with the ocean bottom, Geophysics, 44(12), 1922-1940, (1979).

6. G.V. Frisk and J.F. Lynch, Shallow water waveguide characterization using the Hankel transform, J. Acoust. Soc. Am. 76(1), 205-215, (1984).

7. H.O. Berktay, Parametric Sources - Design Considerations in the Generation of Low-Frequency Signals (this volume).

8. T.G. Muir, C.W. Horton,Sr. and L.A. Thompson, The penetration of highly directional acoustic beams into sediments, J. Sound Vib. 64(4), 539-551, (1979).

9. J.N. Tjotta and S. Tjotta, Theoretical study of the penetration of highly directional acoustic beams into sediments, J. Acoust. Soc. Am. 69, 998-1008, (1981).

INTERFACE WAVE STUDIES ON THE LIGURIAN SHELF USING AN OBS ARRAY: EXPERIMENTAL RESULTS AND PROPAGATION MODELS

Michael Snoek, Guido Guidi, Enzo Michelozzi
SACLANT ASW Research Centre
Viale San Bartolomeo 400
I-19026 La Spezia, Italy

ABSTRACT

Seismic waves travelling in the water/sediment or subbottom sediment/sediment interface have been the subject of considerable interest in recent years. Experiments have confirmed the existence of interface waves in different geological environments. Some progress has been made in understanding the propagation and attenuation characteristics of these waves. However, the generating mechanisms are poorly understood. In particular, what are the roles of geometry and bottom characteristics in coupling waterborne sound into the sea bottom? What is the acoustic-to-seismic energy conversion process? Using explosives as sound sources, an experiment was performed in which the propagation along different interface paths was measured by an array of three tri-axial ocean bottom seismometers. To obtain realistic input data for the propagation models, continuous seismic profiles were run and cores were taken along the propagation path. Results of these experiments and a comparison of measured and modelled data are presented.

INTRODUCTION

Results from SACLANTCEN experiments and other published data show that the propagation and attenuation characteristics for seismic interface waves are still poorly understood and are ofttimes ambiguous (Ali & Schmalfeldt [1] and Jensen & Schmidt [2]).

Rauch [3,4] has outlined the theoretical background for the mathematical treatment of interface waves. Jensen & Schmidt [2] have also presented a modelling approach to reconstruct shear speed and shear attenuation from interface waves for the upper relevant sediment layers.

Unclear, however, is how and under which conditions acoustic energy converts into seismic energy. It has been frequently observed that in changing the bearing of a profile or the frequency spectrum of the source propagation, interface wave characteristics can change dramatically. The changes can range from signal enhancement to disappearance. Before a reasonable prediction of attenuation and propagation characteristics can be made, the driving mechanism for interface wave conversion and propagation have to be carefully studied.

To describe this conversion, one must determine the sensitivity of the process to differences in the physical properties and geometry of the surface layers, to geological structure, to the frequency content of the seismic source and to the bearing and position of the source with respect to the receiving sensors. The interrelations of these parameters affect the complexity of the conversion process. The interpretation of the data has to be supported by a modelling phase based on input data which should be as complete as possible. This requires a multi-parameter survey involving methods and systems schematically shown in Fig. 1.

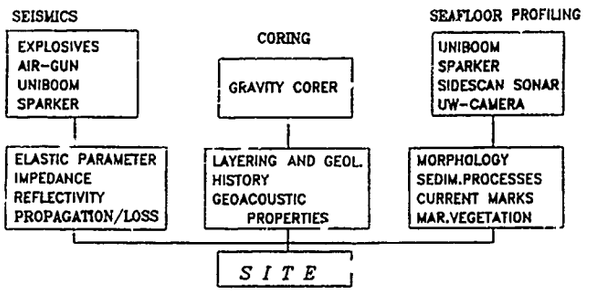

Fig. 1
Direct and indirect methods of investigations for a detailed ocean bottom/subbottom survey

INTERFACE WAVE STUDIES

We have conducted a set of experiments on the Ligurian shelf off La Spezia, Italy, to study the interface waves along different propagation paths (Fig. 2) in a region where we could expect silty clay and clayey silt layers over a more sandy subbottom.

The instrumentation and the setup of SACLANTCEN interface wave experiments have been described in detail by Rauch & Schmalfeldt [5] and Ali & Schmalfeldt [1]. We operated with two ships and deployed three tri-axial ocean bottom seismometers in a triangular configuration, with distances of 537 m, 352 m and 315 m between them. All distances were relative to a marker buoy. Positions were controlled by Loran C, satellite navigation, radar, and terrestrial navigation.

Charges were fired electrically on the sea bottom, their sizes ranging from 180 g (standard size) to 1080 g. The data were available a short time after each shot, thus allowing for correction of charge size if necessary. After the shot instant, the distances to the receivers were controlled by using the unprocessed recordings; all data were bandpass-filtered, 2-14 Hz, and stacked in time-distance plots. The response of the four sensors of seismometer No. 2, for different runs B and C, are displayed in Figs. 3 and 4. In Fig. 5 we see the response of the z-component (the vertical seismometer) for profiles of different azimuth. We can trace interface wave phases up to a range of 4 km; beyond that the signal-to-noise ratio becomes too small. However, even for the close ranges different modes cannot be identified easily. This is a further indication of a rather complex subbottom structure. We marked events of the interface wave train and correlated them with group velocities, as shown in Table 1. The values obtained are in the expected range and typical for the environment encountered. They show a certain scatter, amounting to about 6% for the slow end and 35% for the higher end of the interface wave train for profiles A-B and C-D. On profile F, however, velocities are considerably higher (see Table 1), remarkable because profiles B and F vary in direction by only 9°. The data also contains p-wave phases travelling as headwaves or refracted waves in deeper interfaces with velocities of 1.8 to 2.4 km/s. These data will be included when modelling the full wave field.

We calculated the interface wavelet energy generated by standard charges for different runs and varying ranges. Having only a few profiles, we obtained information on the distribution of interface wave energy for selected azimuthal angles, rather than a continuous azimuthal distribution of energy. We compared two pronounced frequency bands of 4-5 Hz and 8-9 Hz for three different ranges (Fig. 6). There are considerable differences in energy levels, ranging as high as 18 dB. At this stage, however, the results apparently are contradictory, with inconsistency in range and frequency.

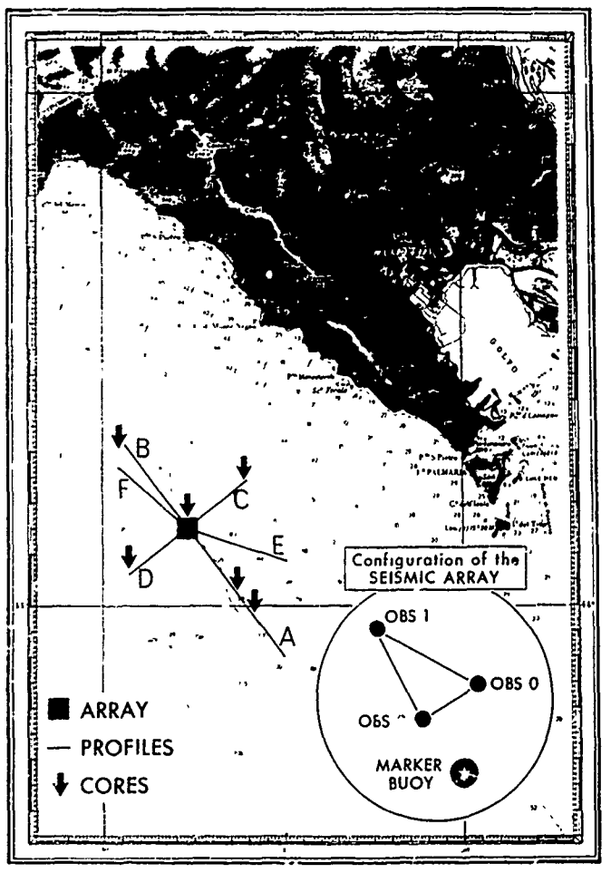

Fig. 2 Area of operation: Ligurian Sea off the coast of Italy

Whereas we can observe a trend in the behaviour for the 8-9 Hz frequency band - lowest attenuation in direction of profile D and highest attenuation on profile B (data were not available at all ranges for profile F) - no general trends can be observed for the 4-5 Hz frequency band. As with the group velocity analysis, the most pronounced effects can be observed on profile F, where we find extremal values for the attenuation, hignest for the 8-9 Hz frequency band and, at the same range, the lowest for the 4-5 Hz frequency band. This analysis was based on only three ranges and two frequency groups; further analysis should reveal a more coherent picture of spatial energy distribution when extended to full range and all frequencies.

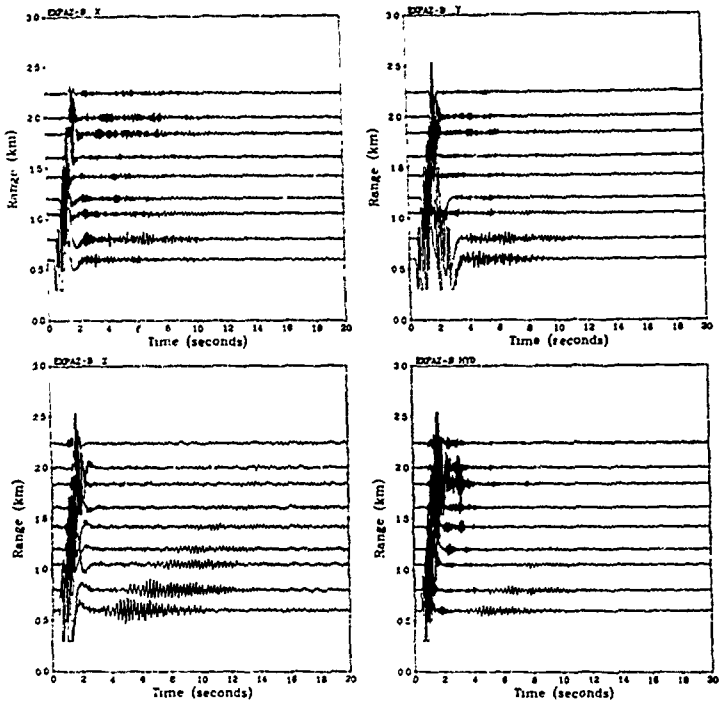

Fig. 3 Stacks of seismograms for profile B, X = radial, Y = transversal, Z = vertical and HYD = hydrophone data

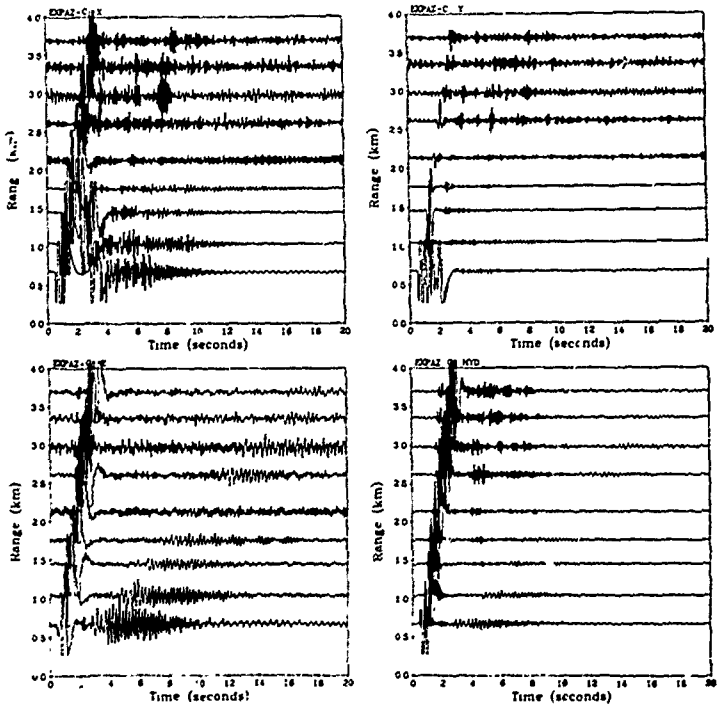

Fig. 4 Stacks of seismograms for profile C, X = radial, Y = transversal, Z = vertical and HYD = hydrophone data

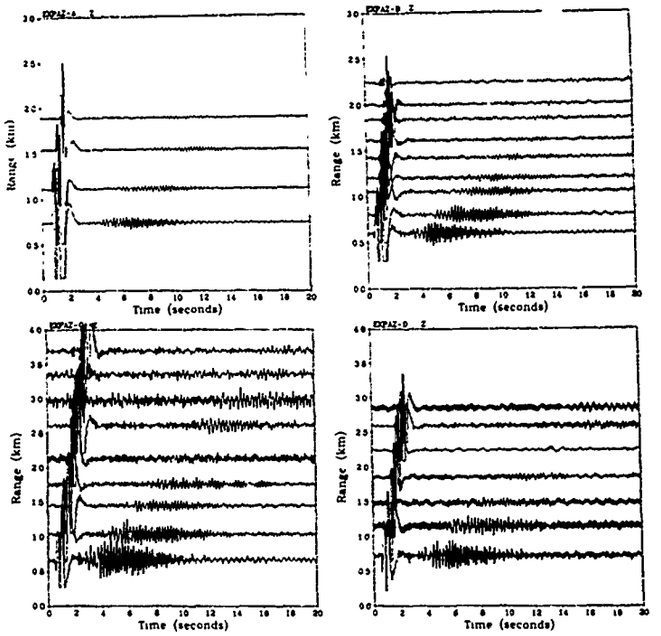

Fig. 5 Stacks of seismograms for profiles A, B, C, D. Only the Z-component is displayed.

PROF.A	65	122	17-	260
PROF.B	60	121	154	190
PROF.C	62	132	228	296
PROF.D	66	14-	192	242
PROF.F	88	210	235	325
	Group velocities (m/s)			

Table 1
Interface mode velocities

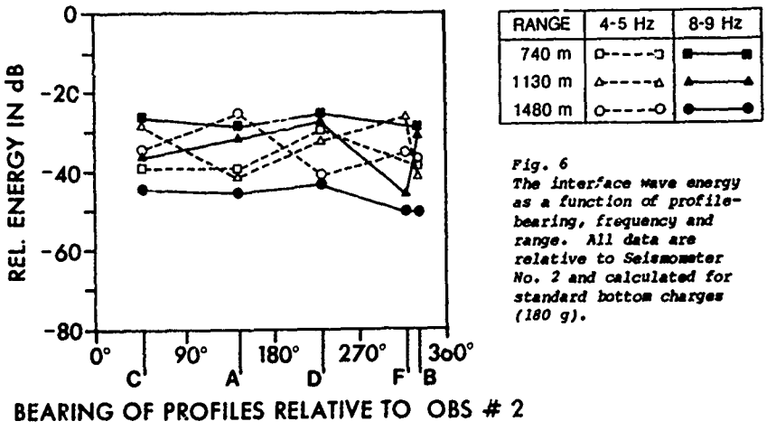

Fig. 6
The interface wave energy as a function of profile-bearing, frequency and range. All data are relative to Seismometer No. 2 and calculated for standard bottom charges (180 g).

A further approach in analyzing the interface wave trains was to apply the multiple filter technique or dispersion analysis suggested by Dziewonski [8]. This technique provides a tool to separate modes of different order in a seismogram. However, this procedure has limitations in this case because the interface wave trains display only a poor modal structure.

We will present herein a characteristic case, which will also be used in modelling the data by applying an inverse method. The dispersion analysis was run and displayed in a Gabor matrix of the data from profile C. Prior to the analysis a conceptual rotation of the geophone orientation was performed, i.e. an operation was applied to obtain maximum response of the radial sensor in the direction of the profile. We determine the radial (R) and transverse (T) components from the actual X and Y components of the seismometer for a given source bearing θ by:

$$R = x \cos\theta + y \sin\theta$$

$$T = -x \sin\theta + y \cos\theta$$

Hence, only Gabor matrices for the radial and vertical components are displayed, (Fig. 7). The most striking feature is the high velocity gradient effective over a very narrow frequency band of 2 Hz. We find a reduction in group velocity from about 260 m/s to 74 m/s over a frequency range from 3.5 to 5.5 Hz. In addition to this we find some further features of interest on the radial geophone data, marked as local maxima, which at this stage are taken as indicators of the complexity of the subbottom structure.

Earlier experiments by Essen et al [6], Rauch & Schmalfeldt [5] and Schmalfeldt & Rauch [7] have clearly demonstrated a correlation between the physical properties of the seafloor and subbottom and the propagation characteristics of interface waves. Therefore in this area, with its pronounced lateral variations in sedimentation rates and processes, the effects depend on the bearing (direction) of the profiles. Further, there is always a certain amount of scatter involved in arrival times of seismic waves travelling near the surface of the crust, or, in this case, in the top sediment layers. Because of this, one cannot attribute with certainty the observed effects to anisotropy or to lateral heterogeneities.

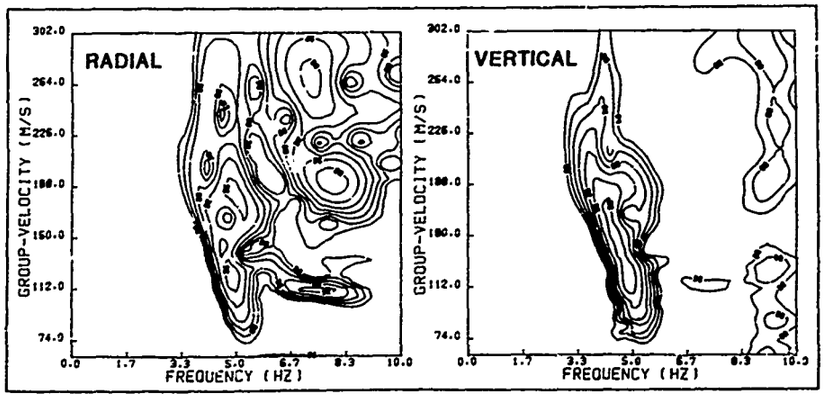

Fig. 7 Gabor matrix for shot No. 2 on profile C (see Fig. 2) for range 0.552 km. Displayed are the vertical and radial components.

Prior to the actual interface wave experiment a set of high resolution seismic UNIBOOM profiles were run. The experiment had three goals: to determine experimentally relevant coring locations, to enable later correlation of geoacoustical parameters and geological features and to map the topography of the top layers.

Two typical profiles are shown: profile A-B with a bearing of 320° (Fig. 8), and profile C-D with a bearing of 25°, representing a sloping

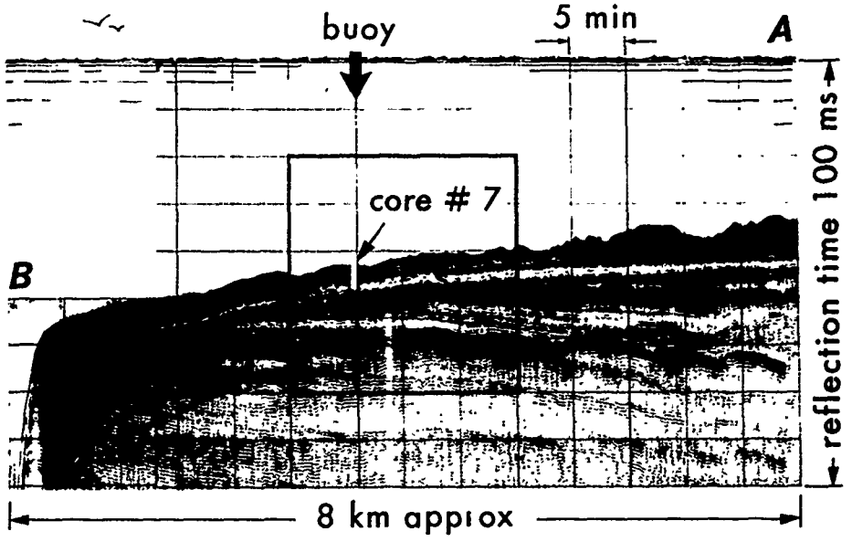

Fig. 8 Reflection seismic UNIBOOM profile A-B

seabottom (Fig. 9). Profile A-B has a uniform water depth (it follows the 100 m contour; all other profiles crossed contour lines).

The major structural feature recorded on profile A-B is a slightly tilted reflecting surface that outcrops on the slope. This reflector, which is interpreted as the bedrock surface during the last glacial period, shows fracturing as well as erosion. It is overlain by sediment wedges that thin out towards the slope and consist of some weaker reflectors, a dark band of sediments with some surface roughness and a laminated top layer. In general we can distinguish two different regions: the western part with a more regular and uniform sedimentation and an eastern part that displays strong lateral variations in sediment accumulation. This coincides with results from the seismic runs, which indicate that at a range greater than 2.5 km eastwards from seismometer No. 2 either poor or no interface wave trains were recorded. On profile C-D the most interesting features are cross bedding and the slumps, indicators of recent sediment dynamics. Marks of earlier gravitational sliding as well as the stratification of the upper sediments can be clearly identified.

Eleven cores were taken with a recovery range from 2.0 to 3.95 m and an average recovery of 3.80 m. Three of the cores were taken along profile A-B: One was taken at the site of the seismometer, one on the slope, and one in the region of anomalous sediment accumulation (see Fig. 2). Eight cores were taken along the other profiles to allow for spatial interpretation of sediment distribution. The No. 7 core, closest to the array, has been analyzed and the others have been inspected.

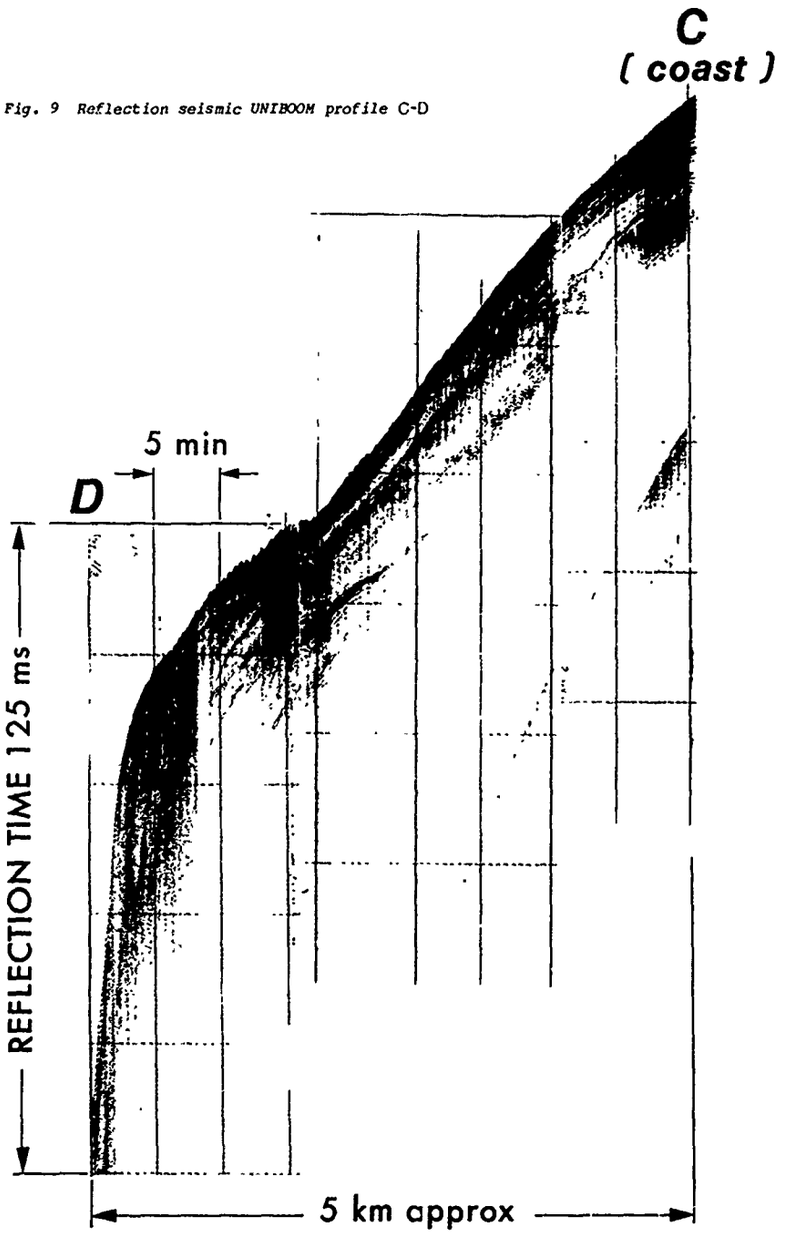

Fig. 9 Reflection seismic UNIBOOM profile C-D

The core analysis shows that the lower end (3.70-3.85 m) has a sandy composition (46.8% sand, 27.6% silt, 25.5% clay) that may correlate with sand at 3.95 m at a nearby core site. We find some dark laminations that correspond to regions of higher p-wave velocities (see Fig. 10). From the available data we can conclude that there exists a sandy interface at about 4 m of depth. We can correlate this event to the reflector S marked in Fig. 7.

The continuous seismic reflection profiles indicate strong lateral heterogeneities. It therefore can be assumed that the observed dependencies of interface velocities and energy on the direction of propagation are caused primarily by lateral inhomogeneities. However, this does not rule out the effects of anisotropy. The further analysis of data from all three ocean bottom seismometers (OBS) should allow more precise discrimination of the various effects involved.

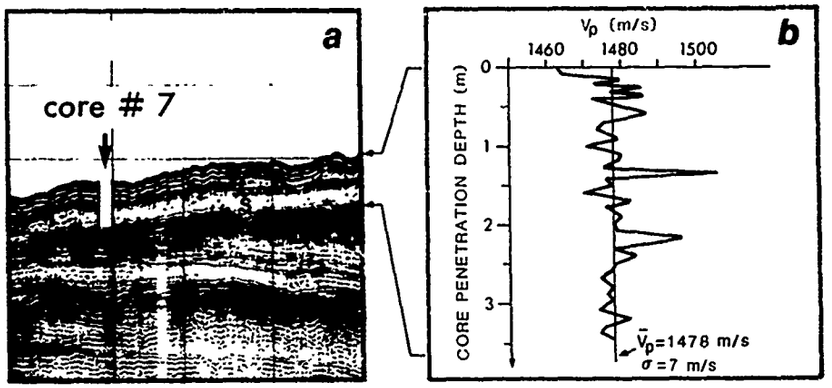

Fig. 10 a) Site of the seismometer array and core No. 7 with indicated analyzed column.
b) P-wave analysis of core No. 7

MODELLING

The inverse method for calculating the dispersion of interface waves trains needs realistic input data, such as measured velocity-depth profiles for P and S waves. We have at this stage the following kind of data and information:

- Sound speed profiles in the water column.
- A velocity depth profile for P waves in the core.
- The actual thickness of the uppermost soft layer.
- Evidence for a sandy substratum.
- Group velocities from seismogram stacks.
- Geoacoustic properties from the core analysis.

Using these data we applied modelling codes from which the group and phase velocities for different modes were calculated as a function of frequency (Fig. 11).

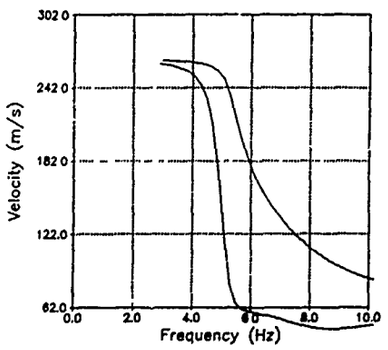

Fig. 11
Calculated dispersion curve from input model based on experimental results.

The first or fundamental mode has been successfully modelled. The results fit the data reasonably well. However, modes of higher order could not be matched to the data, although several models and variations were tried. The final model used was a sandy halfspace subbottom with a shear velocity of V_s=300 m/s, overlain by a 4 m thick layer of soft sediments with a shear velocity profile of 78 m/s on top and 96 m/s on the bottom. A shear velocity of 300 m/s was used for the halfspace, since this has proved to be a realistic value for other measurements in this region.

Not all features seen in the Gabor matrix display can be modelled. This is because the local maxima revealed in the dispersion analysis of the field data may be caused by structural effects of the subbottom rather than higher order modes. Also, the input model needs considerable adjustment to the real world in order to allow the modelling of higher order modes. Nevertheless, if theoretical results agree reasonably with field data for at least the fundamental mode, then the geoacoustic properties of the uppermost layer, that is the dispersion behaviour of interface waves, can be predicted to a reasonable degree of accuracy. With the sensors sitting on the top layer of the seafloor, in general only conversion processes at the seafloor or near seafloor interfaces can be recorded because interface wave energy decreases exponentially perpendicular to the propagation path.

CONCLUSION

By evaluating all of the measured data, we can begin to resolve the pertinent problems that are related to the effects and the role of the geological environment on interface wave propagation. The preliminary data analysis has shown that a multiparameter survey combined with a powerful analysis and modelling phase can provide a deeper understanding of the relevant conversion processes. This will lead to a greater accuracy for predictions of interface wave characteristics.

REFERENCES

1. Ali, H., Schmalfeldt, B. Unpublished report, 1984.
2. Jensen, F., Schmidt, H. Shear properties of ocean sediments determined from numerical modelling of Scholte wave data (this volume).
3. Rauch, D. Seismic interface waves in coastal water: a review, SACLANTCEN SR-42, La Spezia, Italy, SACLANT ASW Research Centre, 1980.
4. Rauch, D. On the role of bottom interface waves in ocean seismo-acoustics: a review (this volume).
5. Rauch, D., Schmalfeldt, B. Ocean-bottom interface waves of the Stonley/Scholte type: properties, observations and possible use. In: Pace, N.G. In: Acoustics and the sea-bed. Bath, U.K., Bath University Press, 1983.
6. Essen, H.-H, Janle, H., Schirmer, F. and Siebert, J. Propagation of surface waves in marine sediments. Journal of Geophysics, 49, 1981.
7. Schmalfeldt, B., Rauch, D. Explosion-generated seismic interface waves in shallow water: experimental results, SACLANTCEN SR-71, La Spezia, Italy, SACLANT ASW Research Centre, 1983.
8. Dziewonski, A., Bloch, S. and Landisman, M. A technique for the analysis of transient seismic signals. Bulletin. Seis. Soc. Am., 59, 1959.

LOW-FREQUENCY ANOMALIES IN THE REFLECTION BEHAVIOUR OF MARINE SEDIMENTS

Markus von Haumeder
SACLANT ASW Research Centre
Viale San Bartolomeo 400
I-19026 La Spezia, Italy

ABSTRACT

It is frequently found that the reflectivity of the sea bottom deviates considerably from the values that are expected by considering its impedance. A type of sea bottom in which anomalies in the reflectivity are particularly strong is a coarse marine sediment consisting of two components: particles that form a stiff frame and a liquid that fills the interstices. Such sediments can be considered porous materials. A theory that analyses the response of a porous material to an elastic wave is the Biot theory. It treats the two components as two interpenetrating elastic continua and predicts some remarkable anomalies in the acoustic behaviour of porous materials. One important prediction of the Biot theory is that acoustic energy of a certain frequency band can penetrate the sediment even in the range of total reflection. The porous material behaves here like a frequency filter with respect to broadband acoustic energy. This energy transfer into the porous material is associated with a relaxation process. We give here a derivation of the pertinent relaxation times and demonstrate how the relaxation time can be evaluated from the reflectivity anomaly. The relaxation time is expressed in terms of parameters descriptive of the internal flow. Use of this interrelation permits us to estimate the flow-permeability of a sediment on the basis of a bottom reflection loss measurement. The method is applied to a real marine sediment.

INTRODUCTION

A large fraction of the naturally occurring marine sediments can be considered porous materials. Being immersed in a fluid, such a porous material consists of two clearly separated components: a porous skeleton or frame and a fluid that fills the pore space. Each of the two components forms a large, interconnected cluster and the two clusters fit exactly into each other. This situation can be viewed as two interpenetrating elastic continua. A pressure wave impinging on such a composite material results not only in a deformation of the single components but also in a relative motion of the two continua with respect to each other. The fluid is free to move through the frame from areas of high local pressure to areas of low local pressure.

The theory that describes the propagation of elastic waves through a porous, fluid-filled material was developed by Maurice Biot [1-3]. The Biot theory is a microscopic theory that takes the particular geometry of the porous skeleton into consideration. It introduces two particle-displacement vectors, one for the solid frame and one for the pore fluid, and expresses the internal flow in terms of a difference vector. The composite nature of the porous material is reflected in the theory by a pair of wave equations that are coupled by a flow term. Thus, the Biot theory is capable of describing the underlying microscopic processes in some detail.

According to the Biot theory, porous materials exhibit some anomalies in their response to a pressure wave. One of these anomalies pertains to the reflection process at the interface between a liquid and a porous material. In an angle-of-incidence range close to grazing angle where total reflection is expected for a solid of equivalent acoustic impedance, a fluid-filled porous material absorbs energy of a certain frequency band. The porous material acts here as a band-pass filter with respect to broad-band acoustic energy, and the fraction of energy that is transferred into the interior of the porous material is used to drive the internal flow. For many frequencies this internal flow will follow the excitation by the pressure wave with a delay. Such a delay results in energy dissipation due to relaxation. Relaxation can be described best in terms of a characteristic response time, the so-called relaxation time, τ.

This paper gives a derivation of the relaxation times for a porous, fluid-filled material on the basis of the Biot theory. The relaxation times are expressed entirely in terms of flow parameters, which gives evidence that the underlying microscopic process is a flow process.

Further we present a measurement of the bottom-reflection loss that shows the reflectivity anomaly and permits the relaxation time to be determined experimentally. This measurement is used in combination with the given formula to calculate the permeability/porosity ratio of the sea bottom. The procedure used can be considered a new technique for remote bottom-permeability determination.

1 THEORY

The Biot theory treats an isotropic, homogeneous, porous material and its pore-filling fluid as two interpenetrating elastic continua [1-5]. Each of the two continua shows its own characteristic response to a pressure wave, and the composite of the two materials requires the use of two particle displacement vectors, one for the skeletal frame, u, and one for the pore fluid, U. The difference between the two displacements is a measure of the internal fluid flow, which is expressed in terms of the vector quantity, w:

$$w = \beta \left[u - U \right]. \tag{1}$$

The quantity w represents the average fluid displacement relative to the frame and β is the porosity defined as the fraction of volume occupied by the pore fluid. By expressing the vectors u and w in terms of scalar potentials, Φ, and vector potentials, Ψ,

$$u = \nabla \Phi_s + \operatorname{curl} \Psi_s \quad , \quad w = \nabla \Phi_f + \operatorname{curl} \Psi_f \tag{2}$$

the Biot equations of motion [3] can be seperated [5] into a pair of

equations involving only dilatational modes and another pair of equations for the rotational mode. The subscript s refers to 'solid' and the subscript f to 'fluid'. We start our consideration with the simpler set of wave equations for the shear-wave:

$$\mu \nabla^2 \Psi_s = \rho \ddot{\Psi}_s - \rho_f \ddot{\Psi}_f \quad , \quad \eta/k \; \dot{\Psi}_f = \rho_f \ddot{\Psi}_s - \rho_f/\beta \ddot{\Psi}_f \tag{3}$$

where μ is the shear modulus, ρ and ρ_f are the densities of the fluid and of the fluid-filled porous material, respectively, η stands for the fluid viscosity, and k designates the flow permeability. The composite nature of the porous, fluid-filled material is reflected in the theoretical description by a set of two coupled wave equations. The term on the left-hand side of the second equation is a flow term that has to be compared to the lag term in relaxation theory. This term contains the particular physics of porous materials. Its prefactor η/k is the viscous resistance to fluid flow. For high frequencies the fluid viscosity, η, is not constant and the viscous resistance to fluid flow must be made frequency dependent. Considering the friction forces within pore channels of simplified geometry, Biot derived [1] a complex correction factor, $F(\kappa) = F_r(\kappa) + i F_i(\kappa)$, for oscillatory motion. The factor η/k may be replaced by $F\eta/k$ in the frequency domain, where

$$F(\kappa) = \frac{1}{4} \frac{\kappa \, T[\kappa]}{1 - T[\kappa]/i\kappa} \quad , \quad T[\kappa] = \frac{\mathrm{ber}'[\kappa] + i \, \mathrm{bei}'[\kappa]}{\mathrm{ber}[\kappa] + i \, \mathrm{bei}[\kappa]} \; . \tag{4}$$

The functions ber(κ) and bei(κ) are the real and imaginary parts of the Kelvin function with ber'(κ), bei'(κ) being their derivatives. The argument, κ, of the correction factor, F,

$$\kappa = a\sqrt{\rho_f \omega/\eta} \tag{5}$$

is non dimensional and depends on the pore-size parameter a, the fluid density ρ_f, the viscosity, η, and the angular frequency, ω. Since we are going to make use of this correction factor $F(\kappa)$ in a quantitative way, we show the variation of its real and imaginary part with frequency in Fig. 1.

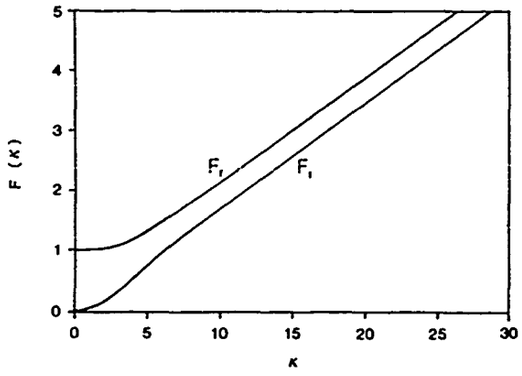

Fig. 1
Real part (F_r) and imaginary part (F_i) of the frequency correction function for three-dimensional, oscillatory flow.

For very low frequencies $F(\kappa)$ approaches unity, resulting in the same equation as when Poiseuille flow is assumed. For high frequencies, and hence large values of κ, the curves become straight lines with a slope of $1/4\sqrt{2} = 0.177$. The derivation of the complex correction factor is valid only for frequencies where the wave length is large compared with the

pore size. For sands, this puts the upper limit on frequencies at about 10^5 to 10^6 Hz.

Incorporating the complex correction factor into Eq. 3 by replacing η by $\eta F(\kappa)$, we derive now an explicit relationship between attenuation and frequency.

By Fourier transforming Eq. 3 into the frequency domain and assuming plane-wave type potentials, the two equations can be combined to give one homogeneous wave equation of the form:

$$\nabla^2\hat{\Psi} + \frac{\omega^2}{V^2}\hat{\Psi} - \frac{\rho_f^2\omega^4/\mu}{\rho_f\omega^2/\beta - i\omega\eta F/k}\hat{\Psi} = 0 \ . \qquad (6)$$

which permits solutions of the type

$$\hat{\Psi}[x,\omega] = A \exp i[\omega t + kx] + B \exp i[\omega t - kx] \ . \qquad (7)$$

Equation 6 can be cast into the form of a lossy Helmholtz equation of the general type $(\Delta^2 + \vec{k}^2) = 0$, with $\vec{k}^2 = (k - i\alpha)^2$. In this form it appears as

$$\left[\nabla^2 + \left\{\frac{\rho\omega^2}{\mu} - \frac{\rho_f^2\omega^4/\mu}{\rho_f\omega^2/\beta - i\omega\eta F/k}\right\}\right]\hat{\Psi} = 0 \ . \qquad (8)$$

The complex k-vector, $\vec{k}$, is to be identified with the expression in the brackets. Separating the real and imaginary parts of the wave vector renders two equations from which we derive the attenuation coefficient:

$$\alpha = \frac{\omega}{V\sqrt{2}}\sqrt{-1 + \frac{1}{1+[\omega\tau+F_i/F_r]^2}\left\{\left[K\omega^2\tau^2 + F_i/F_r\right] + \sqrt{\left[1+\left\{\omega\tau+F_i/F_r\right\}^2\right]\left[1+\left\{\left[\omega\tau+F_i/F_r\right]-K\omega\tau\right\}^2\right]}\right\}} \qquad (9)$$

$$K = \frac{\beta\rho_f}{\rho} \qquad \tau = \frac{\rho}{\beta}\frac{k}{\eta F_r} \qquad (10)$$

in which τ has the dimension of a time and can be identified as a relaxation time. This typical response time of the porous material is entirely expressed in terms of parameters that are descriptive of the internal flow of the pore fluid through the frame, i.e. permeability, k, fluid density, viscosity, and the real part of the frequency correction factor, F_r . K is a dimensionless factor that is determined by the density ratio of the fluid and the porous material ($\rho = \beta\rho_f + (1-\beta)\rho_r$). This factor introduces an altered frequency into the attenuation formula, which largely affects the reflection coefficient.

If we now assume the resistance to fluid flow to be frequency independent by setting the correction factor, $F(\kappa)=1$, we obtain for the attenuation the simpler formula:

$$\alpha = \frac{\omega}{V\sqrt{2}}\sqrt{-1 + \frac{1}{1+\omega^2\tau^2}\left\{K\omega^2\tau^2 + \sqrt{\left[1+\omega^2\tau^2\right]\left[1+\omega^2\tau^2\left\{1-K\right\}^2\right]}\right\}} \ . \qquad (11)$$

Equation 9, which is valid for all frequencies, takes the form of Eq. 11 when $f \to 0$, $F_i/F_r \to 0$. For the case of a pure liquid ($\beta = 1$), K equals one and Eq. 11 takes the form of the well-known formula for the relaxation attenuation in a viscous fluid:

$$\alpha = \frac{\omega}{V\sqrt{2}}\sqrt{-1 + \frac{1}{1+\omega^2\tau^2}\left[\omega^2\tau^2 + \sqrt{1+\omega^2\tau^2}\right]} \ . \qquad (12)$$

This shows that the derived formula is capable of producing the proper results in the limit $\beta = 1$. We now want to test in how far Eq. 11 reproduces the overall variation of the attenuation as obtained by the Biot computations.

For this purpose the attenuation according to Eq. 11 is plotted versus the frequency for a porosity of 0.5 (curve 'b' of Fig. 2). In this case of a frequency-independent flow resistance (Poiseuille flow) the attenuation tends towards a constant value at higher frequencies. Curve 'a', however, represents a plot of Eq. 9 in which the flow resistance is made frequency dependent. The important effect of a frequency-dependent flow resistance is apparent, mainly at high frequencies. These curves are in very good agreement with corresponding curves shown by Stoll [5,6], which were obtained as a result of a Biot model computation.

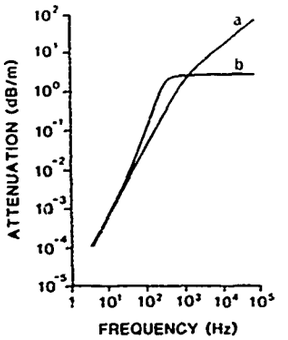

The agreement gives evidence that the derived formula reflects the attenuation in porous materials as considered by the Biot theory. In the following chapters we make use of the bottom-reflection loss anomaly in order to determine τ experimentally.

Fig. 2
Frequency dependence of the attenuation for a frequency dependent flow resistance (a) and a constant flow resistance (b).

2 BIOT PREDICTIONS OF BOTTOM-REFLECTION LOSS

The frequency dependence of the bottom-reflection loss exhibits one of the most significant anomalies in porous materials. In an angle-of-incidence range where total reflection would normally be expected, a liquid/porous-composite interface acts as a band-pass filter with respect to broadband energy. Figure 3 shows the Biot predictions for the frequency dependence of the reflection coefficient for different grazing angles. At high grazing angles the energy is reflected almost independently of frequency. At grazing angles below about 10°, however, energy of a certain frequency band penetrates the porous material, whereas the energy of higher and of lower frequencies is reflected. The line shape of the minimum resembles that of an inverted relaxation curve. In order to verify that the internal flow-

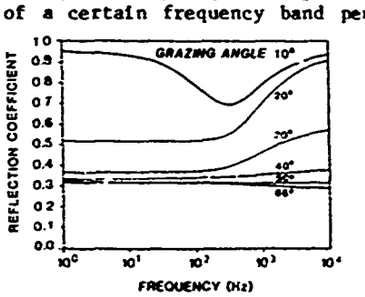

Fig. 3
Frequency dependence of the reflection coefficient for different grazing angles as predicted by the Biot theory.

relaxation creates such a minimum in the reflectivity we display the relaxation and reflectivity curves together in Fig. 4. A maximum of the relaxation manifests itself most clearly in the logarithmic decrement of the viscous losses, which are plotted in the lower part of Fig. 4 for different permeability/pore-size combinations. The appearance of the maximum in the relaxation is closely correlated to the appearance of the minimum in the reflection loss.

By varying the permeability, the curve is strongly shifted within the frequency spectrum; for comparison we display on top of Fig. 4 the corresponding minima in the bottom-reflection loss. It turns out that the corresponding minima and maxima do not show up at the same frequency. Instead they are offset by a constant ratio: the frequency at which the minimum in the bottom-reflection loss occurs is 0.53 times the frequency at which the maximum of the logarithmic decrement is observed. This is a direct result of the Biot theory and will be used later for the evaluation of T.

The location of the maximum of the logarithmic decrement in the frequency spectrum permits T to be determined via the peak-condition $\omega T = 1.1 - \frac{F_1}{F_r}$.

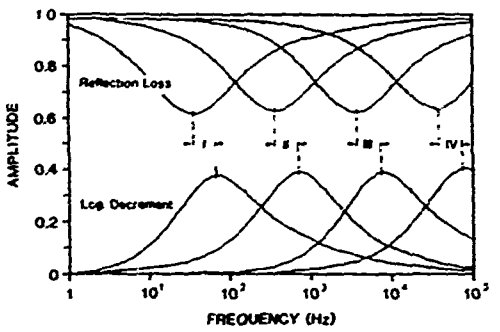

Fig. 4
Comparison of the viscous loss per wave-length (log.decrement) with corresponding reflection loss for four different permeability(k)/pore-size(a) combinations:

I : $a = 1.5 \cdot 10^{-4}$ m, $k = 10^{-9}$ m²
II : $a = 4.0 \cdot 10^{-5}$ m, $k = 10^{-10}$ m²
III : $a = 1.0 \cdot 10^{-5}$ m, $k = 10^{-11}$ m²
IV : $a = 4.0 \cdot 10^{-6}$ m, $k = 10^{-12}$ m²

We are now in the position to use the minimum in the reflection loss to find the maximum of the corresponding logarithmic decrement, and from the frequency where this maximum occurs, to find the relaxation time. In principle, the minimum in the bottom-reflection loss can be measured, although it is not clear whether the Biot effect is large enough to be measurable in a real marine sediment.

3 MEASUREMENT OF BOTTOM-REFLECTION LOSS

In 1978 the SACLANT ASW Research Centre had used a vertical array of twelve hydrophones to measure the bottom-reflection loss in certain deep basins of the central Mediterranean at frequencies from 50 Hz to 7 kHz [7]. To measure the reflection losses over this wide frequency band, explosive sources of 500 g TNT were used. The experimental set-up is sketched in Fig. 5. The receiving ship suspended a 750-m long vertical hydrophone string,

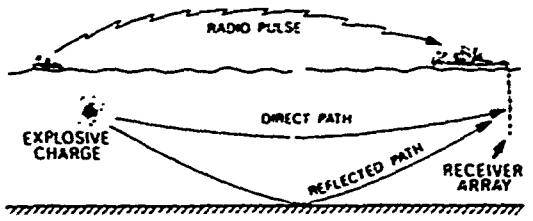

Fig. 5
The experimental set-up for bottom-reflection loss measurements [7].

while the source ship moved on a predetermined fixed course, launching charges set to explode at 550 m depth. The direct and reflected acoustic signals were recorded in digital form by the receiving ship together with a radio pulse transmitted from the source ship at the moment when it received the direct acoustic pulse from the charge. Some of the data collected in those studies will be used here.

Because the sea bottom often exhibits surface roughness and/or layering, the reflection anomaly studied in this paper is frequently masked by distortion of the acoustic signals. To isolate the reflection features related to the Biot effects from those related to the bottom morphology we choose a measuring site that shows a negligible degree of geomorphological discontinuities. This choice was made by examining underwater photographs and profiles of relative sound speed (0.98), relative density (1.5), and porosity (0.5), deduced from core samples. The area selected for the measurements used in this paper was on the Messina abyssal plain in comparatively deep water (3700 m). The morphology of the sea floor over the abyssal plain is extremely flat, with a very soft top layer of fine clay. The area is homogeneous enough to permit the measurement of the Biot reflectivity anomaly.

Accordingly the signals themselves are undistorted, almost textbook-like, which easily permits Fourier analysis. As one result of this analysis, we obtain the impulse response for different angles of incidence, as shown in Fig. 6.

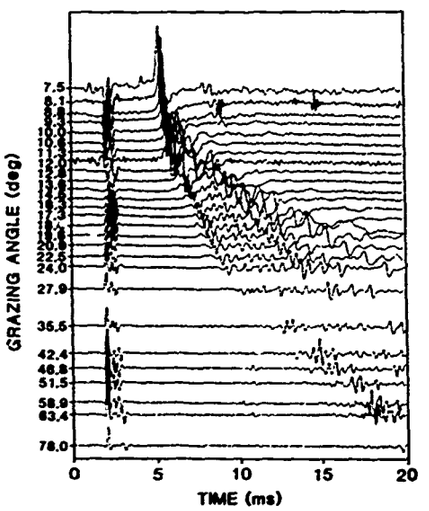

Fig. 6
Detailed display of the first 20 ms of impulse responses for different grazing angles [7].

An analysis of the signal pattern indicates a very soft sea-bottom. This bottom type, with high permeability and high porosity, implies that the sound speed in the bottom is less than that in sea water, which represents an intromission-angle situation for the frequencies discussed here. Accordingly, the first reflection remains small for all grazing angles. However, the first layer is terminated at a depth of 14 m by another, high-velocity layer, as can be deduced from the signal pattern in Fig. 6 (extrapolation to vertical incidence). As long as the grazing angle is less than 10°, all reflections/refractions merge here to create a single, large-amplitude, phase-shifted pulse. It is mainly at this 14-m interface that a reflectivity anomaly similar to the one predicted by the Biot theory was measured.

4 COMPARISON BETWEEN MODEL PREDICTIONS AND MEASUREMENTS

By Fourier analyzing the measured signal we obtain the bottom-reflection loss at different frequencies. If we use the whole signal for

the computation, i.e. the full-length signal of Fig. 6 comprising the contributions of all layers, we obtain the oscillating curve depicted in Fig. 7. The bottom-reflection loss is here shown for a very small grazing angle of 10°.

It is striking that the overall tendency of this curve resembles very much the one predicted by the Biot theory for liquid/porous-composite interfaces, as shown in Fig. 3. Some features are different, due to the layering and mixing of different materials in a real sea floor and due to the fact that the signal is also effected by the refracted arrival. Nevertheless, an appropriate choice of the input parameters to the Biot model permits the measured curve to be fitted in a way that reproduces the overall tendency; this is particularly true for the position of the minimum which is strongly shifted in frequency by small changes of the permeability (see Fig. 4). The superimposed solid line in Fig. 7 represents the fit by the Biot theory. The values of the parameters used for this computation are given in Table 1 and were chosen to obtain agreement between the experimental and the theoretical curves in Fig. 7. However, in choosing their values, constraints were imposed in order to keep them within physically realistic limits. Accordingly they are of the same order of magnitude as commonly used parameter sets given by Stoll [8].

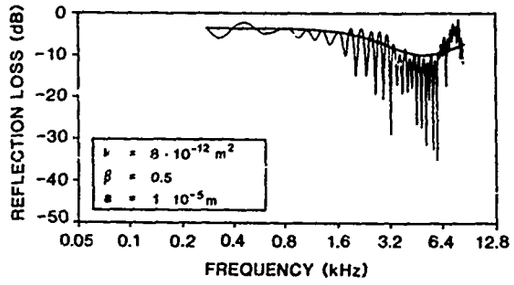

Fig. 7
Bottom-reflection loss versus frequency for a 10° grazing angle. The smooth line represents the prediction by the Biot theory.

TABLE 1

POROSITY	$\beta = 0.5$	ISOTROPY FACTOR	$\alpha = 3$
PERMEABILITY	$k = 8 \cdot 10^{-12}$ m²	BULK MODULUS OF FRAME	$K_b = 4.2 \cdot 10^7$ Pa
PORE SIZE	$a = 1 \cdot 10^{-5}$ m	SHEAR MODULUS OF FRAME	$\mu = 2.5 \cdot 10^7$ Pa
DENSITY OF GRAIN MATERIAL	$\varrho_s = 2.5 \cdot 10^3$ kg/m³	LOG DECREMENT FOR SHEAR VIBRATIONS OF THE FRAME	$\delta_\mu = 0.015$
DENSITY OF FLUID	$\varrho_f = 10^3$ kg/m³	LOG DECREMENT FOR BULK VIBRATIONS OF THE FRAME	$\delta_K = 0.015$
VISCOSITY	$\eta = 10^{-3}$ Pa·s		

Regarding the position of the minimum in the frequency spectrum, which is critically influenced by the input parameters, the fit can be considered accurate. From this fit we obtain values for the bottom parameters, in particular for those determining the above-derived relaxation time, τ . This allows us to apply our concept of a relaxation time directly to a measurement. On the one hand the relaxation time is known

by the frequency at which the measured minimum occurs according to the peak condition: $\tau = (1.1\text{-}F_1/F_2)/2\pi(1.8f)$, where the factor 1.8 is determined by the shift factor of Eq. 10. On the other hand we can easily calculate τ by introducing the fit parameters into our derived formula. A comparison of the two values of τ shows close agreement and proves the applicability of the derived formula to real marine sediments. Experimentally we obtain $\tau = 1.5\times10^{-5}$s; the formula gives $\tau = 1.6\times10^{-5}$s. The close agreement convinces us that we are dealing with a measured Biot effect. It opens up the possibility of determining bottom parameters from a measurement of the bottom-reflection loss.

CONCLUSIONS

The derived expression for the relaxation time — which correlates an overall response time with the parameters of the microscopic structure — can be used for determining bottom parameters remotely. The idea is first to use the minimum in a measured bottom-reflection-loss curve to evaluate the relaxation time and then to employ Eq. 10 to deduce values for the correlated structure parameters. The relaxation time itself is expressed in terms of the permeability/porosity ratio and of additional parameters descriptive of the liquid. With a simple assumption concerning the relation between flow permeability and porosity we are thus in a position to determine the flow permeability of the bottom under examination. This method of remotely sensing the permeability may not only be useful for characterizing the sea bottom, but may also have applications to the sensing of liquid-carrying layers. By analyzing bottom-reflection losses in the central Mediterranean we have demonstrated the applicability of this method to an actual sea-floor measurement.

ACKNOWLEDGMENTS

The author wishes to thank O. Hastrup and T. Akal of SACLANTCEN for the permission to use their bottom-reflectivity measurements.

REFERENCES

1. M.A. Biot, 'Theory of propagation of elastic waves in a fluid-saturated porous solid. I. Low-frequency range, II. Higher frequency range', J. Acoust. Soc. Am., 28: 168-191 (1956).
2. M.A. Biot, 'Mechanics of deformation and acoustic propagation in porous media', J. Appl. Phys., 33: 1482-1489 (1962).
3. M.A. Biot, 'Generalized theory of acoustic propagation in porous dissipative media', J. Acoust. Soc. Am., 34: 1254-1264 (1962).
4. R.D. Stoll and T.K. Kan, 'Reflection of Acoustic Waves at a water-sediment interface', J. Acoust. Soc. Am., 70: 149-156 (1981).
5. R.D. Stoll, 'Acoustic waves in saturated sediment'. In: L. Hampton, ed. Physics of Sound in Marine Sediments, New York, Plenum, 19-39 (1974).
6. R.D. Stoll and G.M. Bryan, 'Wave attenuation in saturated sediments', J. Acoust. Soc. Am., 47: 1440-1447 (1970).
7. T. Akal, 'Acoustical characteristics of the sea floor: experimental techniques and some examples from the Mediterranean Sea'. In: L. Hampton, ed. "Physics of Sound in Marine Sediments", New York, Plenum, p. 447 (1974).
8. R.D. Stoll, 'Experimental studies of attenuation in sediments', J. Acoust. Soc. Am., 66: 1152-1160 (1979).